Temperature-induced magnetization reversals in micromagnetic systems

Sergei Y. Liashko

Faculty of Physical Sciences
School of Engineering and Natural Sciences
University of Iceland
2017

Temperature-induced magnetization reversals in micromagnetic systems

Sergei Y. Liashko

180 ECTS thesis submitted in partial fulfillment of a
Doctor Philosophiae degree in Chemistry

Ph.D. Supervisors:
Hannes Jónsson
Valery M. Uzdin

Ph.D. Committee:
Hannes Jónsson
Pavel F. Bessarab
Unnar B. Arnalds

Opponents:
Peter Derlet
Robert Stamps

Faculty of Physical Sciences
School of Engineering and Natural Sciences
University of Iceland
Reykjavík, November 2017

Temperature-induced magnetization reversals in micromagnetic systems

Dissertation submitted in partial fulfillment of a *Philosophiae Doctor* degree in Chemistry

Faculty of Physical Sciences
School of Engineering and Natural Sciences
University of Iceland
Dunhaga 5
107, Reykjavík
Iceland

Telephone: +354 525-4000

Bibliographic information:
Sergei Y. Liashko, 2017, *Temperature-induced magnetization reversals in micromagnetic systems*, Ph.D. dissertation, Faculty of Physical Sciences, University of Iceland, 79 pp.

ISBN 978-9935-9383-4-3

Printing: Háskólaprent ehf., Fálkagötu 2, 107 Reykjavík
Reykjavík, Iceland, November 2017

Abstract

Microscopic magnetic particles can be found in a wide range of systems, from asteroids in outer space and minerals in the Earth's crust to living organisms on land and in the ocean. Often they determine critical functional properties of these systems and form the basis of modern technology such as high-density data storage devices. An essential task for fundamental magnetism and applications is to describe the behavior of such particles at a given temperature and in the presence of an applied magnetic field. In this thesis, a theoretical method is developed for estimating the lifetime of magnetic states of microscopic particles based on harmonic transition state theory. It represents an extension of Stoner-Wohlfarth theory by introducing the effect of temperature. An analytical expression for the lifetime is presented as a function of magnetic field strength and temperature for certain field directions. This theory is applied in the calculations of switching field distribution of sub-micron CoPt islands with out-of-plane anisotropy and in the estimation of nucleation volume for magnetization reversal in such islands. After considering magnetization reversal of a single island, collections of micromagnetic particles in elements of spin ice systems are analyzed. Micromagnetic, dipole-dipole and dumbbell numerical models for the description of the interaction between islands in spin ice magnetic elements are compared. The lifetime of magnetic states in one and two hexagonal rings of a kagome spin ice system is calculated and found to compare well with reported results of experimental measurements. The magnetization reversal processes in an element of the shakti lattice are quantitatively described using various paths on the energy surface with estimation of the energy variation along each path for a range in the value of the lattice constant.

Útdráttur

Örsmæðar segulagnir koma fyrir víða, allt frá loftsteinum í himinhvolfinu til steinda í jarðskorpunni, og í lifandi verum á láði og legi. Oft á tíðum gegna þær lykilhlutverki og eru t.a.m. grundvöllurinn fyrir nútíma tækni svo sem í háþéttni gagnageymslum. Mikilvægt er að skilja grundvallareiginleika slíkra agna og geta metið líftíma segulástandanna við tiltekið hitastig og ytra segulsvið. Í þessari ritgerð er þróuð aðferð til að meta líftíma segulástanda örsmæðar segulagna með því að nota virkjunarástandskenninguna innan kjörsveifilsnálgunarinnar. Þar með er Stoner-Wohlfarth aðferðin útvíkkuð til að taka áhrif hitastigs með í reikninginn. Einföld líking er leidd út fyrir líftímann sem fall af hitastigi og styrkleika segulsviðsins fyrir tilteknar stefnur sviðsins. Þessari aðferð var beitt í reikningum á vendisviðsdreifinu smárra CoPt eyja með þverstæðan stefnuás til að meta kjarnarúmmálið fyrir umseglun eyjanna. Eftir að umselgun stakra eyja hafði verið rannsökuð voru greindir eiginleikar eyjaklasa sem eru einingar í spunaís. Tvískauts- og handlóðarnálganir til að lýsa víxlverkun milli eyja í spunaíseiningum voru bornar saman við míkrósegulreikninga. Líftími segulástanda í einum og tveimur sexhringjum kagome spunaíss var reiknaður og niðurstöðunum bar vel saman við birtar mæliniðurstöður. Umseglun í einingu af shakti spunaís var lýst ítarlega með ýmsum hvarfleiðum á orkuyfirborðinu og mati á orkunni eftir ferlunum fyrir ýmis gildi á grindarfastanum.

Table of Contents

List of publications

Publications included in the thesis

A1: S.Y. Liashko, H. Jónsson, V.M. Uzdin, *The effect of temperature and external field on transitions in elements of kagome spin ice*, New Journal of Physics **19**, 113008 (2017).

A2: S.Y. Liashko, I.S. Lobanov, V.M. Uzdin, H. Jónsson, *Thermal stability of magnetic states in submicron magnetic islands*, Nanosystems: Physics, Chemistry, Mathematics **8(5)**, 572-578 (2017).

A3: S.Y. Liashko, H. Jónsson, V.M. Uzdin *Calculations of switching field and energy barrier for magnetic islands with perpendicular anisotropy*, Nanosystems: Physics, Chemistry, Mathematics (accepted for publication).

Publications not included in the thesis

B1: S.Y. Liashko, V.M. Uzdin, H. Jónsson, *Rate of thermal transitions in kagome spin ice*, Journal of Physics: Conference Series **741**, 012182 (2016).

B2: S.Y. Liashko, V.M. Uzdin, H. Jónsson, *Energy surface and transition rates in a hexagonal element of spin ice*, Journal of Physics: Conference Series **903**, 012006 (2017).

Acknowledgments

I would like to express my sincere gratefulness to my teachers, professor Valery M. Uzdin and professor Hannes Jónsson, for the invaluable support of my Ph.D. study and related research. Their enthusiasm, immense knowledge and patience were my driving force in the Ph.D. pursuit. I could not have imagined having better mentors.

Besides my advisors, I would like to thank Dr. Unnar Arnalds and Dr. Pavel Bessarab for their insightful comments and helpful discussions on my thesis work. In addition I would like to thank my colleague and friend Sergei M. Vlasov.

Also I would like to thank my parents, Natalia S. Liashko and Yuriy P. Liashko, for supporting me spiritually throughout my life and this thesis.

Last but not the least, I would like to thank all my friends.

1 Hysteresis loops and magnetization reversal in magnetic particles at zero temperature

1.1 Introduction

Microscopic magnetic particles are an essential part of our world. In asteroids from outer space and samples from the moon to rare minerals in the Earth's crust, as well as in living organisms, one can find such magnetic particles. Just one gram of human brain contains up to 10^8 magnetic particles [1]. Almost every cell of a plant or animal contains the protein "ferritin" that has a magnetic nanoparticle in its structure. They play a significant role in a wide range of systems. In Nature, animals use such systems for navigation, in our day-to-day life technologies such as high-density data storage devices and medical treatments use small magnetic particles as the basis. Thus it is clear why research, both theoretical and experimental, has been dedicated to magnetic systems of small size, over more than 70 years. As a result, it is now possible not only to create systems that consist of magnetic particles on the scale down to nanometers but also accurately measure the physical properties of magnetic systems on the atomic scale. Such small particles can have special properties, unlike larger magnetic systems. A magnetic nano-object is a physical object made from a magnetic material that shows a considerable difference in its physical properties from the corresponding bulk material and has at least one dimension that ranges from one to hundreds of nanometers. A material that has key physical properties determined by nanoscopic size is referred to as "nanomaterial." Presently it is possible to construct magnetic nanomaterials in various forms that fall into two categories: Compact materials and nanodispersions. The first type includes so-called "nanostructured" materials that consist of nanometer-sized units as repeating structural elements following a particular pattern (for example, artificial spin ice systems). On the other hand, a material with nanosized particles that are dispersed in a homogeneous base, such as vacuum, gas, liquid or solid that allows to distinctly separate particles from each other, is called "dispersion material". Examples are powder samples and ferrofluids. By choosing and controlling the preparation method of magnetic nano-systems, it is possible to control the microscopic properties of the nanomaterials, and thereby influence the resulting macroscopic properties. For example, one of the most critical properties of these materials is the distance between nano-objects, which can vary on a broad scale from sub-nanometer to hundreds of nanometers. That has led to the discovery of a new variety of physical phenomena, such as giant magnetoresistance (GMR) [2] and extraordinary Hall effect in metallic

systems [3]; large tunneling magnetoresistance (TMR) in insulating materials [4]; remanence [5], coercivity [6] and magnetocaloric effect [7] enhancements; glassy behavior [7] and quantum tunneling of magnetization [8]. Both experimental [9, 10, 11, 12, 13, 14, 15, 16, 17, 18, 19] and theoretical [20, 21, 22, 23, 24] research has showed how magnetization can differ between fine particles and corresponding bulk materials.

These new phenomena have great importance for fundamental science as well as modern technology. Some examples are magnetic high-density data storage devices, and industry technology in the form of magnetic sensors, refrigerant materials, and permanent magnets. Their origin lies in the combination of intrinsic properties that are consequences of the system's small size and interactions between elements of the nanomaterial. An important task is to describe the behavior of such particles at a given temperature and in the presence of an applied magnetic field. From the theoretical point of view, the most accurate way to model the magnetic system is to apply a quantum mechanical approach based on *ab initio* calculations. However, such an approach is computationally too demanding as the effort increases exponentially with increasing number of elements in the system. Therefore, various simplified models have been proposed for describing the behavior of ferromagnetic materials on the microscopic scale. Each model tends to simplify the task by bringing some assumptions about the particular system it is meant for. The most common way to distinguish systems is the size scale. On a larger scale, magnetic materials show multidomain structure that breaks the sample into different regions, each with a uniform magnetization direction. These domains are separated by domain walls (DW). The micromagnetic theory, suggested by Brown Jr. [25] in 1963, describes this accurately on the micron scale. One of the most fundamental questions that are related to the small finite volume of the nanoparticle is the question about the influence of volume on internal domain structure. As the volume of the particle is reduced, it can become comparable to and smaller than the size of domains in bulk material. For some volume, called the critical volume, V_{crit}, the formation of the domain wall becomes energetically too unfavorable. Systems of a size that is comparable with (or lesser than) the size of the domains in the corresponding bulk sample, represent so-called monodomain structures [26] and can be described by Stoner-Wohlfarth model [27].

The critical volume depends on the particle's magnetization, its anisotropy energy and exchange interaction between magnetic spins. The critical diameter of spherical particles is in the range of 10 - 800 nm [28]. For metallic iron and cobalt particles, the critical diameter is between 15 nm and 35 nm, but for $SmCo_5$ particles, it is about 750 nm [29].

Due to incomplete control during the preparation of a magnetic nano-material, the size of the particles is not the same but has some variations. A distribution function $f(V)$ describes the volume of particles in the system. It is common [30, 29] to model such a function with

$$f(V) = \frac{1}{\sqrt{2\pi}\sigma V} \exp\left(-\frac{ln^2(V/V_0)}{2\sigma^2}\right) \tag{1}$$

where V_0 is the most probable value of the particle volume in the system, and σ is the standard deviation of $ln(V)$. Transmission electron microscopy (TEM) and other indirect techniques such as x-ray diffraction and magnetic granulometry have shown

experimentally that this assumption is accurate for many nanosystems [31].

1.2 Micromagnetic modeling

When the peak of the function given by Eq. 1 corresponds to a volume that is larger than V_{crit}, then the micromagnetic theory can be used to accurately describe the behavior of the system. A magnetic material consists of magnetic dipoles or elementary magnets. Such dipoles can be related to atomic spins and angular momenta.

One can assume that elementary magnets, $\vec{m}_i$, located at $\vec{r}_i$ have parallel orientation over some region

$$\vec{m}_i \approx \vec{m}_j \, for \, |\vec{r}_i - \vec{r}_j| < \lambda \tag{2}$$

where the λ defines the range of the exchange interaction. The fundamental assumption of the micromagnetic theory is a uniform density of magnetic dipoles. Then a continuous magnetization vector $\vec{M}(\vec{r})$ is a valid approximation for the orientation of the magnetic moments $\vec{m}_i$ within a region $\Omega > \lambda^3$ Because of the homogeneous distribution of the elementary magnets, the magnetization can be normalized as

$$\vec{M}(\vec{r}) = M_s \vec{m}(\vec{r}) \text{ where } |\vec{m}(\vec{r})| = 1 \tag{3}$$

where M_s is the saturation magnetization.

Superposition and interaction of magnetic dipoles determine the macroscopic magnetic properties of the material. Some of the interactions, such as demagnetizing energy or Zeeman energy, have the origin in classical theory whereas other, such as exchange energy, are of quantum mechanical nature. Because of this mixture of different effects, the micromagnetic theory is sometimes referred to as a semi-classical continuum theory.

1.2.1 Exchange energy

For two neighboring spins, classical electromagnetic interaction favors antiparallel ordering [32]. From this, one would expect that macroscopic magnetic material will not have the uniform magnetization. This is, indeed, true for paramagnetic and diamagnetic materials. However, elementary magnets show different behavior due to the presence of the exchange interaction. Its origin is the Coulomb interaction between electrons and the antisymmetry of the two-particle wave function [33]. The classical Heisenberg Hamiltonian [34] for two localized and neighboring spins is the starting point for introducing exchange energy to micromagnetic continuum theory

$$E_{ij}^{ex} = -J_{i,j} \vec{S}_i \cdot \vec{S}_j \tag{4}$$

where $\vec{S}_i$ and $\vec{S}_j$ are two neighbor spins and $J_{i,j}$ is the exchange integral between them. If the length of the vector is defined as $S = \|\vec{S}_i\| = \|\vec{S}_j\|$, then the total exchange energy of a magnetic body can be written as

$$E_{total}^{ex} = \sum_{i \neq j} -J_{ij} S^2 \left[1 - \frac{1}{2} (\vec{n}_i - \vec{n}_j)^2 \right] \tag{5}$$

where $\vec{n}_i = \vec{S}_i/S$ and $J_{ij} \neq 0$ for neighboring spins. Micromagnetics adopts this expression to the continuum model of $\vec{m}(\vec{r})$. If $\Delta\vec{r}$ is the distance vector between two interacting magnetic moments, then the sum of all contributions from possible $\Delta\vec{r}_i$ defines the exchange energy of the magnetic material

$$E^{ex}_{total} = \int_\Omega \sum_i A_i \vec{m}(\vec{r}) \cdot \vec{m}(\vec{r} + \Delta\vec{r}_i) d\vec{r} \tag{6}$$

where A_i is the exchange constant that includes exchange integral and the number of spins. The expansion of the $\vec{m}(\vec{r} + \Delta\vec{r})$ up to the first member changes the general form of the exchange energy to

$$E^{ex}_{total} = \int_\Omega \sum_{i,j} A_j \left(\frac{\partial m_i}{\partial x_j} \right)^2 d\vec{r}. \tag{7}$$

The fact that the exchange constant does not depend on the dimensionality for isotropic materials and materials with cubic lattice simplifies the expression 7 further

$$E^{ex}_{total} = A \int_\Omega \sum_i (\nabla m_i)^2 d\vec{r} = A \int_\Omega (\nabla \vec{m})^2 d\vec{r}. \tag{8}$$

Typically, the exchange constant A is determined experimentally.

The expression above accurately describes most magnetic materials, and it is the most common way to calculate exchange interaction in numerical simulations. In metallic ferromagnets the spins are not truly localized and, therefore, the Heisenberg model is only a rough approximation. However, even for such materials, Eq. 8 can be used to describes exchange interactions phenomenologically [35].

1.2.2 Demagnetization energy

The demagnetization or magnetostatic energy is the energy of the magnetization in a magnetic field. It originates from the dipole-dipole interaction between spins. The starting point for the calculation within micromagnetic theory are Maxwell equations [36]

$$\nabla \cdot \vec{B} = 0 \tag{9}$$

$$\nabla \times \vec{H} = 0 \tag{10}$$

where $\vec{B}$ is the magnetic flux and $\vec{H}$ is the magnetic field. There is a relation between them

$$\vec{B} = \mu_0 \left(\vec{H} + \vec{M} \right) \tag{11}$$

where μ_0 is the permeability of vacuum. The general solution to the Eq. 10 can be found by expressing $\vec{H}$ as the gradient of a scalar potential U. The demagnetizing field $\vec{H}_{demag}$ is then a solution to

$$\nabla U = \nabla \cdot \vec{M} \tag{12}$$

$$\vec{H} = -\nabla U \tag{13}$$

with the asymptotic boundary condition $U(\vec{r}) = O(1/\|\vec{r}\|)$ for $\|\vec{r}\| \to \infty$. In case of finite magnetic body, the magnetization behaves continuously in a finite region Ω

$$\|\vec{M}(\vec{r})\| = \begin{cases} M_s \; if \; \vec{r} \in \Omega \\ 0 \; else \end{cases} \tag{14}$$

By using a Green's function of the Laplacian [32] to solve Eq. 12 and Green's theorem to calculate magnetization at the edge of the Ω

$$\vec{H}_{demag} = -\nabla U(\vec{r}) = \int_{\Omega} N(\vec{r} - \vec{r}')\vec{M}(\vec{r}')d\vec{r}' \tag{15}$$

where the $N(\vec{r} - \vec{r}')$ the so-called demagnetizing tensor can be expressed as

$$N(\vec{r} - \vec{r}') = -\frac{1}{4\pi}\nabla\nabla' \frac{1}{\|\vec{r} - \vec{r}'\|}. \tag{16}$$

Therefore, the form of the demagnetizing energy becomes

$$E_{total}^{demag} = -\frac{\mu_0}{2}\int_{\Omega} \vec{M} \cdot \vec{H}_{demag} d\vec{r} = \frac{\mu_0}{2}\iint_{\Omega} \vec{M}(\vec{r})N(\vec{r} - \vec{r}')\vec{M}(\vec{r}')d\vec{r}d\vec{r}'. \tag{17}$$

1.2.3 Zeeman energy

The energy of the magnetization in the presence of the external magnetic field $\vec{H}$ or Zeeman [36] energy

$$E_{total}^{Z} = -\mu_0 \int_{\Omega} \vec{M} \cdot \vec{H} d\vec{r}. \tag{18}$$

1.2.4 Anisotropy energy

The anisotropy depends on the crystal structure of the material [35] and its shape [37]. The orientation of the magnetization along a particular axis then becomes energetically more favorable, or in other words, this axis becomes an "easy-axis". This effect arises from numerous reasons including the spin-orbit coupling (magnetocrystalline anisotropy), and deviation of the particle shape from a perfect sphere (shape anisotropy). The particular direction along the easy-axis is not important, e.g., a local minimum at direction $\vec{m}_{min}$ has same energy as a local minimum for direction $-\vec{m}_{min}$, i.e., $E^{anis}(\vec{m}_{min}) = E^{anis}(-\vec{m}_{min})$.

For the simplest case of one easy-axis or uniaxial anisotropy case, one can write a phenomenological expression

$$E_{uniax}^{anis} = \int_{\Omega} \left[K_{u1}(\vec{m} \cdot \hat{\kappa}_u)^2 + K_{u2}(\vec{m} \cdot \hat{\kappa}_u)^4\right] d\vec{r} \tag{19}$$

where the unit vector $\hat{\kappa}_u$ is aligned with the easy-axis, K_{u1} and K_{u2} are anisotropy constants. This equation is the result of a Taylor expansion of direction cosines of magnetization along anisotropy axis. Since the energy has to be independent of the direction of the easy-axis, no odd powers are present in the series expansion. Uniaxial

anisotropy is typical for materials such as cobalt [38], which has hexagonal or tetragonal crystal lattice.

For materials with cubic lattices, such as nickel with face-centered cubic lattice [39] or iron with body-centered cubic lattice [40], the anisotropy has three pairwise orthogonal axes $\hat{\kappa}_i \cdot \hat{\kappa}_j = \delta_{ij}$. That leads to following Taylor expansion with even powers

$$E_{cubic}^{anis} = \int_{\Omega} \left[K_{c1}(\vec{m}_1^2\vec{m}_2^2 + \vec{m}_2^2\vec{m}_3^2 + \vec{m}_3^2\vec{m}_1^2) + K_{c1}(\vec{m}_1^2\vec{m}_2^2\vec{m}_3^2) \right] d\vec{r} \tag{20}$$

where $\vec{m}_i = \hat{\kappa}_i \cdot \vec{m}$ is component of the magnetization along the i-th easy-axis. During a numerical simulation, it is usually enough to include only the lowest powers [36].

If the shape of the material is not perfectly spherical, then there is an anisotropy that solely depends on the shape of the particle - shape anisotropy. The origin of shape anisotropy lies in the demagnetization energy and, in this case, the anisotropy constant K_1 has the form of a difference between values of demagnetizing energy when all magnetic moments are oriented along the easy-axis and perpendicular to it

$$K_1 = E_{\perp}^{demag} - E_{\parallel}^{demag} = \frac{M_s^2(D_w - D_l)}{2} \tag{21}$$

where D_w and D_l are so-called demagnetizing factors and can be calculated analytically for some particular shapes such as general ellipsoid [41] and rectangular prism [42].

The micromagnetic theory assumes a set of simplifications compared to the quantum theory. Such approach is justified for a broad range of applications but has its limitations. For example, there are points of singularity, where the magnetization changes rapidly and breaks the homogeneous assumption, e.g., Bloch points. Even though magnetic simulations can accurately describe processes with such singularities [43] the energy density at Bloch points is not accurate. Another reason for the non-uniform magnetization is the temperature effect and local perturbation of the magnetic moments. However, mean field theory or a fluctuating field addition in the equation of motion [44] can help to account for such effects. Unfortunately, both approaches do not deal with local changes of the magnetization. This limitation can be handled by using Landau-Lifshitz-Bloch equation of motion that considers a change of the length of the magnetization vector [45]. Composite materials, which consist of two materials that interact via the interface, bring another limit to the model. Magnetic interaction near the interface often proves to be quite complicated and can be correctly described only by considering quantum effects. Examples of such interaction are Ruderman-Kittel-Kasuya-Yosida interaction (RKKY) [46] and Dzyaloshinskii-Moriya interaction (DMI) [47]. These kinds of interactions can be taken into account in calculations [48, 49].

When the volume of a magnetic particle is small enough, it starts to behave as monodomain particle and then the Stoner-Wohlfarth model ca be used to describe the remagnetization dynamics.

1.3 Stoner - Wohlfarth model of a monodomain particle

The Stoner - Wohlfarth model assumes the magnetic particle has a single domain. This is a good assumption when the the volume distribution function 1 has a peak, V_0, below the critical volume V_{crit}. In the absence of a magnetic field, the energy of the particle is determined by the anisotropy energy, which depends on the angle between anisotropy axis and magnetic moment. Typically, the anisotropy energy of a monodomain magnetic particle is proportional to the volume V and has a form of

$$E(\theta) = -K_1 V \cos^2 \theta \tag{22}$$

where θ is an angle between a direction of the magnetization vector $\vec{M}$ and the easy-axis. K_1 is the anisotropy constant, that in case of the shape anisotropy can be calculated for the particular particle in accordance with Eq. 21. In the absence of an external magnetic field $\vec{H}$, two easy directions along the anisotropy easy-axis correspond to the angles $\theta = \pi$ and $\theta = 0$. Anisotropy constant and the volume of the particle, $K_1 V$, determine the energy barrier between those two "easy" directions of the magnetization. In the case when a single domain particle is under an external magnetic field $\vec{H}$, its total energy becomes

$$E = -K_1 V \cos^2 \theta - (\vec{H} \cdot \vec{M}). \tag{23}$$

Stoner and Wohlfarth described such a system, and it is usually referred to as Stoner-Wohlfarth (SW) model [27]. They showed that for the monodomain magnetic particle with uniaxial anisotropy the energy achieves its minimum when the magnetization reversal process happens in the plane formed by anisotropy axis and the external field. Therefore, the problem of finding the magnetization equilibrium states for a given $\vec{H}$, becomes a search of the minima of the energy function (see Fig. 1.1).

$$E(\theta) = -K_1 V \cos^2 \theta - M_s H \cos(\psi - \theta) \tag{24}$$

where the M_s is the value of the saturation magnetization of the particle, and H is the value of the external magnetic field.

If the value of H is less than a critical value referred to as the switching field at zero temperature H^0_{sw}, the energy of the system has two minima corresponding to two stable states of the system. The two minima are separated by an energy barrier corresponding to the activation energy, ΔE. When the external field is parallel to the easy-axis, the expression for the activation energy ΔE becomes [50]

$$\Delta E = -K_1 V \left(1 - \frac{H}{H^0_{sw}}\right)^2. \tag{25}$$

As the field strength is increased at zero temperature, $\vec{M}$ irreversibly rotates toward the direction of $\vec{H}$ when the value of H becomes equal to $H^0_{SW} = 2K_1/M_s$. Therefore, the H^0_{sw} is the minimum strength of the external magnetic field at which the anisotropy energy barrier, $K_1 V$, vanishes.

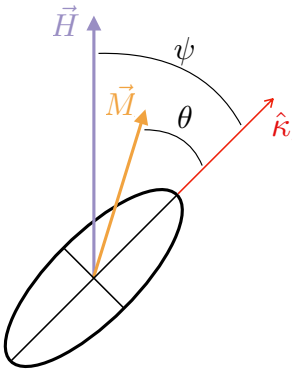

Figure 1.1. Schematic representation of the Stoner-Wohlfarth model for a monodomain magnetic particle in the presence of an external field. $\vec{M}$ gives the direction of the magnetization of the particle, specified by the angle θ. The orientation of the external magnetic field $\vec{H}$ in the plane of the particle is defined by the angle ψ. The unit vector $\hat{\kappa}$ is aligned with the anisotropy easy-axis.

An analytical solution for an arbitrary orientation of the external magnetic field has not been found. However, a phenomenological approximation has been used

$$\Delta E = -K_1 V \left(1 - \frac{H}{H_{sw}^0}\right)^k \tag{26}$$

where k is the phenomenological constant that depends on the angle ψ. For small deviations from the parallel orientation [51], $k = 1.5$. For the general case, e.g., arbitrary ψ angle, a phenomenological approximation for k has been suggested by Pffeifer [52] of the following form

$$k = 0.86 + \frac{1.14 H_{sw}^0}{2K_1 V}. \tag{27}$$

The SW model can be used to predict hysteresis loops for uniaxial monodomain particles for different angles of the external magnetic field as seen in Fig. 1.2.

Experimental tests of the accuracy of SW theory were not obtained right away. Only with the development of new modern experimental measurements and material processing techniques, it becomes possible to obtain quantitative information to test the predictions of the SW model. Especially important was the development of near-field microscopy and nanolithography. The measurements by Wernsdorfer et al. were the first experimental work that showed the SW astroid and confirmed the SW model predictions for nanowires and fine magnetic particles at low-temperature [53, 54, 55, 56, 57, 58]. Before Wernsdorfer work, it was suggested that the magnetization reversal process occurs via a complex path and cannot be described via the SW model even for single-domain particle [59, 60]. Later, other techniques were applied to this problem, in particular: Hall probe magnetometry [61], GMR [62, 63] and spin-dependent tunneling with Coulomb blockade [64, 65], but again results were not conclusive enough. In

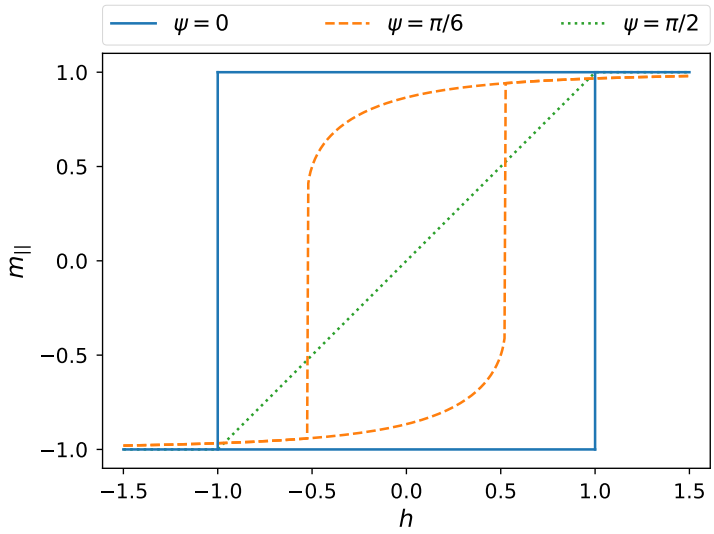

Figure 1.2. Hysteresis loops predicted by SW model for different angles between easy-axis and external field. $m_{\parallel}$ is the cosine of magnetization that has been projected to the external field direction. h is the dimensionless constant that is defined as $h = HM_s/2K_1$.

the measurements of Wernsodrfer et al., the direct current superconducting quantum interference device (DC-SQUID) was used to study fine magnetic particles. The experimental set-up consisted of a planar Nb micro-bridge (created with electron-beam lithography [66, 67]) and a magnetic nanoparticle or nanowire made of Co, Ni, Fe or $BaFe_{12-2x}Co_xTi_xO_{19}$ placed on one side of the bridge. This experimental configuration made it possible to detect the change in the direction of the magnetization on the scale of 10^4 μ_B [68]. The first experiments showing the dependence of H^0_{sw} on angle ψ were based on measurements of the hysteresis loops and their angle dependency at low temperature [54]. To obtain such data, the external magnetic field was generated in the plane of the SQUID bridge, and the angle ψ between anisotropy and the generated field was measured. This process was reversible up to the switching field value at which point the magnetization changed its orientation and became aligned with the direction of the external magnetic field. Subsequently, a more convenient method was used. There the strength of the magnetic field was increased at some fixed rate at a particular temperature and as soon as the magnetization changed its orientation H_{sw} was measured. This procedure was repeated over 100-200 cycles, and a histogram of the switching field was obtained, from which the mean value of the H_{sw} and the width of the distribution was obtained [54, 55, 56]. As a result, it has been showed that for small enough magnetic nanoparticles the magnetization reversal process occurs coherently, and the system could be described as a macro-spin object [57]. In particular, the angle dependency of the magnetization predicted by SW astroid was confirmed [54, 55, 56]. Moreover, experiments with 3-dimensional external field also showed the accuracy of

the SW model, but for some systems, the uniaxial anisotropy approximation is not good enough, and higher order anisotropy is required [69].

1.4 Magnetic dynamics

In order to describe the dynamics of the magnetization vector, a continuous model can be used where the magnetization is characteristic of particular states of the ferromagnetic body. The magnetization is the total magnetic moment of small macroscopic volumes $\vec{M} = \sum \vec{m}/(\Delta V)$. The equation of motion of the isotropic ferromagnet was introduced by Landau and Lifshitz in 1935. Because of the quantum nature of exchange interaction this equation cannot be strictly derived from classical theory. It is assumed that the ferromagnet is presented by a set of 'gyroscopes', solid bodies that are pinned. Each of these bodies has an angular moment $\vec{J}$ and magnetic moment $\vec{m}$. Then equation of motion is written [34] as

$$\hbar \frac{\vec{J}}{t} = \vec{m} \times \vec{H}. \tag{28}$$

By multiplying this expression by the number of magnetic moments N in the volume, we obtain the equation of motion for the magnetization precession

$$\frac{\vec{M}}{t} = -\gamma \vec{M} \times \vec{H} \tag{29}$$

where γ is the characteristic of the collective motion of the moments in the ferromagnet. In the framework of continuum theory, this factor should be regarded as phenomenological and determined from experiment. However, if the material has a particular easy direction that is energetically favorable, then it is not isotropic and the equation of motion can be generalized [34] as

$$\frac{\partial \vec{M}}{\partial t} = -\gamma \vec{M} \times \frac{\partial E_{mag}}{\partial \vec{M}} \tag{30}$$

where $E_{mag} = -\vec{M} \cdot \vec{H}$ is the energy of the magnetization in external magnetic field $\vec{H}$. In this case, the equilibrium state of the magnetization of the anisotropic ferromagnet is achieved when the energy does not change over time, and the length of the magnetization vector remains constant. As a result, the Landau - Lifshitz equation [34], without dissipation is written as

$$\frac{\partial \vec{M}}{\partial t} = -\gamma \vec{M} \times \vec{H}_{eff} \tag{31}$$

where $\vec{H}_{eff}$ is the effective magnetic field that is defined as

$$\vec{H}_{eff} = -\frac{\partial E}{\partial \vec{M}}. \tag{32}$$

In the adiabatic limit, this equation can be split into two equations for spherical polar angles θ and ϕ

$$\dot{\theta} = -\frac{\gamma}{M_s \sin\theta} \frac{\partial E}{\partial \phi} \tag{33}$$

$$\dot{\phi} = \frac{\gamma}{M_s \sin\theta} \frac{\partial E}{\partial \theta}. \tag{34}$$

In orer to take dissipation into the account [34], these equations become

$$(1+\alpha^2)\frac{\partial \vec{M}}{\partial t} = -\gamma \vec{M} \times \vec{H}_{eff} - \frac{\alpha\gamma}{M_s} \vec{M} \times \left[\vec{M} \times \vec{H}_{eff}\right] \tag{35}$$

where α is a dimensionless damping constant.

2 Magnetization reversal of monodomain magnetic particles at finite temperature

2.1 Introduction

The stability of magnetic systems with respect to thermal fluctuations is an important topic in fundamental science and modern technology [70, 71]. In particular, systems consisting of nano-particles are found to be useful for various technological applications. For example, nano-patterned arrays of magnetic islands theoretically can increase the density of magnetic data storage devices to greater than 160 Gbits per cm^2 [72]. However, with reduction of the size the nanoscale, the thermal stability also decreases. While the SW model, described in the previous chapter, is an experimentally proven model for describing a monodomain magnetic particle in the presence of an external magnetic field at zero temperature, it does not take into account an important factor, namely finite temperature. For example, the switching field at non-zero temperature is less than the value predicted by SW model [73] since thermal activation brings the system over the energy barrier. By applying transition state theory, the SW model can be extended to finite temperature, as described below.

2.2 Energy surfaces and transition state theory

Rate theory was originally developed in studies of chemical reactions. Back in the 1880s, Arrhenius and van't Hoff were analyzing experimental data and formulated the empirical law that well describes the dependence of the rate constant of a chemical reaction on temperature [74], known today as the Arrhenius law

$$k = \nu \exp\left(-\frac{\Delta E}{k_B T}\right). \tag{36}$$

Here, ν is a pre-exponential factor with units of inverse time, T is the temperature, k_B is Boltzmann constant and ΔE is referred to as the activation energy. The mechanism of chemical reactions involves rearrangements in the configurations of the atoms [75, 76, 77]. A reaction starts in an initial state corresponding to the region around some local minimum on the multidimensional energy surface characterizing the system. An energy barrier separates the reactant state from the rest of configuration space. An example of such configuration presented in the Fig. 2.3. It is useful to introduce the concept of a reaction coordinate X that describes how the system changes during the transition. Usually, it has geometrical interpretation. For example, in the disassociation

of a molecule, the distance between its two parts that are separated in the final state can be taken as the reaction coordinate. Consequently, the energy of the system changes along the reaction coordinate.

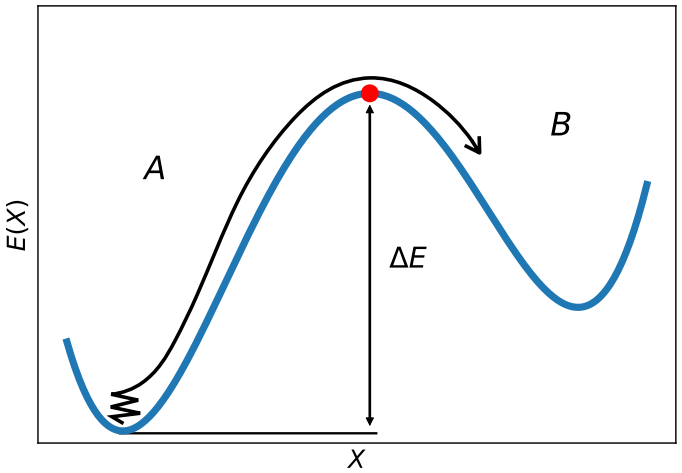

Figure 2.3. Schematic representation of a reaction that starts at the initial state, A, corresponding to the left potential well, and proceeds to the right potential well corresponding to the final state, B. Typically, an energy barrier significantly higher than the thermal energy $\Delta E >> k_B T$ separates these two states. The energy of the system changes as a function of the reaction coordinate, X. Due to the Boltzmann distribution, it is highly unlikely to observe the system near the top of the energy barrier, however thermal fluctuations due to coupling to a heat bath can allow the system to overcome the barrier. Compared with the vibrational periods of the atoms in the initial state, a transition is typically a rare event.

We assume that the system is in contact with a heat bath and it achieves thermal equilibrium. Moreover, the height of the activation energy barrier is assumed to be much higher than the thermal energy, $\Delta E >> k_B T$. As a result the probability to observe the system at particular configuration corresponding to reaction coordinate, X, is given by the Boltzmann distribution $p(X) \sim exp\left(-\frac{E(X)}{k_B T}\right)$. Due to thermal fluctuations, there is a finite probability that the system obtains enough energy to overcome the energy barrier and leave the initial state. In chemical reactions, such a transition corresponds to the breakup of some chemical bonds in reactants and formation of new bonds in the products. Due to the low probability of finding a system there, the narrow region at the barrier is a natural dividing surface between the initial and final states. This region is referred to as the transition state [78].

This type of analysis of chemical reactions has developed into a more general theory of thermally induced transitions. For the simplest case of two potential wells, the transition rate is related to the probability of finding the system near the transition state. The key assumption in transition state theory (TST) that the transition state is only crossed once. That is, if the system overcomes the energy barrier and is heading

away from the initial state there, it is assumed that it will end up in the final state. Re-crossings of the transition state are neglected. In general, TST is able to describe accurately experimental data on the dependence of transition rates on temperature. The pre-exponential factor ν in the Arrhenius law 36 is connected to the vibrational frequency of the atoms in the initial state and within the transition state dividing surface [79, 80]. Later, Kramers presented work [81] where an expression for the transition rate is given that takes recrossings into account based on Brownian dynamics. The effect of recrossings always decreases the TST estimate of the transition rate.

TST can easily be applied to multidimensional systems. A system of N atoms has dimensionality $D = 3N$ and the transition state dividing surface is then a subspace with $D-1$ degrees of freedom. The dividing surface should be placed in configuration space where the probability of finding the system is lowest while all trajectories going from the initial state to the final state must cross it. Based on Kramers formulation, the first attempts to calculate a rate coefficient for a multidimensional system were those of Brinkman in 1956 [82] and Landauer and Swanson in 1961 [83]. However, a more general approach was developed by Langer [84]. The rate constant was related to the stationary flux through the dividing surface. To calculate it for a general multidimensional system, Langer used linearized Fokker-Plank equation.

However, the TST approach applies to any thermally induced process where the configuration of the system is changing from one stable state to another. It was applied to study the diffusion [85], liquid crystal relaxation [86] as well as for first-order phase transition [87, 88]. Moreover, thermally activated magnetic transitions can also be described within TST. First work in this direction was done by Néel [89] and Brown [90] on monodomain magnetic particles. Later Langer's method was applied to an arbitrary Hamiltonian by Klik and Gunther [91, 92]. It is important to note that the Kramers/Langer approach relies on the assumption of Brownian movement. This approximation has proven to be inaccurate in some cases, see for example [93]. An alternative approach can be adopted to overcome these limitations. First one should obtain a transition rate within TST, i.e., by neglecting recrossings. Then, as a second step, this approximation is revised by calculating short time dynamical trajectories starting from various positions within the transition state [94]. By counting multiple recrossings in these short trajectories, a dynamical correction to the TST rate estimate can be calculated. Consequently, the TST is merely an intermediate approximation in this two-step approach. Such an approach has been formulated for multidimensional magnetic systems. First work on this topic was introduced by Bessarab et al. [95] who developed a harmonic approximation to TST for magnetic states. An expression of the transition rate constant for a general magnetic Hamiltonian was presented based on Landau-Lifshitz equations of motion. This approach has been applied to a variety of magnetic systems, such as magnetic skyrmion annihilation in CoPt(111) films [96], skyrmion lifetime in narrow magnetic tracks [97] and the effect of impurities on skyrmion lifetime [98], kagome spin ice element made of large permalloy islands [99], remagnetization of Fe islands on a W(110) surface [100], hysteresis loops of spring magnets [101] and magnetization reversal in a small Fe cluster at a tip interacting with an antiferromagnetic surface [102]. The method can be applied to systems where the energy obtained from iterative self-consistent calculations [103, 104].

HTST is used here to derive an expression for remagnetization transitions in a single

domain magnetic island supported on a solid surface as seen in Fig. 2.4 with both easy-axis anisotropy and easy-plane anisotropy. In the presence of an external magnetic

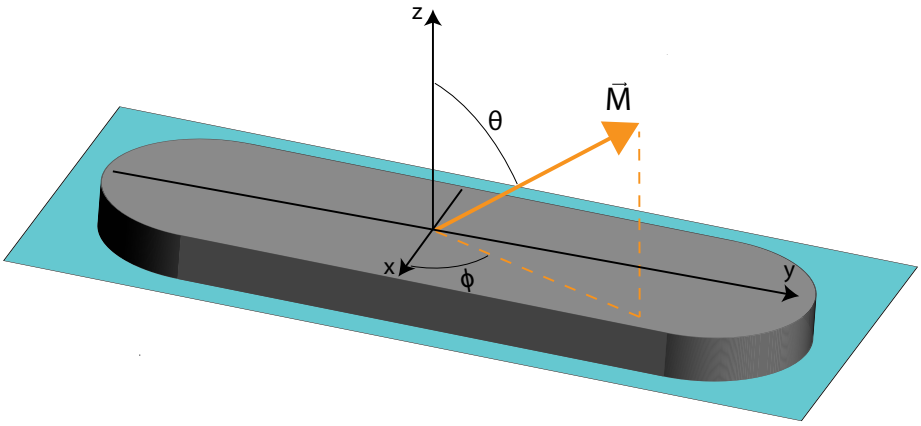

Figure 2.4. Schematic representation of the single domain particle that is supported on a solid surface. Magnetisation vector $\vec{M}$ is defined by two polar angles θ and ϕ. Anisotropy easy-axis is aligned with the y-axis. Easy plane anisotropy axis is aligned with the Z-axis.

field, the total energy also contains a Zeeman energy term

$$E_{total}/V = E_{anis}/V + E_Z/V = -K_1 \sin^2\theta \sin^2\phi + K_2 \cos^2\theta - \left(\vec{H}\cdot\vec{M}\right) \tag{37}$$

where K_1 and K_2 are anisotropy constants and $\vec{H}$ is the external magnetic field vector, with orientation defined by spherical polar angles ϕ_H and θ_H.

It is convenient to express the energy density in a dimensionless form

$$\eta = \frac{E}{2VK_1} = -\frac{\sin^2\theta\sin^2\phi}{2} + \frac{c\cos^2\theta}{2} - h\left(\sin\theta\sin\theta_H\cos(\phi-\phi_H) + \cos\theta\cos\theta_H\right) \tag{38}$$

where $h = \frac{HM}{2K_1}$ and $c = K_2/K_1$ are dimensionless parameters.

A search for extrema of Eq. 38 yields minimum condition for the θ coordinate as $\theta = \theta_H = \pi/2$, while for the ϕ coordinate the equation

$$\frac{\partial\eta}{\partial\phi} = h\sin(\phi-\phi_H) - \sin\phi\cos\phi = 0|_{\theta=\theta_H=\frac{\pi}{2}} \tag{39}$$

needs to be solved. By making the substitution $h\sin\phi_H = h_{||}$ and $h\cos\theta_H = h_\perp$, this can be rewritten as

$$\frac{\partial\eta}{\partial\phi} = h_\perp\sin\phi - h_{||}\cos\phi - \sin\phi\cos\phi = 0|_{\theta=\theta_H=\frac{\pi}{2}}. \tag{40}$$

For the given condition $\theta = \theta_H = \frac{\pi}{2}$, there are two important cases where an analytical solution for the extrema can be obtained, namely

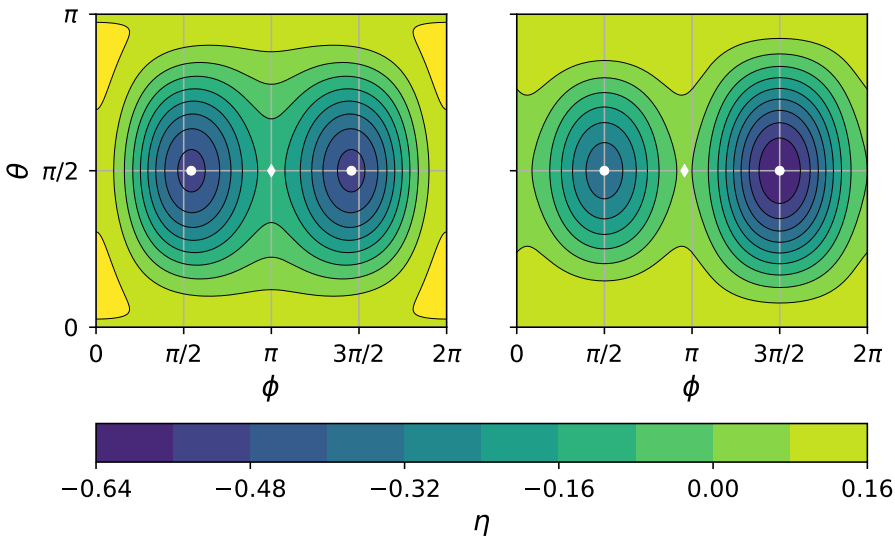

Figure 2.5. Energy surface of the magnetic island illustrated in Fig. 2.4. On the left, the external field is applied perpendicular to the anisotropy easy-axis. On the right, the field is parallel to it. The local minima and first-order saddle points are marked with white dots and diamonds respectively. The parameter values used in the calculations are $c = 0.3$ *and* $h = 0.13$.

- Parallel case, when $h_\perp = 0$
- Perpendicular case, when $h_{||} = 0$.

For an arbitrary orientation of the external field, it is more convenient to use minimization and saddle point search (such as NEB [105, 106] or GNEB [107]) algorithms rather than a search for an analytical solution.

Table 2.1. Extremum and lowest energy barriers for parallel and perpendicular cases

	Perpendicular	**Parallel**
local minimum ϕ	$\pi \pm \arccos(h)$	$\pi \pm \pi/2$
saddle point ϕ	π	$\pi + \arcsin(-h)$
minimum and saddle θ	$\pi/2$	$\pi/2$
lowest ΔE	$K_1 V(1-h)^2$	$K_1 V(1-h)^2$

As seen from the table 2.1, the condition $|h| < 1$ needs to be satisfied in order for two stable states to exist. When this condition is not satisfied, the energy landscape has only one global minimum, and no transitions can take place.

2.3 Rates of the magnetic transitions

Within TST the rate of transitions can be estimated as the probability of reaching the narrow region of the transition state near a first-order saddle point on the energy surface multiplied by the flux out of the transition state. We assume that the system is in thermal equilibrium and that the energy is Boltzmann distributed in all degrees of freedom. Then, if the energy is defined as $E(\theta,\phi)$, the probability that (θ,ϕ) is in the range$\{\theta,\theta+d\theta\}$ and $\{\phi,\phi+d\phi\}$ is

$$P(\theta,\phi)d\phi d\theta = C\exp\left(-\frac{E(\theta,\phi)}{k_BT}\right)d\phi d\theta \tag{41}$$

where C is a normalization factor.

One can obtain C by assuming that the system is in the A state, meaning that the probability of finding it there is equal to one, $P(\theta,\phi)=1$

$$P(\theta,\phi)=1=\int_A \exp\left(-\frac{E(\theta,\phi)}{k_BT}\right)C\sin\theta d\phi d\theta = \\ = C\int_A \exp\left(-\frac{E(\theta,\phi)}{k_BT}\right)\sin\theta d\phi d\theta. \tag{42}$$

Therefore,

$$C=\left(\int_A \exp(-\frac{E(\theta,\phi)}{k_BT})\sin\theta d\phi d\theta\right)^{-1}. \tag{43}$$

The flux out of the transition state is the projection of the velocity vector, $\vec{V}$, onto the local normal of the dividing surface (that points to the final state B). This is referred to as the perpendicular velocity component $\vec{V}_\perp$

$$V_\perp = \frac{\nabla\vec{F}}{\|\nabla\vec{F}\|}\cdot\vec{V}. \tag{44}$$

Thus the TST estimate of the rate constant becomes

$$k^{TST}=\frac{\iint_{TS} e^{E/k_BT}V_\perp\sin\theta d\theta\phi}{\iint_A e^{E/k_BT}\sin\theta d\theta\phi}. \tag{45}$$

One approach to calculate the Eq. 45 is to use the harmonic approximation. A quadratic approximation of the energy E in terms of the spherical polar angles θ and ϕ is calculated near minimum corresponding to the initial state, A, and near the first order saddle point, S. The energy surface is approximated in the vicinity of these two points as a Taylor series up to and including the quadratic term.

$$E^c(\theta,\phi)=E(\theta_c,\phi_c)+[(\theta-\theta_c)g_1^c+(\phi-\phi_c)g_2^c] \\ +\frac{1}{2}\left[(\theta-\theta_c)^2\chi_{1,1}^c+2(\theta-\theta_c)(\phi-\phi_c)\chi_{1,2}^c+(\phi-\phi_c)^2\chi_{2,2}^c\right] \tag{46}$$

where $c=s$ corresponds to the expansion near the saddle point and $c=m$ corresponds to the expansion near the minimum. g_i^c is the element of the gradient at the critical point

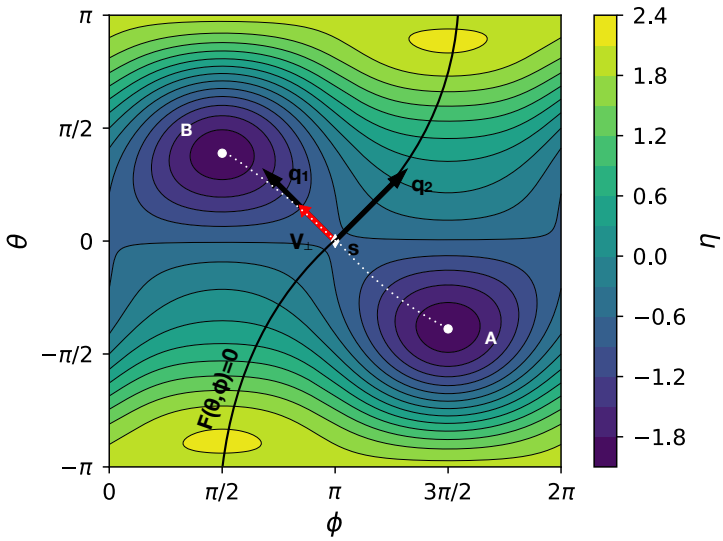

Figure 2.6. There are two local minima, A and B, on the energy surface corresponding to stable magnetic states. The dividing surface which separates these states can be represented as a continuous curve. An MEP between stable states can be found using the geodesic nudged elastic band method. The exact position of the saddle point, marked as s, can be determined using the climbing image algorithm. The velocity component along the MEP near the saddle point, which is perpendicular to the surface is shown as a red arrow starting at the saddle point. Parameters are $b = 1.3$ $h = 1.8$ $\phi_H = \pi/2$ $\theta_H = \pi/4$.

c and χ^c_{ij} is the matrix element of the Hessian at the critical point c. Taking into account that the gradient at the critical point is equal to zero

$$E^c(\theta,\phi) = E(\theta_c,\phi_c) + \frac{1}{2}\left[\chi^c_{1,1}(\theta-\theta_c)^2 + 2\chi^c_{1,2}(\theta-\theta_c)(\phi-\phi_c) + \chi^c_{2,2}(\phi-\phi_c)^2\right]. \quad (47)$$

To eliminate mixed terms in the quadratic approximation, it is convenient to define a new coordinate system in terms of the eigenvectors of the Hessian matrix, i.e., the vibrational normal coordinates q^c_1 and q^c_2

$$E^c(q^c_1,q^c_2) = E(\theta_c,\phi_c) + \frac{1}{2}\left[\lambda_{c,1}(q^c_1)^2 + \lambda_{c,2}(q^c_2)^2\right] \quad (48)$$

where, $\lambda_{c,1}$ and $\lambda_{c,2}$ are the eigenvalues of the Hessian matrix at the saddle point or initial state minimum. The dividing surface is chosen to be a hyperplane going through the first order saddle point, with a normal pointing along the MEP. The velocity is given by the Landau-Lifshitz equation, which can be written in terms of the normal

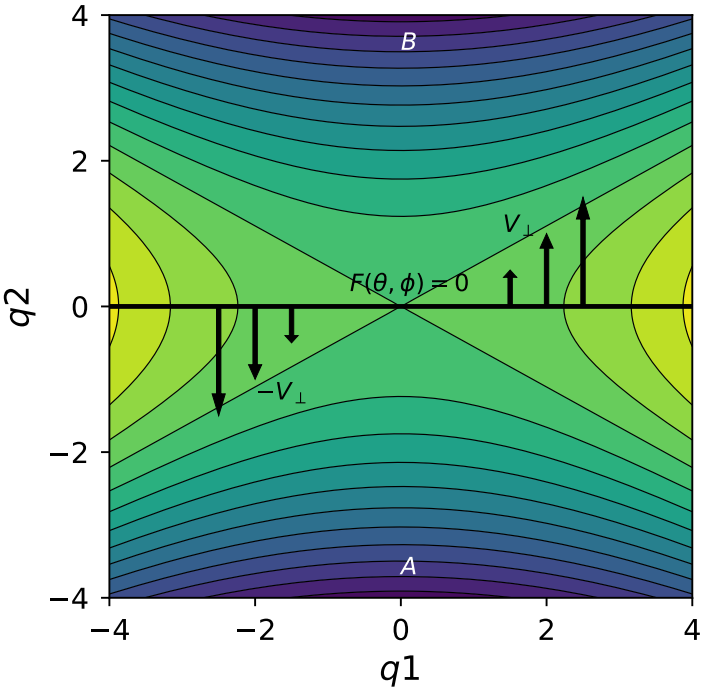

Figure 2.7. A region near the first order saddle point s on an energy surface illustrated in Fig. 2.6. The dividing surface, $F(\theta,\phi)=0$, is shown as a thick black line. It includes the first order saddle point and has a normal pointing along the unstable mode. At the saddle point, the velocity is zero in accordance with the Landau-Lifshitz equation of motion. However, in one half of the hyperplane, the velocity towards the final state B increases the farther one goes away from the saddle point. Since the HTST transition rate includes integration over the dividing surface, a non-zero rate is obtained.

coordinates in the proximity of the first order saddle point

$$\dot{q}_1^s = \frac{\gamma\lambda_{s,2}}{VM_s\sin\theta_s}q_2^s \tag{49}$$

$$\dot{q}_2^s = -\frac{\gamma\lambda_{s,1}}{VM_s\sin\theta_s}q_1^s. \tag{50}$$

If $\lambda_{s,1}<0$ and $\lambda_{s,2}>0$ at the saddle point, then $V_\perp=\dot{q}_1^s\sin\theta_s$. Otherwise, if $\lambda_{s,1}>0$ and $\lambda_{s,2}<0$, then $V_\perp=\dot{q}_2^s\sin\theta_s$. An integral is carried out over Eq. 45 for regions where $V_\perp>0$, or in other words for transitions that go from the initial state A to the final state B. Notably, in accordance with the equation of motion, the velocity is equal to zero at the saddle point, but non-zero contributions to the flux are obtained from one half of the hyperplanar dividing surface. The integration yields

$$k^{HTST} = \frac{\gamma\sqrt{\lambda_{s,1}\lambda_{s,2}}}{2\pi M_s V\sin\theta_m}e^{-\Delta E/k_BT}. \tag{51}$$

It turns out that the pre-exponential factor does not depend on the Hessian at the saddle point. This happens because in this simple case $V_\perp$ proves to be proportional to the one positive eigenvalue of Hessian at the saddle point. The same eigenvalue also appears in the denominator and cancels out, so only Hessian eigenvalues at the initial minimum remain. The pre-exponential factor is also independent of the volume, V, of the system, because the eigenvalues of the Hessian are proportional to it they are presented both in the denominator and the nominator, so the volume cancels out in the expression for the rate constant.

For an external magnetic field $\vec{H}$ orientated perpendicular or parallel to the easy-axis of the island, an analytical expression for the energy barrier as well as locations of the minima and saddle points can be obtained (see table 3.3). This leads to analytical Hessian matrices at the minimum, and thus one can obtain analytical expressions of the k^{HTST} for these two particular cases. When the field is aligned with the anisotropy axis, the expression for the transition rate within harmonic approximation is

$$k_\perp^{HTST} = f_{0\perp} e^{-\Delta E/k_B T} = \frac{\gamma K_1 \sqrt{(1-h)(2c+1-h)}}{\pi M_s} \exp\left[-\frac{K_1 V}{k_B T}(1-h)^2\right]. \quad (52)$$

When the field is parallel to the anisotropy axis, the expression is

$$k_\parallel^{HTST} = f_{0\parallel} e^{-\Delta E/k_B T} = \frac{\gamma K_1 \sqrt{(1-h^2)(2c+1)}}{\pi M_s} \exp\left[-\frac{K_1 V}{k_B T}(1-h)^2\right]. \quad (53)$$

When a magnetic field is absent, both expression yield the same transition rate, which allows us to see how the pre-exponential factor depends on the anisotropy parameters K_1 and K_2, as shown in the Fig. 2.8. A decrease of the anisotropy parameter K_1 leads to a decrease of the pre-exponential factor but at the same time reduces the activation barrier. These results show that a value of 10^9 Hz, as was assumed in refs. [73, 108], is a reasonable approximation.

2.4 Temperature induced switching field distribution (SFD)

The theory of magnetization reversals developed in the previous section can be used to interpret measurements of the hysteresis of small magnetic islands as a function of temperature. As was shown above, a single domain particle can have two stable states separated by an energy barrier ΔE. In order to overcome this barrier at zero temperature, one needs to apply a so-called switching field or saturation field, that can be written as $H_{SW}^0 = 2K_{eff}/M_s$ for the case when the $\vec{H}$ is aligned with the anisotropy easy-axis. However, at finite temperature, there is a chance that the system jumps between the energy minima before the H value becomes equal to the switching field H_{SW}^0 due to the thermal fluctuations. The process can be described with Poisson process statistics, where the probability that the system has switched to the other stable state increases with time as

$$P_{sw}(\tau) = 1 - e^{-\tau/k}. \quad (54)$$

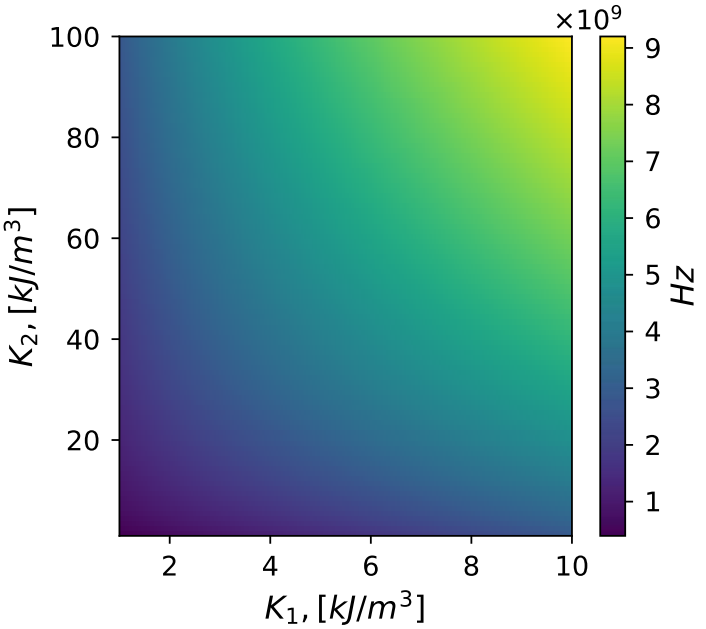

Figure 2.8. The dependence of the pre-exponential factor on the parameters, K_1 and K_2, for magnetization reversals of a single domain magnetic island when an external magnetic field is not presented, $H = 0$. The saturation magnetization is $M_s = 200\ kA/m$.

Here, k is the transition rate for the magnetization reversal process on the Arrhenius law defined by Eq. 36 and τ is the time until a switch occurs. When a hysteresis loop is measured, the field is slowly ramped up from negative saturation field value in small steps of ΔH and the reversal of magnetization monitor after each step for a waiting time $\Delta\tau$, small enough to avoid double magnetization reversals. The probability that a switch of the magnetization has occurred within the waiting time equals to the probability that system has not switched already multiplied by the probability that a switch occurs at the given time interval. In a typical experiment, the magnetic field depends linearly on time, $R = \Delta H/\Delta t = const$. In this case, the probability density of magnetization switching at a field value H can be calculated as [73, 108]

$$p_{sw}(H) = \frac{f_0(H)}{R}\exp\left(-\frac{\Delta E(H)}{k_B T}\right) \times \exp\left[-\frac{1}{R}\int_{-H_{sat}}^{H'} f_0(H')\exp\left(-\frac{\Delta E(H')}{k_B T}\right)dH'\right]. \quad (55)$$

The value $p_{sw}(H)dH$ gives the probability that the magnetization will switch when the field is in the interval [H, H+dH], given that it has not happened at a smaller field. Expression 55 is the temperature-induced SFD.

2.5 Nucleation Volume

An investigation of the stability and temperature dependence of the switching field of a sub-micron magnetic island with perpendicular magnetic anisotropy has been carried out by J. de Vries et al. [73] based on anomalous Hall effect. They measured the magnetization reversal of individual CoPt island of diameter 220 nm. The results can be seen in the Fig. 2.9.

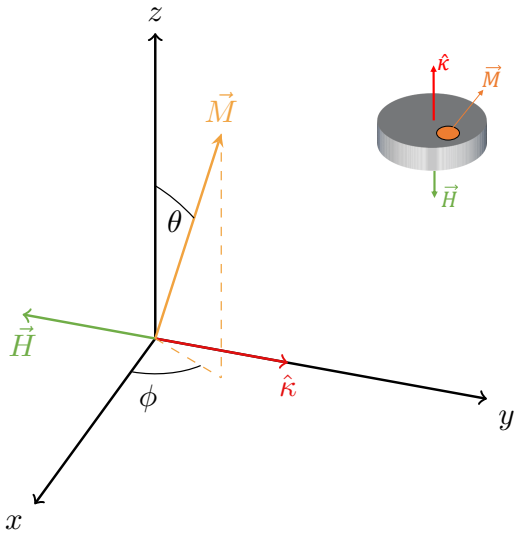

Figure 2.9. Schematic illustration of the magnetic islands measured by de Vries et al. and the coordinate system used in the calculations. The inset shows the assumed shape of the magnetic dot and the orientation of the anisotropy easy-axis as well as nucleation region. The external magnetic field, $\vec{H}$, is aligned with the y-axis, perpendicular to the plane of the island. $\vec{M}$ is the total magnetic moment of the nucleation region with directions specified by angles θ and ϕ. $\hat{\kappa}$ is aligned with the easy-axis.

Table 2.2. Parameters used in the SW calculations of de Vries et al. [73].

	Value
Magnetization, M_s	829 kA/m
Ramp at 10 K, R_{10}	39 A/ms
Ramp at 300 K, R_{300}	3.9 A/ms

In the context of high-density data storage devices, a narrow distribution of the switching field is desired. Patterned systems made from thin multilayers have, however, been shown to have broad SFDs. This broadening had been attributed to several sources, including lithographic variations [109], particle orientation and/or boundary variations [110]. However, it was later shown that the reason for the broad SFDs is due

to variations in the material properties of the multilayers [111, 72]. In the analysis of their measurements, de Vries et al. [73] attempted to use the SW model to describe the experimental observations. There, a magnetic island (Fig. 2.9) was treated as a single domain magnetic particle with uniaxial anisotropy and parameters from table 2.2 used in the evaluation of Eq. 55. However, the result of the calculations was a tenfold overestimate of H_{sw} and the SW model was deemed inapplicable for this system.

On the other hand, it can be assumed that the magnetic switching begins by nucleation of a small volume, V_{nuc}, followed by rapid domain wall propagation [109, 111]. Then, the SW model extended to finite temperature can be used to estimate the nucleation volume. In the experiment of de Vries et al., the SFD for each magnetic island has a well-defined peak that varies with temperature. As a result, they categorize their system to have two types of extreme islands, "weak" and "strong" with respect for the H_{sw} that is needed to induce the magnetization reversal. The values of the parameters K_1 and V_{nuc} in Eq. 55 were adjusted to reproduce the experimental peak positions of the SFDs shown in shown in Fig. 2.10. As can be seen in the figure, the width of the SFDs are then also accurately reproduced by the calculations. The same values of the parameters were used for the two different values of the temperature.

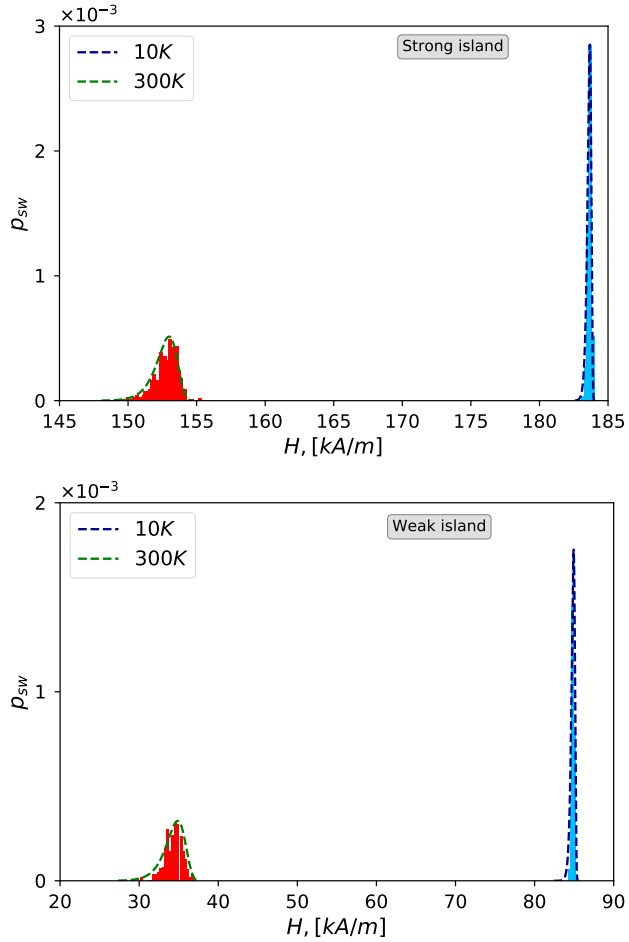

Figure 2.10. The switching field distribution for weak and strong islands obtained from the experiment of de Vries et al. [73] and from numerical calculations using the extended SW model. Histograms represent the measured switching field in over 150 reversals of a weak and a strong island measured at 10 K (blue) and 300 K (red). Dashed lines represent the corresponding numerical calculations.

3 Magnetisation reversal in elements of artificial spin ice

3.1 Introduction

Artificial spin ice is a frustrated system consisting of magnetic islands, typically of submicrometer size. In general, the islands are chosen to be small enough so the switching behavior can be described by a single domain particle model while being large enough to suppress rapid thermal fluctuations. The distance between the islands is large enough, so they only interact by magnetostatics. The strength of the dipolar-coupling can be tuned by varying the distance between the islands. This makes it possible to control how the system responds to an applied magnetic field and temperature.

The term "artificial spin ice" has its origin in the discovery of inability of the rare earth material $Ho_2Ti_2O_7$ to satisfy all its interactions simultaneously due to the geometry, i.e., geometric frustration [112]. This leads to non-zero entropy at zero temperature and to a high degeneracy of low energy states. There is a close correspondence to the well known residual entropy in water ice. The $Ho_2Ti_2O_7$ material has magnetic spins in a lattice of tetrahedra with anisotropy along the (111) direction. The spins point either towards or away from the center of the tetrahedron. If we consider corners between multiple tetrahedra, the rule for lowest energy configuration will be defined as two in/one out or vice versa. Extensive studies have been made of such materials [112, 113, 114, 115]. However, even with modern experimental methods, the orientation of each spin is not easy to detect.

In 2006 Schiffer came up with an approach to re-create the behavior of spin ice crystal with a two-dimensional arrangements of magnetic islands coupled by dipolar interaction, or artificial spin ice [116]. The advantage of this approach is that one can define an arbitrary geometry of the system, i.e., not only on lattices that are presented in nature but also in various exotic geometries. Moreover, magnetic elements in such systems are relatively easy to measure and observe under various external conditions [117, 118, 119].

Artificial spin ice systems make it possible to study various new physical phenomena such as magnetic monopoles [120, 121], temperature induced disordering or melting [122], new kinds of thermodynamic phase transitions [123] and screening chargers effects [124]. Artificial spin ice systems consisting of a large number of islands are referred to as extended systems. While theoretical work on transitions between magnetic states in such arrangments of magnetic islands can be made by direct dynamic simulations based on LLG equation or Monte Carlo simulations, there are limits to those approaches. For the direct simulation, it is the short timescale that can be simulated,

due to the fast vibrational motion of the magnetic moments around the equilibrium orientation. The time evolution of such systems involves overcoming energy barriers that are typically prohibitively large on the short timescale that can be represented in direct LLG dynamics simulations. On the other hand, Monte Carlo simulations are purely statistical and give thermally averaged quantities with no information about the time of the transitions. Moreover, the Monte Carlo simulations have so far mainly been based on simplified Hamiltonians without direct connection to the microscopic degrees of freedom. The kinetic Monte Carlo (KMC) method can, however, be used to simulate the long time scale evolution. However, as a prerequisite for a KMC simulation, it is good to study first the building blocks of artificial spin ice lattices.

3.2 Interaction between islands in artificial spin ice

The interaction between the islands affects the properties of artificial spin ice systems, and several different ways have been used to model it. The most accurate approach, but also the one that requires largest computational effort, is micromagnetics. A simpler approach is to place a magnetic dipole at the center of each island and evaluate the dipole-dipole interaction. Then the energy can then be written as

$$E_{ij}^{dipole} = -V_i V_j \left(\frac{\left(\vec{M}_i \cdot \vec{M}_j\right)}{\left\|\vec{r}_{ij}\right\|^3} - \frac{\left(\vec{M}_i \cdot \vec{r}_{ji}\right)\left(\vec{M}_j \cdot \vec{r}_{ij}\right)}{\left\|\vec{r}_{ij}\right\|^5} \right). \tag{56}$$

Where the vector r_{ij} is pointing between the centers of islands i and j and $\vec{M}_i$ is the magnetization vector of the i-th island.

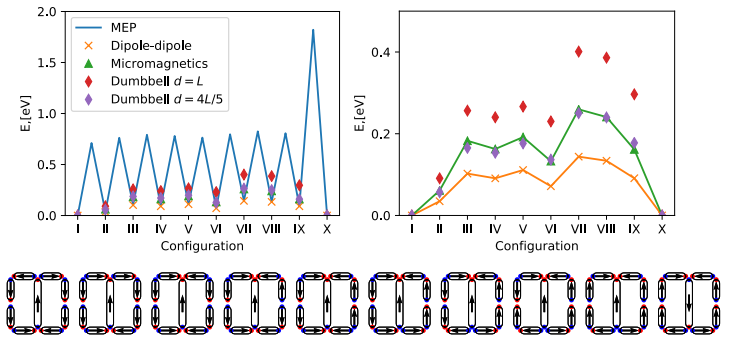

Figure 3.11. Minimum energy path (MEP) for magnetization reversal of shakti lattice element and the energy of the minima along the path calculated using various models for the interaction between islands. Configurations at the minima are shown below the graphs. The length, L, of the smaller islands is 450 nm while it is 1050 nm for the big island.

In the third approach, the dumbbell approximation [125, 126, 124], two magnetic

charges of the same magnitude $|q|$ are placed on each island separated by a distance, d.

$$E_{ij}^{dumbell} = \frac{q_i q_j}{d_i d_j}\left[\frac{1}{\left|r_{a_i} - r_{a_j}\right|} - \frac{1}{\left|r_{a_i} - r_{b_j}\right|} - \frac{1}{\left|r_{b_i} - r_{a_j}\right|} + \frac{1}{\left|r_{b_i} - r_{b_j}\right|}\right] \tag{57}$$

where r_{a_i} and r_{b_i} correspond to locations of the positive and negative charges on the i-th magnetic island. The magnitude of the magnetic charge, q_i, is chosen so as to give the right magnetic moment for the island, $M_{s_i}V_i$. The distance between charges on the i-th island is d_i. Fig.3.11 shows calculated results using the various approaches with parameter values listed in table 3.4. Micromagnetic calculations were performed with mumax3 software [127]. Dumbell calculations include two different choices for d_i, namely $d_i = 4L_i/5$ and $d = L_i$, where L_i is the length of the islands, 450 nm for small islands and 1050 nm for the big island. The volume and magnetization are given in 3.4. In each case, the magnetic dipole is the same, consistent with the saturation magnetization of material times the volume of the islands. The different choices of d affect the calculated energy of the various states of the system. Our results show that by adjusting d to a smaller value than the length of the island, about 2/3, the dumbbell model can accurately reproduce the micromagnetic calculations.

3.3 One and two ring element of kagome lattice

Studies of the building block of a lattice can help understand the behavior of the extended system. The mechanism of the elementary transitions and rate can be calculated for the element and the information then used in larger scale KMC simulations. While it is possible to simply fit these parameters, it is better to apply HTST and obtain values consistent with the energy surface. Also, experimental measurements of temperature induced magnetic switching have been made and give information about the rates [117, 128]. The latter one reports how the lifetime of the ground state of one, two and tree rings of kagome spin ice lattice ranges from seconds to days depending on temperature.

A hexagonal element of Kagome spin ice consists of six prolate islands. The geometry of each island is described illustrated in Fig. 3.12. Parameters that were used in the present calculations are shown in the Table 3.3. The magnetization is within the range of estimates given by the experimental data. The shape is taken to correspond to the experimental measurements. Anisotropy parameters were calculated by the micromagnetic simulation, by using only experimentally determined parameters characterizing the material and the shape of the islands.

Using the geometry that is defined in Fig. 3.12 and the dipole-dipole interaction 56, the energy of an island corresponds to Eq. 37 and the total energy of the kagome system

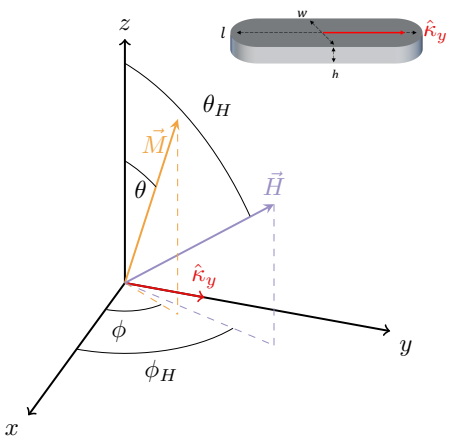

Figure 3.12. Representation of the geometry of the magnetic islands used in simulations of elements of kagome spin ice in the presence of an external magnetic field. The direction of the magnetization and the external magnetic field is defined by the vectors $\vec{M}$ (specified by polar angles ϕ and θ) and $\vec{H}$ (specified by polar angles ϕ_H and θ_H). The inset shows the assumed shape of the island, such as height h, width w and length l and the orientation of the anisotropy axis.

Table 3.3. Parameter values used in the present calculations and in the calculations of ref [128]

Parameter	**Present calc.**	**ref. [128]**
Magnetisation, A/m·10^5	2.00	2.00
$l \times w \times h$, cm·10^{-7}	$470 \times 170 \times 3.2$	$470 \times 170 \times 3$
Volume, cm^3 ·10^{-16}	2.36	
Anisotropy, Jm^{-3}	538	618

with N islands is

$$E/V = -\sum_i^N K_1(\hat{m}_i \cdot \hat{\kappa}_i)^2 - \sum_i^N (\vec{M}_i \cdot \vec{H}) - \frac{V}{2}\sum_{i\neq j}^N \left(\frac{\left(\vec{M}_i \cdot \vec{M}_j\right)}{\left\|\vec{r}_{ij}\right\|^3} - \frac{\left(\vec{M}_i \cdot \vec{r}_{ji}\right)\left(\vec{M}_j \cdot \vec{r}_{ij}\right)}{\left\|\vec{r}_{ij}\right\|^5} \right). \quad (58)$$

Where the vector r_{ij} is pointing between the centers of islands i and j and $\hat{m}_i = \vec{M}/\|\vec{M}\|$. This energy expression defines an energy surface as a function of the orientation of the magnetic moments of the islands in the system. A state is defined as a local minimum on this energy surface and is found by setting up a rough approximation of the orientations of the magnetic moments and then minimizing the energy with respect to the orientation

of all the magnetic moments. Two equivalent ground states exist when the external magnetic field is absent, as shown in Fig. 3.13.

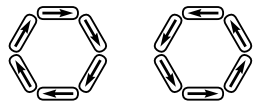

Figure 3.13. Ground states of a kagome hexamer ring in the absence of an external field.

Minimum energy paths for magnetic reversals were calculated to estimate energy barriers for the various elementary steps, see Fig. 3.13. The calculations of MEPs were carried out using the geodesic nudged elastic band (GNEB) method [107]. The presence of an external magnetic field is found to strongly affect the energy landscape of the system as shown in Fig. 3.15. Even a field of 4mT can eliminate states that correspond to ground states in the absence of a field.

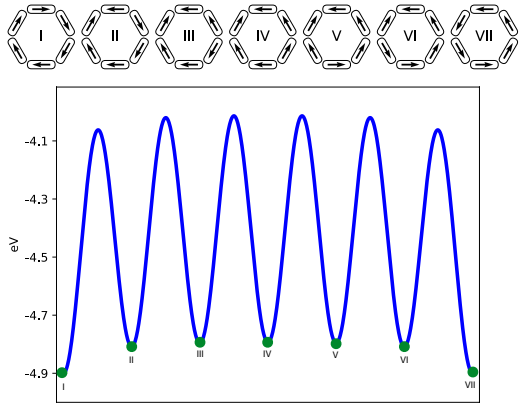

Figure 3.14. MEP between the two ground states for a hexamer ring element of the kagome lattice in the absence of a magnetic field. The curves show the energy along the minimum energy path between the local minima. The array of system configurations on top show the direction of the magnetic moments at minimum energy configurations along the path.

The rate of each elementary transition between metastable states j and k is calculated using HTST and the multidimensional Hamiltonian [95, 107]

$$W_{jk}^{HTST} = \frac{1}{2\pi}\frac{J_s}{J_m}\sqrt{\sum_{i=2}^{D}\frac{a_i^2}{\varepsilon_{s,i}}}\frac{\prod_{i=1}^{D}\sqrt{\varepsilon_{j,i}}}{\prod_{i=2}^{D}\sqrt{\varepsilon_{s,i}}}e^{-(E_s-E_j)/k_BT} \tag{59}$$

where s denotes to the saddle point between metastable states j and k. J is Jacobian, ε corresponds to eigenvalues of the Hessian matrix, a for coefficients in the expansion

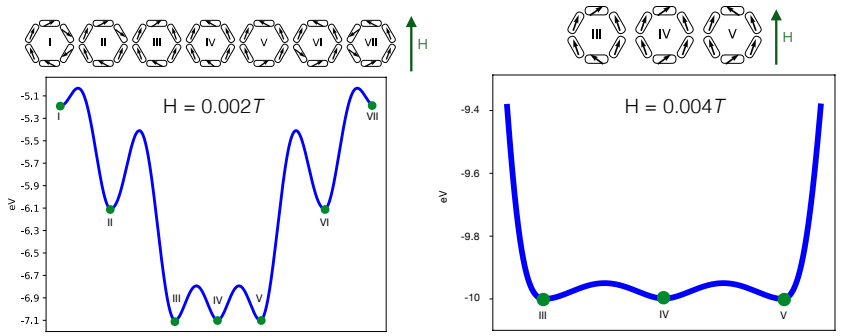

Figure 3.15. Two MEPs for a hexamer ring element of the kagome lattice in a magnetic field of 2 mT on the left and 4 mT on the right. The curves show the energy along the minimum energy paths between the local energy minima. The array of system configurations on top show the direction of the magnetic moments at minimum energy configurations along the path.

of the velocity at the saddle point in terms of the eigenvectors of the Hessian, and the energy. The sum of eigenvalues at the saddle point excludes the negative eigenvalue corresponding to the unstable mode, i.e., the mode for which the energy is maximal at the saddle point.

Because of the geometric symmetry, the kagome hexamer ring has more than one MEP depending on the direction of the rotation of te magnetic vectors. When an external magnetic field is introduced the symmetry is broken, and a lower number of equivalent paths are present as shown in Fig. 3.16.

The overall transition rate between equivalent ground states can be calculated by using the stationary state approximation including all possible transition paths. A set of master equations combine the rate of the various elementary steps. This is a set of differential equations for the time derivative of the probabilities, n_i, of finding the system at each of the various degenerate states i. In our case, n_i is a particular energy level, and W_{jk} is the rate constant for transitions between states belonging to n_j and n_k. In order to obtain the lifetime of the initial state, $\frac{dn_1}{dt}/n_1$ needs to be determined. By taking into account all possible paths for the case of the hexamer kagome ring in the absence of the external field, the master equation is (roman numerals are used in Fig. 3.16):

$$\frac{dn_1}{dt} = -12W_{12}n_1 + 12W_{21}n_2 \tag{60}$$

$$\frac{dn_i}{dt} = -\left(2W_{ii+1} + 2W_{ii-1}\right)n_i + 2W_{i-1\,i}n_{i-1} + 2W_{i+1\,i}n_{i+1} \tag{61}$$

$$\frac{dn_6}{dt} = -(2W_{67}n_n + 2W_{65})n_6 + 2W_{56}n_5 \tag{62}$$

In order to obtain the lifetime of the system, we need to make the assumption that n_7 is the final state and when the system goes there it does not return for an extended

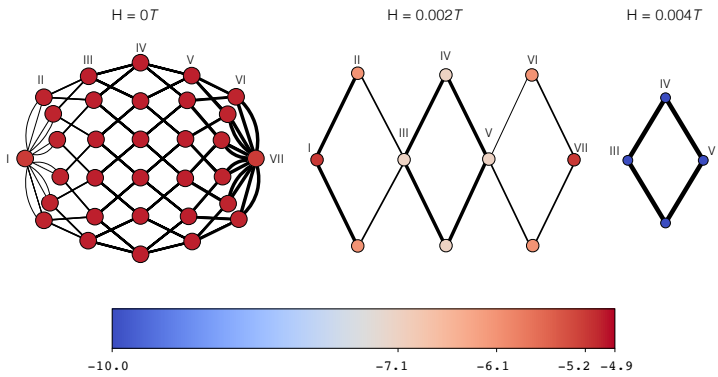

Figure 3.16. Schematic diagrams showing the local energy minima, color-coded according to their energy and connected with lines where the thickness indicates the magnitude of the rate of the elementary transition. From left to right: no field, 0.002 T and 0.004 T field. When the external field is not present, transitions between states I and II as well as between states VI and VII, have the same rate for clockwise and anticlockwise rotations, but for transitions between the other pairs of states, either clockwise or anticlockwise rotation is the favored mechanism.

period of time. Furthermore, we apply the steady-state approximation, namely $\frac{dn_i}{dt}$ is assumed to be zero for all intermediate states, i.e., that the probability of intermediate states does not change with time. Then, the set of master equations for intermediate states becomes

$$\frac{dn_i}{dt} = -2\left(W_{ii+1} + W_{ii-1}\right)n_i + 2(W_{i-1i}n_{i-1} + W_{i+1i}n_{i+1}) = 0 \tag{63}$$

$$\frac{dn_6}{dt} = -(2W_{67}n_n + 2W_{65})n_6 + 2W_{56}n_5 = 0 \tag{64}$$

The rate of decrease in the probability of the initial state can then be written as $\frac{dn_1}{dt} = -n_1 \times G$, where G is a combination of W_{ij}. More precisely $G = A/C$, where

$$A = 12W_{12}W_{23}W_{34}W_{45}W_{56}W_{67} \tag{65}$$

$$\begin{aligned} C = {} & W_{21}W_{32}W_{43}W_{54}W_{65} + W_{21}W_{32}W_{43}W_{54}W_{67} \\ & + W_{21}W_{32}W_{43}W_{56}W_{67} + W_{21}W_{32}W_{45}W_{56}W_{67} \\ & + W_{21}W_{34}W_{45}W_{56}W_{67} + W_{23}W_{34}W_{45}W_{56}W_{67}. \end{aligned} \tag{66}$$

Therefore, the overall rate constant for transition between the two ground states is expressed as $k_{tot} = \frac{1}{n_1}\frac{dn_1}{dt}$. The lifetime is the inverse of the rate constant, $t = 1/k_{tot}$.

By using parameters characterizing the system measured by Farhan *et al.* [128], a lifetime of $t = 14$ s is obtained at 420 K. This is in excellent agreement with the experimental measurements showing a lifetime of 11 seconds at 420 K [128]. At 320K, the lifetime is much longer, calculated to be several days. Variation in the thickness of the islands has a strong effect on the lifetime of the ground states of the hexamer,

as observed by Farhan *et al.*. If the island thickness is reduced to 2 nm, the lifetime becomes 10^{-5} s at 420 K, and an increased thickness of 4 nm brings the lifetime to 10^{6} s.

Similar calculations were carried out for a double ring element of a kagome lattice consisting of 11 islands see Fig. 3.18.

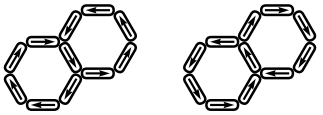

Figure 3.17. Illustration of two ground states for a double kagome ring with 11 islands in the absence of an external field.

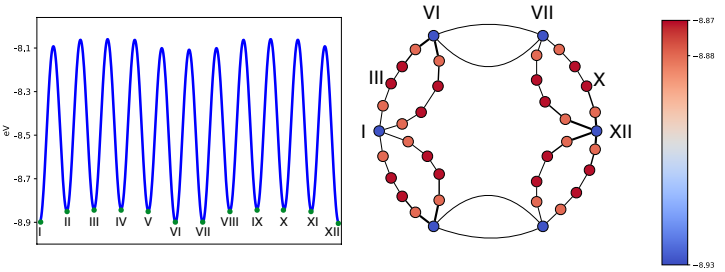

Figure 3.18. Energy landscape for a double ring element of the kagome lattice in the absence of an external magnetic field. The blue curve on the right shows the energy along the minimum energy path between the local minima. The configuration shown on top represent saddle points on the energy surface. Schematic diagrams to the right, show the local energy minima, color-coded according to their energy, and connected with lines where the thickness indicates the rate of the elementary transitions. For transitions between states between states VI and VII, clockwise and anticlockwise rotation have the same rate, but for transitions between the other pairs of states, either clockwise or anticlockwise rotation is favored.

The calculated lifetime of a ground state of the double ring within the steady state approximation turns out to be longer than for the single ring, 22 s at 420 K, as the lowering of the prefactor has a larger effect than the lowering of the activation energy in this case. Again, excellent agreement is obtained between these calculations and the experimental measurements of Farhan *et al.* [128] that indeed gave a longer lifetime for the double ring than for the singe ring, 29 s vs. 11 s. The results on the double ring further illustrate that close agreement can be obtained with the experiment using the present theoretical approach and parameters determined from properties of a single island.

3.4 Shakti lattice

Another interesting spin ice system is the shakti lattice. A unit element of this lattice consists of four unit elements of a square lattice with lattice constant, a, where two internal islands have been removed, while two other islands inside the square have been united into one (as shown in Fig. 3.19).

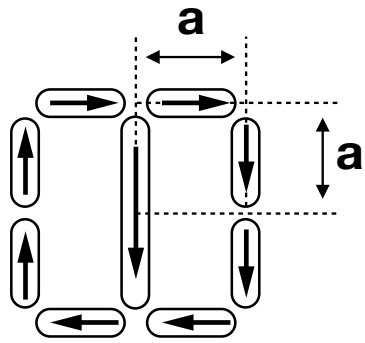

Figure 3.19. Schematic representaion of the shakti unit element with a lattice constant a.

It is possible to separate the big island into two smaller islands [129]. The difference in size and, therefore, volumes of the magnetic islands in the system, leads to richer magnetization reversal processes, than for the kagome lattice.

This element of the shakti lattice was studied using the point dipole approximation for the inter-island interaction given by Eq. 56. The magnetization as well as anisotropy parameters used in the calculations are presented in the Table 3.4. Given the dipole

Table 3.4. Parameter values in the present calculations

Parameter	Small island	Big island
Magnetisation, A/m$\cdot 10^5$	2.00	2.00
Volume, cm^3 $\cdot 10^{-16}$	1.88	4.58
Anisotropy, Jm^{-3}	588	621

approximation of the interaction between islands, there are two energentically equivalent sets of ground states. The MEPs between them were obtained with the GNEB algorithm for a range of values of the lattice constant, a. Path 1 is shown in Fig. 3.20 and path 2 is presented in Fig. 3.21 along with configurations in the ground and intermediate states. For both possible paths, the transition between ground states is determined by the barrier for rotating the magnetic vector of the large island. Therefore, one can say that small islands and large island are not coupled. By applying HTST, the dependence of the effective barrier and pre-factor on the lattice constant was calculated for both

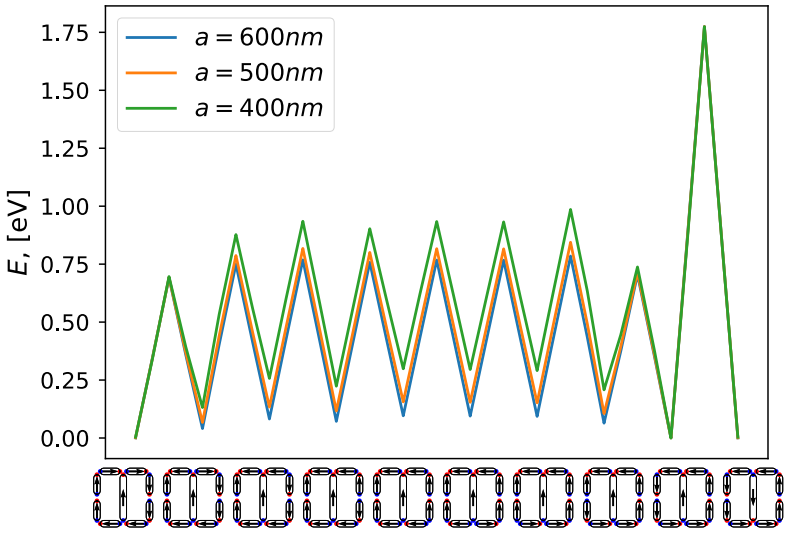

Figure 3.20. Schematic representation of path 1 when the small islands have arranged in a clockwise or anticlockwise manner, and the big island flips. Curves represent the MEP between the two ground states. On the bottom, there are system configurations in the ground and intermediate states. Each peak between adjacent minima corresponds to a saddle point configuration. Different curves correspond to a change in the lattice constant, a.

small islands and the large island and for various MEPs. The dependency of the time on temperature to change orientation for all small islands and the large island in both paths were calculated for various values of the lattice constant.

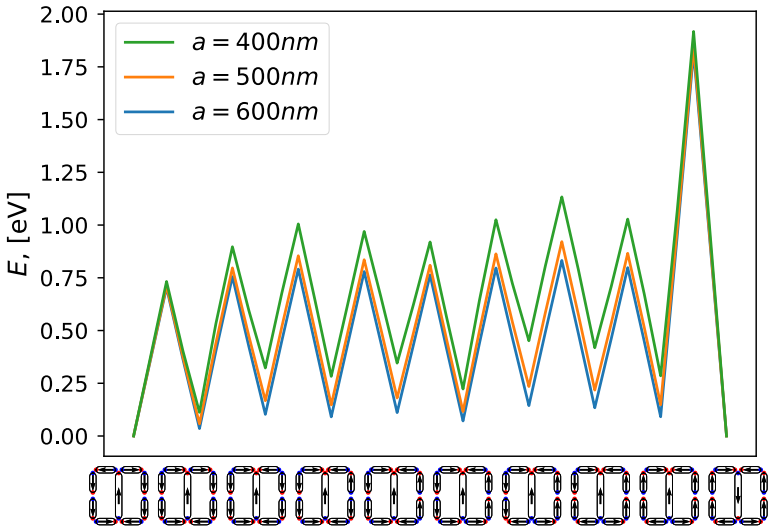

Figure 3.21. Schematic representation of path 2, where the small islands form a closed loop. Curves represent the MEP between the two ground states. The images below show the system configurations in the ground and intermediate states. Each peak between two minima corresponds to a saddle point configuration. Different curves correspond to different values of the lattice constant, a.

Article I

The effect of temperature and external field on transitions in elements of kagome spin ice

S.Y. Liashko, H. Jónsson, V.M. Uzdin

New Journal of Physics **19**, 113008 (2017)

IOP Publishing New J. Phys. 19 (2017) 113008 https://doi.org/10.1088/1367-2630/aa8b96

New Journal of Physics
The open access journal at the forefront of physics

Deutsche Physikalische Gesellschaft DPG
IOP Institute of Physics
Published in partnership with: Deutsche Physikalische Gesellschaft and the Institute of Physics

OPEN ACCESS

RECEIVED
24 April 2017

REVISED
3 August 2017

ACCEPTED FOR PUBLICATION
11 September 2017

PUBLISHED
7 November 2017

PAPER

The effect of temperature and external field on transitions in elements of kagome spin ice

Sergei Y Liashko[1,2], **Hannes Jónsson**[2,3] **and Valery M Uzdin**[1,4]

[1] St. Petersburg National Research University of Information Technologies, Mechanics and Optics, St. Petersburg, 197101, Russia
[2] Faculty of Physical Sciences and Science Institute, University of Iceland, 107 Reykjavík, Iceland
[3] Department of Applied Physics, Aalto University, Espoo, FI-00076, Finland
[4] Department of Physics, St. Petersburg State University, St. Petersburg, 198504, Russia

E-mail: hj@hi.is

Keywords: spin ice, rate theory, life time, transition mechanism, simulation

Abstract

Transitions between magnetic states of one and two ring kagome spin ice elements consisting of 6 and 11 prolate magnetic islands are calculated and the lifetime of the ground states evaluated using harmonic transition state theory and the stationary state approximation. The calculated values are in close agreement with experimental lifetime measurements made by Farhan and co-workers (Farhan *et al* 2013 *Nat. Phys.* **9** 375) when values of the parameters in the Hamiltonian are chosen to be best estimates for a single island, obtained from measurements and micromagnetic modeling. The effective pre-exponential factor in the Arrhenius rate law for the elementary steps turns out to be quite small, on the order of 10^9 s^{-1}, three orders of magnitude smaller than has been assumed in previous analysis of the experimental data, while the effective activation energy is correspondingly lower than the previous estimate. The application of an external magnetic field is found to strongly affect the energy landscape of the system. Even a field of 4 mT can eliminate states that correspond to ground states in the absence of a field. The theoretical approach presented here and the close agreement found with experimental data demonstrates that the properties of spin ice systems can be calculated using the tools of rate theory and a Hamiltonian parametrized only from the properties of a single island.

1. Introduction

Lithographic processing and film growth technologies make it possible to construct complex magnetic systems spanning a wide range in length scale, from nanoscale to microns [1, 2]. Of particular interest are artificial spin ice systems which are frustrated and have ground state entropy. Extensive studies, both experimental and theoretical, are currently being carried out on these systems. Interesting physical effects have been observed, such as magnetic monopoles [3], thermally activated changes (even melting) [4–8], and novel thermodynamic phase transitions [9]. The strength of the interaction between the islands, modified by their spatial separation, strongly affects the onset of thermally activated dynamics and transitions in these systems.

Detailed measurements of elements of kagome spin ice, in particular a hexamer ring and a double ring with 11 islands, have been carried out at a temperature of 320 and 420 K with observations of magnetic transitions over a timescale ranging from seconds to days [10]. This is an important model system which is useful for testing and refining theoretical tools for calculating rates of transitions in spin ice systems.

Theoretical work on transitions between magnetic states in overlayers, individual islands and assemblies of islands such as spin-ice has mainly made use of direct dynamical simulations based on the Landau–Lifschitz–Gilbert equation or Monte Carlo simulations [11]. The former has limited applicability because of the short time scale that can be simulated, limited by the fast vibrational motion of the magnetic moments. This problem is analogous to the limitations of direct classical dynamics simulations of atomic rearrangements in chemistry and condensed matter physics [12]. Energy barriers that can readily be overcome on a laboratory time scale are typically prohibitively large for dynamics on such a short time scale. The evolution of systems of interest on a

IOP Publishing New J. Phys. 19 (2017) 113008 S Y Liashko et al

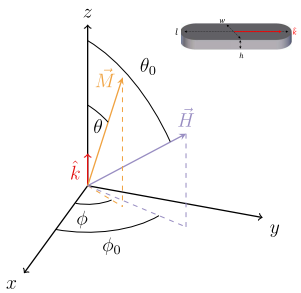

Figure 1. Schematic representation of a magnetic island in three dimensions in the presence of an external field. $\vec{M}$ is the magnetic moment of the island with direction specified by angles ϕ and θ. The direction of the external field, $\vec{H}$, is specified by ϕ_0 and θ_0. The z-axis is aligned with the anisotropy vector, $\hat{k}$. The inset shows the assumed shape and dimensions of an island as well as the direction of the anisotropy axis. The dimensions of an island are taken to be $h = 3.2$ nm, $w = 170$ nm and $l = 470$ nm, as estimated by Farhan *et al* [10].

laboratory time scale cannot, therefore, be simulated by direct dynamics. The Monte Carlo simulations on the other hand are purely statistical and give only thermally averaged quantities with no information about time evolution. Furthermore, the Monte Carlo simulations have so far been based on simplified Hamiltonians without direct connection to the microscopic degrees of freedom and the energy landscape of the system. The kinetic Monte Carlo (KMC) method can be used to simulate such systems over an extended time scale, but it requires as input knowledge of the mechanism and rate of the elementary transitions that can take place [10]. While it is possible to guess what such input should be, it is better to have a well defined procedure for deriving such input from the basic properties of the individual islands. This can be done by using tools of rate theory to find the mechanism and rate of the thermally activated transitions. In this way, the KMC method can be made more rigorous and consistent with basic physical properties of the system. Such approaches have been developed for systems undergoing atomic rearrangements [13–15], for example dynamics at proton disordered ice surfaces [16, 17], but have yet to be developed for magnetic systems.

In the present article, we report results of calculations of magnetic transitions in a 6 island ring and 11 island double ring elements of the kagome lattice. The energy landscape of the system is described by a point dipole representation of each island and is characterized by finding local minima and minimum energy paths (MEPs) for transitions between the local minima. The rate of the magnetic transitions is evaluated using harmonic transition state theory (HTST) for magnetic systems. The calculated lifetime of the ground magnetic state is found to agree well with the experimental observations of Farhan and coworkers [10] when the values of the parameters in the Hamiltonian are taken from experimental estimates as well as micromagnetic modelling of a single island. The effect of external magnetic field on the energy landscape and the transition rates is, furthermore, estimated.

2. Methods

2.1. Single magnetic island

In order to determine the properties of an individual island, we have carried out micromagnetic simulations. Farhan *et al* estimated the dimensions of their islands to be $470 \times 170 \times 3.2$ nm and the saturation magnetization, M, to be 2.00×10^5 A m^{-1} [10]. We have chosen the shape of the islands in our calculations to be as shown in figure 1 with these dimensions, giving a volume of 2.36×10^{-16} cm^3.

The in-plane shape anisotropy constant, K, was evaluated as the difference in magnetostatic self energy when the total magnetic moment is pointing in the direction of the long axis of the island, e_l, and when it is pointing in the direction of the short axis of the island, e_s. This gives $K = e_l - e_s = 538$ J m^{-3}. Similarly, the out of plane shape anisotropy was evaluated and found to be about 40 times larger than the in-plane anisotropy, 2.3×10^4 J m^{-3}. As a result of this large difference, the magnetic moments can be assumed to rotate only in plane during the remagnetization transitions. The OOMMF software [18] was used for the micromagnetic calculations. A

Table 1. Parameter values used in the present calculations as well as values used in the calculations of [10], and results obtained for an isolated island, a single ring and a double ring element of the kagome lattice.

Parameter:	Value used	[10]
Magnetization, A $m^{-1} \cdot 10^5$	2.00	2.00
Volume, $cm^3 \cdot 10^{-16}$	2.36	
Anisotropy, J m^{-3}	538	618
Results:		
Isolated island rotation:		
Pre-exponential factor, 1 s^{-1}	9.9×10^8	
Activation energy, eV	0.79	
Single ring, first rotation:		
Pre-exponential factor, 1 s^{-1}	1.0×10^9	1.0×10^{12}
Activation energy, eV	0.84	0.925
Single ring, overall transition:		
Pre-exponential factor, 1 s^{-1}	2.5×10^9	
Activation energy, eV	0.88	
Double ring, overall transition:		
Pre-exponential factor, 1 s^{-1}	4.2×10^8	
Activation energy, eV	0.83	

summary of the parameter values used in our simulations as well as the values used in the KMC simulations of Farhan *et al* is given in table 1.

The magnetic island is taken to be a single-domain, ferromagnetic particle with uniaxial anisotropy. The transition mechanism is assumed to be a uniform, in-plane rotation of the magnetic moments of the atoms in the island, i.e. all atomic magnetic moments in the island are taken to be parallel and lie in the plane of the island [19]. Then, the energy of an island, E, can be expressed as

$$E/V = -K(\hat{m} \cdot \hat{\kappa})^2 - (\vec{M} \cdot \vec{H}), \tag{1}$$

where $\vec{M}$ is the magnetic moment of the island, $\hat{m} = \vec{M}/\|\vec{M}\|$, is a unit vector giving its direction, $\hat{\kappa}$ is a unit vector in the direction of the long axis of the island (see figure 1) and V is the volume of the island. The first term on the right represents the anisotropy energy and the second term represents the Zeeman energy arising from an external field $\vec{H}$.

Using the angles illustrated in figure 1, the energy can be rewritten as

$$\begin{aligned} E/V = &-K\cos^2\theta - \|\vec{M}\|\|\vec{H}\|(\sin\theta_0 \sin\theta \cos\phi_0 \cos\phi \\ &+ \sin\theta_0 \sin\theta \sin\phi_0 \sin\phi + \cos\theta_0 \cos\theta) \end{aligned} \tag{2}$$

The energy of the island is minimized by pointing the magnetic moment in such a way that $\phi = \phi_0$ so MEPs for remagnetization transitions can be described using only the two polar angles θ_0 and θ

$$E/V = -K\cos^2\theta - \|\vec{M}\|\|\vec{H}\|\cos(\theta_0 - \theta). \tag{3}$$

2.2. Kagome single ring

A single ring element of a kagome lattice consisting of a hexamer of islands was simulated as shown in figure 2. The distance between parallel islands was chosen to be 1 μm to mimic a system studied by Farhan *et al* [10]. The interaction between the islands was approximated as dipole–dipole interaction with a single dipole centered on each island. For a hexamer of islands, the energy can then be written as

$$\begin{aligned} E/V = &-\sum_i^6 K(\hat{m}_i \cdot \hat{\kappa})^2 - \sum_i^6 (\vec{M}_i \cdot \vec{H}) \\ &- \frac{V}{2}\sum_{i\neq j}^6 \left(\frac{(\vec{M}_i \cdot \vec{M}_j)}{\|\vec{r}_{ij}\|^3} - \frac{3(\vec{M}_i \cdot \vec{r}_{ij})(\vec{M}_j \cdot \vec{r}_{ij})}{\|\vec{r}_{ij}\|^5} \right), \end{aligned} \tag{4}$$

where the vector $\vec{r}_{ij}$ is pointing between the centers of islands i and j.

This energy expression defines an energy surface as a function of the orientation of the magnetic moments of the islands in the system. A state is defined as a local minimum on this energy surface and is found by setting up a rough approximations of the orientations of the magnetic moments and then minimizing the energy with respect to the orientation of all the magnetic moments. Two equivalent ground states exist corresponding to clockwise and anticlockwise arrangements of the magnetic moments of the islands. The energy along a MEP for

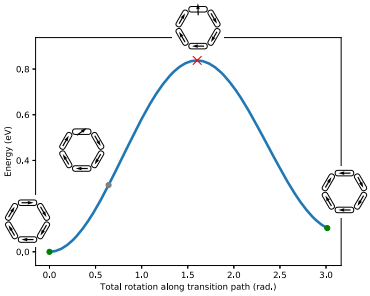

Figure 2. Energy along the minimum energy path for an anticlockwise rotation of one of the magnetic moments of a single ring element of the kagome lattice, starting from the clockwise oriented ground state, as a function of the total displacement of all the magnetic moments. The saddle point is marked with a red ×. One other intermediate image in the GNEB calculation is shown for completeness, but the calculation of the path involved 10 intermediate images.

the rotation of one of the magnetic moments starting from a ground state is shown in figure 2. The MEP is defined in such a way that at each point on the path the energy is at a minimum with respect to all degrees of freedom except the direction along the path tangent. The calculations of MEPs were carried out using the geodesic nudged elastic band (GNEB) method [20]. The maximum energy along the MEP corresponds to a first order saddle point on the energy surface and gives an estimate of the activation energy of the transition within HTST.

The rotation of one of the magnetic vectors creates two points where magnetic moments meet in a way that increases the energy, i.e. two 'defects' are formed (states labeled II in figure 3). All other configurations where additional magnetic moments have been rotated without introducing more defects where generated and the state corresponding to a local minimum in energy found. Then, the GNEB method was used to find MEPs between local minima corresponding to successive rotations. Both clockwise and anticlockwise rotations were studied. The climbing image algorithm was used to converge the highest energy image on the saddle point. The MEPs are the paths of highest statistical weight for the magnetic transitions and show the mechanism of the transitions. The essential part of the energy surface of the system is characterized by the local minima corresponding to configurations with only two defects in the hexamer and the MEPs connecting those minima.

HTST [21, 22] is used to calculate the rate constant for each elementary transition $j \to k$

$$W_{jk}^{\mathrm{HTST}} = \frac{1}{2\pi}\frac{J_s}{J_j}\sqrt{\sum_{i=2}^{D}\frac{a_i^2}{\epsilon_{s,i}}}\frac{\prod_{i=1}^{D}\sqrt{\epsilon_{j,i}}}{\prod_{i=2}^{D}\sqrt{\epsilon_{s,i}}}\mathrm{e}^{-(E_s-E_j)/k_BT}. \tag{5}$$

Here, the subscript j refers to the energy minimum corresponding to the initial state and s refers to the saddle point. J stands for Jacobian, ϵ for eigenvalues of the Hessian, a for coefficients in the expansion of the velocity at the saddle point in terms of the eigenvectors of the Hessian, and E the energy. The sum over eigenvalues at the saddle point excludes the negative eigenvalue corresponding to the unstable mode, i.e. direction for which the energy is maximal at the saddle point.

For a single island, with energy given by equation (3) and parameters listed in table 1, the activation energy for a rotation of the magnetic vector is found to be 0.79 eV. The calculated pre-exponential factor turns out to be small, 9.9×10^8 s^{-1}, three orders of magnitude smaller than has been assumed in previous Monte Carlo simulations of this system [10].

The MEP for the rotation of the magnetic vector of one of the islands in a kagome hexamer is shown in figure 2. In this case, clockwise and anticlockwise rotations have equivalent MEPs, with equal activation energy and rate constants. The rate of transition between the two states is therefore twice the rate obtained from equation (5). The activation energy is quite a bit higher than for an isolated island, 0.84 eV, but the pre-exponential factor is similar, 1.0×10^9 s^{-1}.

For subsequent transitions, the lowest activation energy is obtained by rotating one of the neighboring islands, (one example shown as state III in figure 3(a)). In those cases, the activation energy for clockwise and anticlockwise rotations is slightly different, by a few percent, and one of the two possible mechanisms dominates. An MEP for a complete transition from one of the ground states of the kagome hexamer to the other

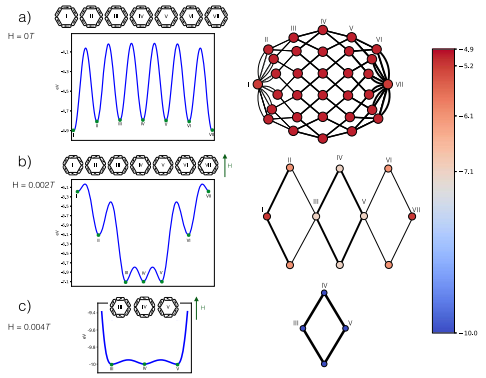

Figure 3. Left column: Energy landscape for a single ring element of the kagome lattice: (a) in the absence of a magnetic field, (b) in a field of 2 mT, and (c) in a field of 4 mT. The curves show the energy along the minimum energy paths between the local minima. Right column: Schematic diagrams showing the local energy minima, color coded according to their energy, and connected with lines where the tickness indicates the rate of the elementary transition. For transitions between states I and II as well as between states VI and VII, clockwise and anticlockwise rotations have the same rate, but for transitions between the other pairs of states either clockwise or anticlockwise rotation dominates.

is shown in figure 3(a) and the possible paths of elementary transitions indicated in the inset. HTST is used to calculated the rate of each of the elementary steps using equation (5). The pre-exponential factor for the elementary steps in the MEP shown in figure 3(a) is found to range from 9.7×10^8 to 1.0×10^9 s^{-1}. A reasonable approximation to the pre-exponential factor for the elementary steps can, therefore, be obtained by using the value for a single island. The highest energy saddle points, corresponding to rotations between states III and IV, and between states IV and V, have energy 0.885 eV above the ground state (see figure 3(a)).

The overall rate from one of the ground states of the kagome hexamer to the other can be calculated by combining the rates of the various elementary steps in a master equation, i.e. a set of differential equations for the time derivative of the probabilities, n_i, of finding the system in each of the various energy levels, i (roman numerals are used in figure 3)

$$\begin{aligned}
\frac{\mathrm{d}n_1}{\mathrm{d}t} &= -12W_{12}n_1 + 12W_{21}n_2, \\
\frac{\mathrm{d}n_i}{\mathrm{d}t} &= -(2W_{i\,i+1} + 2W_{i\,i-1})n_i + 2W_{i-1\,i}n_{i-1} + 2W_{i+1\,i}n_{i+1}, \\
\frac{\mathrm{d}n_6}{\mathrm{d}t} &= -(2W_{67} + 2W_{65})n_6 + 2W_{56}n_5,
\end{aligned} \tag{6}$$

where $i = 2 \ldots 5$. The coefficient 12 multiplying the elementary rate constants W_{12} and W_{21} takes into account the number of different ways to get between the two levels, and similarly for the coefficient 2 multiplying some of the other rate constants, as illustrated in figure 3. For transitions between states I and II as well as between states VI and VII, clockwise and anticlockwise rotations have the same rate, so there are two equivalent, parallel mechanisms. But, for transitions between the other pairs of states either clockwise or anticlockwise rotation dominates. Transformations back from the final state, $i = 7$, are not included since the goal is to calculate the lifetime of the ground states.

In order to obtain a closed expression for the overall rate, the steady state approximation is invoked. There, it is assumed that the probability of intermediate states does not change with time

$$\begin{aligned}
\frac{\mathrm{d}n_i}{\mathrm{d}t} &= -2(W_{i\,i+1} + W_{i\,i-1})n_i + 2(W_{i-1\,i}n_{i-1} + W_{i+1\,i}n_{i+1}) = 0, \\
\frac{\mathrm{d}n_6}{\mathrm{d}t} &= -(2W_{67} + 2W_{65})n_6 + 2W_{56}n_5 = 0,
\end{aligned} \tag{7}$$

where $i = 2 \ldots 5$. The rate of decrease in the probability of the initial state can then be written as a continued fraction

$$\frac{\mathrm{d}n_1}{\mathrm{d}t} = -12n_1\left(W_{12} - \frac{W_{12}W_{21}}{W_{21} + W_{23} - \dfrac{W_{23}W_{32}}{W_{32} + W_{34} - \dfrac{W_{34}W_{43}}{W_{43} + W_{45} - \dfrac{W_{45}W_{54}}{W_{54} + W_{56} - \dfrac{W_{56}W_{65}}{W_{65} + W_{67}}}}}}\right) \tag{8}$$

and the overall rate constant for transitions from a ground initial state expressed as $k_{\mathrm{tot}} = \frac{1}{n_1}\frac{\mathrm{d}n_1}{\mathrm{d}t} = \frac{A}{C}$, where A and C are a combination of the elementary rates, W_{ij}, given by

$$\begin{aligned} A &= 12W_{12}W_{23}W_{34}W_{45}W_{56}W_{67}, \\ C &= W_{21}W_{32}W_{43}W_{54}W_{65} + W_{21}W_{32}W_{43}W_{54}W_{67} + W_{21}W_{32}W_{43}W_{56}W_{67} \\ &\quad + W_{21}W_{32}W_{45}W_{56}W_{67} + W_{21}W_{34}W_{45}W_{56}W_{67} + W_{23}W_{34}W_{45}W_{56}W_{67}. \end{aligned} \tag{9}$$

The lifetime of the ground state is then obtained as the inverse of the rate constant, $\tau = 1/k_{\mathrm{tot}}$. By using the calculated MEPs and HTST to estimate the rate constant for each elementary step given the Hamiltonian in equation (4) and the parameters derived for a single island, a lifetime of $\tau = 14$ s is obtained at 420 K. This is in excellent agreement with the experimental measurements of Farhan and co-workers showing a lifetime of ca 11 s at 420 K (see figure 3(b) in [10]). At 320 K, the lifetime is much longer, calculated to be several days.

In order to determine the overall pre-exponential factor and activation energy for transitions between the ground states, the lifetime was calculated for a wide range in temperature, from 80 to 1000 K, using equation (9). The calculated lifetime was found to vary exponentially with $1/T$, following closely the Arrhenius law. From this, the effective pre-exponential factor and effective activation energy were found to be 2.5×10^9 s^{-1} and 0.88 eV. The effective activation energy turns out to be essentially equal to the difference between the energy of the highest saddle point and the initial state energy. The presence of the intermediate states reduces the pre-exponential factor for the overall transition as compared with the pre-exponential factor of the elementary steps, but the presence of multiple transition paths increases it. The two effects cancel out to some extent.

Variation in the thickness of the islands has a strong effect on the lifetime of the ground states of the hexamer, as observed by Farhan and co-workers [10]. If the island thickness is reduced to 2 nm, the lifetime becomes 10^{-5} s at 420 K, and an increased thickness to 4 nm brings the lifetime to 10^6 s.

2.3. Single ring in an external field

An important question is how an external magnetic field affects the properites of a spin ice system. Calculations were carried out for the hexamer ring in a field applied as shown in figure 3 with magnitude of 2.0 and 4.0 mT. The effect of the field on the energy landscape is illustrated in figures 3(b) and (c). Even such a small field clearly has a dramatic effect on the energy landscape. At a field of 2 mT, states I and VII no longer correspond to the ground state, but rather states III and V. When a larger field of 4 mT is applied, several of the of the local minima on the energy surface disappear and the corresponding states no longer exist. This is an important consideration in experimental measurements were external magnetic field may be present, on purpose or inadvertently.

2.4. Kagome double ring

Similar calculations were carried out for a double ring element of a kagome lattice consisting of 11 islands, shown in figure 4. Using the same values of parameters as for the single ring hexamer and a fit to the calculated rate over an extended temperature range, the effective activation energy for transitions between equivalent ground states of the double ring is found to be lower than for the single ring, 0.83 versus 0.88 eV. Again, this is essentially the difference in energy between the highest first order saddle point along the MEP and the ground state energy. As can be seen by comparing the energy landscapes in figures 3(a) and 4, the intermediate states of the double ring are not as high above the ground state as of the single ring. For example, state II in the double ring is up in energy by 0.052 eV while for the single ring the enegy increase is 0.091 eV. The presence of the junctions where three islands meet in the double ring make it easier to accomodate one of the defects formed when an island rotates from the ground state configuration. This smaller increase in the energy of the intermediate states of the double ring is also reflected in the energy of the first order saddle points.

The pre-exponential factor for the elementary transitions in the double ring is similar as for the elementary transitions in the single ring, between 9.8×10^8 and 1.0×10^9 s^{-1}. From these considerations, one would expect that the lifetime of the ground states of the double ring to be shorter than that of the single ring. However, the effective prefactor is significantly smaller for the double ring, 4.2×10^8 s^{-1}. The reason for this is essentially the reduced symmetry of the double ring. While there are 12 equivalent ways for transitions out of the ground state of the single ring, there are only 4 equivalent ways for transitions out of the ground state of the double ring.

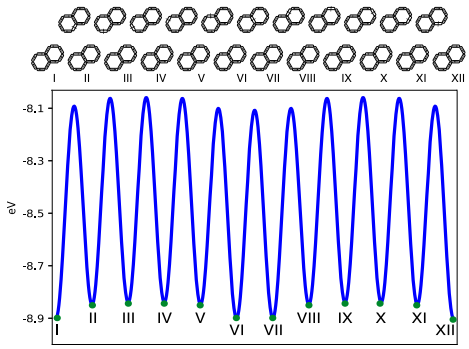

Figure 4. Energy landscape for a double ring element of the kagome lattice. The curve shows the energy along the minimum energy path of lowest activation energy between the two global minima. Schematic diagrams on top show the orientation of the magnetic vectors at each of the local energy minima (lower row) and the saddle points for the elementary transitions (upper row).

Futhermore, there are more intermediate states for the double ring, each one offering the possibility of a return to the initial ground state. The calculated lifetime of a ground state of the double ring within the steady state approximation turns out to be longer than for the single ring, 22 s at 420 K, as the lowering of the prefactor has a larger effect than the lowering of the activation energy in this case.

Again, excellent agreement is obtained between these calculations and the experimental measurements of Farhan and coworkers which indeed observed a longer lifetime for the double ring than for the singe ring, 29 s versus 11 s [10]. The results on the double ring further illustrate that close agreement can be obtained with experiment using the present theoretical approach and parameters determined from the properties of a single island.

3. Discussion

The theoretical approach presented here and the good agreement found with the measurements of Farhan *et al* [10] on the lifetime of the ground state of the single and double ring kagome elements, demonstrates that the properties of spin ice systems can be calculated using the tools of rate theory and a Hamiltonian parametrized from the basic properties of individual islands. The parameter values used here were not obtained by fitting to the measurements of the kagome ring or double ring, but were obtained from estimates obtained from micromagnetic calculations and experimental measurements on a single island. This is a powerful approach that opens the door for rigorous simlations of melting and other interesting phenomena in extended spin ice systems. In particular, the pre-exponential factor is evaluated from HTST and found to be three orders of magnitude smaller than what had previously been assumed [10]. The calculated effective activation energy is correspondingly smaller than had previously been extracted by fitting to the experimental data while using the postulated value of the pre-exponential factor. This difference between the calculated and fitted values of the activation energy together with the difference between the calculated and previously assumed values of the pre-exponential factor will lead to different estimates of the rate of transitions at temperature outside the narrow range used in the fitting.

We note that the methodology used here for calculating pre-exponential factors in the Arrhenius rate expressions for magnetic transitions, HTST, has been shown to give results in good agreement with experimentally measured prefactors for remagnetization of Fe islands on a W(110) surface [23] and simulations of hysteresis loops of spring magnets [24]. Also, the calculated activation energy for annihilation of a magnetic skyrmion obtained with this methodology is in close agreement with direct Landau–Lifshitz–Gilbert simulations carried out at a relatively high temperature (where the life time is short enough for such direct simulations) [25]. Full transition state theory, without the harmonic approximation, where both the location and orientation of the transition state is variationally optimized (as has been done for atomic rearrangement

transitions [26]) followed by dynamical corrections involving direct simulation of trajectories starting at the transition state (the two step WKE procedure, see review in [12]), will, however, give more accurate estimates of the transition rates and may be required for systems where the energy landscape is more complex and has low second order saddle points in comparison with the first order saddle points.

Acknowledgments

We thank Dr Unnar B Arnalds and Dr Pavel F Bessarab for helpful discussions. This work was supported by the Icelandic Research Fund, and the Academy of Finland (grant 278260).

References

[1] Wang R F, Nisoli C, Freitas R S, Li J and McConville W 2006 *Nature* **439** 303
[2] Braun H B 2012 *Adv. Phys.* **61** 1
[3] Castelnovo C, Moessner R and Sondhi S L 2008 *Nature* **451** 42
[4] Morgan J P, Stein A, Langridge S and Marrows C H 2011 *Nat. Phys.* **7** 75
[5] Kapaklis V, Arnalds U B, Harman-Clarke A, Papaioannou E T, Karimipour M, Korelis P, Taroni A, Holdsworth P C W, Bramwell S T and Hjörvarsson B 2012 *New J. Phys.* **14** 035009
[6] Arnalds U B, Farhan A and Chopdekar R V 2012 *Appl. Phys. Lett.* **101** 112404
[7] Zhang S, Gilbert I, Nisoli C, Chern G W and Erickson M J 2013 *Nature* **500** 553
[8] Kapaklis V, Arnalds U B and Farhan A 2014 *Nat. Nanotechnol.* **9** 514
[9] Anghinolfi L, Luetkens H, Perron J, Flokstra M G, Sendetskyi O, Suter A, Proksch T, Derlet P M, Lee S L and Heyderman L J 2015 *Nat. Commun.* **6** 8278
[10] Farhan A, Derlet P M, Kleibert A, Balan A, Chopdekar R V, Wyss M, Anghinolfi L, Nolting F and Heyderman L J 2013 *Nat. Phys.* **9** 375
[11] Heyderman L J and Stamps R L 2013 *J. Phys.: Condens. Matter* **25** 363201
[12] Jónsson H 2011 *Proc. Natl Acad. Sci.* **108** 944
[13] Henkelman G and Jónsson H 2001 *J. Chem. Phys.* **115** 9657
[14] Chill S T, Welborn M, Terrell R, Zhang L, Berthet J-C, Pedersen A, Jónsson H and Henkelman G 2014 *Modelling Simul. Mater. Sci. Eng.* **22** 055002
[15] Pedersen A and Jónsson H 2009 *Acta Mater.* **57** 4036
[16] Batista E R and Jónsson H 2001 *Comput. Mater. Sci.* **20** 325
[17] Pedersen A, Karssemeijer L J, Cuppen H M and Jónsson H 2015 *J. Phys. Chem.* C **119** 16528
[18] http://math.nist.gov/oommf/
[19] Stoner E C and Wohlfarth E P 1991 *IEEE Trans. Magn.* **27** 3475
[20] Bessarab P F, Uzdin V M and Jónsson H 2015 *Comput. Phys. Commun.* **196** 335
[21] Bessarab P F, Uzdin V M and Jónsson H 2012 *Phys. Rev.* B **85** 184409
[22] Bessarab P F, Uzdin V M and Jónsson H 2013 *Z. Phys. Chem.* **227** 1543
[23] Bessarab P F, Uzdin V M and Jónsson H 2013 *Phys. Rev. Lett.* **110** 020604
[24] Moskalenko M, Bessarab P F, Uzdin V M and Jónsson H 2016 *AIP Adv.* **6** 025213
[25] Lobanov I, Jónsson H and Uzdin V M 2016 *Phys. Rev.* B **94** 174418
[26] Jóhannesson G H and Jónsson H 2001 *J. Chem. Phys.* **115** 9644

Article II

Thermal stability of magnetic states in submicron magnetic islands

S.Y. Liashko, I.S. Lobanov, V.M. Uzdin, H. Jónsson

Nanosystems: Physics, Chemistry, Mathematics **8(5)**, 572-578 (2017)

NANOSYSTEMS: PHYSICS, CHEMISTRY, MATHEMATICS, 2017, 8 (5), P. 572–578

Thermal stability of magnetic states in submicron magnetic islands

S. Y. Liashko[1,2], I. S. Lobanov[1], V. M. Uzdin[1,3], H. Jónsson[2,4]

[1]ITMO University, Kronverkskiy, 49, St. Petersburg, 197101, Russia
Kronverkskiy, 49, St. Petersburg, 197101, Russia

[2]Science Institute and Faculty of Physical Sciences, University of Iceland
107 Reykjavík, Iceland

[3]St. Petersburg State University, St. Petersburg, 198504, Russia

[4]Center for Nonlinear Studies, Los Alamos, NM 87545, USA

sergei.liashko@gmail.com, lobanov.igor@gmail.com, v_uzdin@mail.ru, hj@hi.is

PACS 75.75.-c, 75.75.Jn, 75.60.Jk **DOI 10.17586/2220-8054-2017-8-5-572-578**

The lifetime of magnetic states in single domain micromagnetic islands is calculated within the harmonic approximation to transition state theory. Stable magnetic states, minimum energy paths between them and first order saddle points determining the activation energy are analyzed and visualized on two-dimensional energy surfaces. An analytical expression is derived for the pre-exponential factor in the Arrhenius rate expression for the reversal of the magnetic moment when the external field is directed either along the anisotropy axis or perpendicular to it.

Keywords: pre-exponential factor, magnetic islands, activation energy, rate theory, spin ice.

Received: 19 September 2017

Revised: 14 October 2017

1. Introduction

The stability of magnetic states with respect to thermal fluctuations and external perturbations is an important topic in fundamental science as well as for technological applications [1, 2]. Thermal stability is a particularly important issue in the context of nanoscale information storage devices. The thermal stability of the magnetic states decreases as the size of such devices is reduced. Estimates of the rate of magnetic transitions are, therefore, important when designing such systems.

In this context, thermally-activated magnetic transitions are rare events on the time scale of oscillations of the magnetic moments, making direct simulations of spin dynamics an impractical way to estimate the lifetime. This separation of time scales, however, makes it possible to apply statistical approaches such as transition state theory (TST) [3] or Kramers theory [4]. The transitions are slow enough that a Boltzmann distribution is established and maintained in the initial state of the system. Within the harmonic approximation to TST (HTST) [5] and within Kramers theory, the activation energy of a transition is given by the energy difference between the local minimum on the energy surface corresponding to the initial state and the highest energy on the minimum energy path (MEP) connecting the initial and final state minima. The MEPs between minima are the transition paths of largest statistical weight and characterize the mechanism of the corresponding transitions. A maximum along an MEP corresponds to a first order saddle point on the energy surface and gives an estimate of the activation energy within HTST. In adaptions of these rate theories to magnetic systems [6–12], the magnitude of the magnetic vectors is either assumed to be constant as orientation changes, or it is treated as a fast variable obtained from self-consistency calculations for fixed values of the slow variables specifying orientation [13]. The energy surface of a system of N magnetic moments is then a function of 2N degrees of freedom defining the orientation of the magnetic moments.

If all degrees of freedom in the system can be included within the harmonic approximation (no zero modes, i.e. degrees of freedom for which the energy is constant) HTST and Kramers estimate give an Arrhenius expression for the rate constant, $k(T) = f_0 \exp\left[-\Delta E/k_B T\right]$ where ΔE is the energy difference between the relevant first order saddle point and the initial state minimum. The pre-exponential factor, f_0, often referred to as the attempt frequency, can be determined by calculating the eigenvalues of the Hessian matrix, the matrix of second derivatives of the energy with respect to the angles specifying the orientaiton of the magnetic moments, at the first order saddle point and at the initial state minimum [11].

While the activation energy for magnetic transitions has frequently been calculated, fewer estimates of the pre-exponential factor have been reported. Brown [6, 7] estimated the pre-exponential factor for remagnetization

transitions in a single domain, uniaxial magnetic particle to be on the order of 10^9 – 10^{12} sec^{-1}. The size and shape of the particle as well as the materials properties will affect the value. Experimental measurements by Wernsdorfer et al. [14] on 30 nm diameter Co nanoparticles gave an estimate of 4×10^9 sec^{-1}.

Recently, the HTST approach has been used to estimate the pre-exponential factor as well as the activation energy for various magnetic transitions. For remagnetization transitions in small Fe nanoislands on W(110), significantly larger values of the pre-exponential factor were obtained, ranging from 10^{13} to 10^{18} sec^{-1}, depending on the size and shape of the islands [15]. The higher range of values was found where the remagnetization occurs via formation of a temporary domain wall ('soliton' mechanism [2]). Experimental estimates for islands falling within a more limited range in shape and size are in close agreement with the calculated values [16]. An HTST estimate for larger permalloy islands used in kagome spin ice systems [17] gave a smaller value, 9.9×10^8 sec^{-1} [18] while analysis of the experimental data had assumed a value of 10^{12} sec^{-1} [17].

On the other hand, HTST calculations of magnetization reversal in a small Fe cluster at a tip interacting with an antiferromagnetic surface gave values in the range of 10^{12} to 10^{18} sec^{-1} [19], while previous analysis of such measurements had assumed a pre-exponential factor of 10^9 sec^{-1} [20]. Since the values of the pre-exponential factor quoted here range over several orders of magnitude, it is clearly important to carry out calculations based on the energy landscape characterizing the magnetic system of interest, rather than just assuming some value *a priori*.

Calculations of the value of the pre-exponential factor using HTST are in principle straightforward, even when the energy of the system is obtained from iterative self-consistent calculations [12, 13]. Other examples of HTST calculations of transition rates include magnetic skyrmion annihilation in CoPt(111) films [21], skyrmion lifetime in narrow magnetic tracks [22] and the effect of impurities on skyrmion lifetime [23]. The dimensionality of the energy surface used for those calculations ranged from several hundreds up to tens of thousands. Good agreement has been found between HTST calculations and experimental measurements of lifetimes of both single and double kagome rings when the parameters in the calculations were determined from basic properties of a single island and no adjustment made to fit the data [18].

While robust methods are available for finding MEPs in complex magnetic systems [24, 25], the visualization of the transition mechanism is in general a difficult task. To simplify the problem, one can consider a projection of the multidimensional surface on a two-dimensional surface, where the energy is given by a two-parameter function specifying the orientation of the magnetic moments in the system. This has, for example, been done in studies of magnetization reversals in an exchange spring magnet, where the mechanism was described as propagation of a temporary domain wall along the soft magnet toward the interface with the hard magnet and beyond [26]. The position and the width of the wall are the two parameters used to parametrize the projection of the energy surface.

A particularly simple and yet important example of a magnetic system is a single domain magnetic particle with shape anisotropy, possibly in the presence of a magnetic field. This system has been studied over a long period of time and is often referred to as a Stoner-Wohlfarth particle [27]. It is, for example, relevant for modeling of transitions in artificial spin ice systems which consist of arrays of magnetic islands on a solid surface. The energy of the magnetic particle can be described by two angles in a spherical coordinate system so the energy surface can be visualized easily. Previously, thermal effects on the lifetime of the magnetic states of such a particle have been studied using kinetic equations [7] and by calculations of the smallest non-vanishing eigenvalue of the Fokker-Plank equation [28]. Theoretical and experimental studies of the effect of temperature on dynamic hysteresis [29] have been carried out as well as studies of the effect of thermal fluctuations on magnetic anisotropy determinations [30]. However, the dependence of the pre-exponential factor in the rate constant on the size and shape of the magnetic particle as well as the materials properties is not well known and, as mentioned above, analysis of experimental data often relies on assumed values rather than accurate estimates.

In the present article, we report HTST calculations of the lifetime of magnetic states of a single domain magnetic particle with shape anisotropy with and without an applied magnetic field. The activation energy and pre-exponential factor for magnetic transitions are reported for various values of the anisotropy parameters. For the cases where the applied magnetic field is directed either along the anisotropy axis or perpendicular to it, explicit analytical expressions are obtained for the pre-exponential factor as well as the activation energy.

2. Model

We will consider a single domain magnetic island supported on a solid surface in the presence of an external magnetic field **H**. The direction of the magnetic moment of the island is determined by two angles, θ and ϕ, as shown in Fig. 1. The direction of the magnetic field will be characterized by angles θ_H and ϕ_H.

The energy density can be written as the sum of an anisotropy term and a Zeeman term

$$E/V \;=\; E_{anis}/V \;+\; E_Z/V. \tag{1}$$

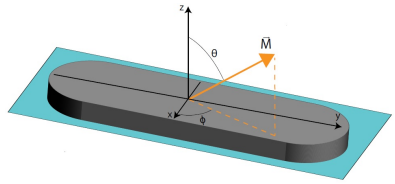

FIG. 1. Single domain magnetic island on a solid surface. $\vec{M}$ is the total magnetic moment of the island and its direction with respect to the anisotropy axis and the surface normal is given by the spherical polar angles θ and ϕ.

Here, the anisotropy term can be written as

$$E_{anis}/V \;=\; -K_1 \sin^2\theta \sin^2\phi + K_2 \cos^2\theta, \tag{2}$$

where K_1 and K_2 are anisotropy constants. For a permalloy island in a spin ice structure [17], $K_1 > 0$ and $K_2 > 0$ describe easy axis shape anisotropy and easy plane shape anisotropy, respectively. For CoPt islands [31,32], there is an intrinsic out of plane anisotropy and $K_2 < 0$ whereas $K_1 \approx 0$ due to the round shape of the islands. The same system can be described by $K_1 < 0$ and $K_2 \approx 0$ when the y-axis is chosen to be perpendicular to the island plane.

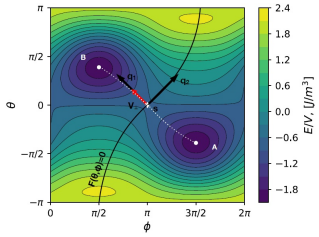

FIG. 2. Energy surface determined by eqs. (1-3) for parameters mimicking CoPt islands [31,32], $c = 1.3$ and $h = 1.8$ with magnetic field $H = 1.33$ MA/m in a direction given by $\theta_H = \pi/10$ and $\phi_H = \pi/2$ (the parameters used in the calculations are $M_0 = 836$ kA/m, $K_1 = 386$ kJ/m^3 and $K_2 = 501.8$ kJ/m^3). The local minima corresponding to the two stable states, A and B, are marked with white disks and the minimum energy path connecting them is shown with a white dotted line. The first order saddle point is marked with **s** and a dividing surface separating the A and B states, defined by $F(\theta, \phi) = 0$, is shown with a black line. The velocity perpendicular to the dividing surface, $V_\perp$, near the saddle point is shown with a red arrow. The two normal mode vectors at the saddle point are shown as black arrows labeled q_1 and q_2

The Zeeman energy is given by the equation

$$E_Z/V \;=\; -\mu_0 H M_0 (\sin\theta \sin\theta_H \sin\phi \sin\phi_H + \sin\theta \sin\theta_H \cos\phi \cos\phi_H + \cos\theta \cos\theta_H), \tag{3}$$

where M_0 is the magnetization of the material and H is the magnetic field strength.

An example energy surface determined by eq. (1–3) is depicted in Fig. 2. The values of parameters are $c \equiv K_2/K_1 = 1.3$ and $h \equiv \mu_0 M_0 H/2K_1 = 1.8$ (The parameters used in the calculations shown in Fig. 2 are $M_0 = 836$ kA/m, $K_1 = 386$ kJ/m^3 and $K_2 = 501.8$ kJ/m^3. In the calculations shown in Fig. 3 the value of K_2 is different, 116 kJ/m^3, to roughly correspond to CoPt islands [31,32]), and the magnetic field is chosen to have strength of $H = 1.33$ MA/m and direction given by $\theta_H = \pi/10$ and $\phi_H = \pi/2$. There are two local minima

A and B on the energy surface corresponding to the stable magnetic states. The dividing surface separating the orientations that correspond to the A and B states can be represented as a continous curve $F(\theta, \phi) = 0$. The MEP between the stable states was found using the geodesic nudged elastic band method [24], a generalization of the frequently used NEB method for atomic rearrangements [33]. The exact position of the first order saddle point was determined with the climbing image algorithm [34].

When the magnetic field is applied along or perpendicular to the easy axis and in the plane of the island, the energy surface is more symmetric and the values of the angles corresponding to stable states, the MEP and saddle point can be obtained analytically. Fig. 3 shows such a case for a magnetic field of $H = 100$ kA/m. If the field is directed perpendicular to the easy axis (the y-axis), the local minima are at $\theta = \pi/2$ and $\phi = \pi \pm \arccos h$. The value of θ is constant along the MEP and the saddle point is at $\theta = \pi/2$, $\phi = \pi$. The activation energy is the same in this case for transitions in both directions $\Delta E/V = K_1(1-h)^2$. If the field is directed parallel to the easy axis, the local minima are at $\theta = \pi/2$ and $\phi = \pi \pm \pi/2$ and the saddle point is at $\theta = \pi/2$, $\phi = \pi + \arcsin(-h)$.

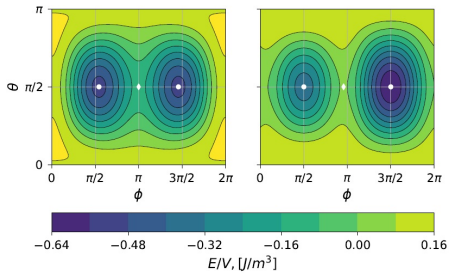

FIG. 3. Energy surface of a single domain magnetic island with parameter values the same as for Fig. 2 except that $c = 0.3$ and the field strength is $H = 100$ kA/m (the parameters used in the calculations are $M_0 = 836$ kA/m, $K_1 = 386$ kJ/m^3 and $K_2 = 116$ kJ/m^3). The field is pointing perpendicular to the easy axis (the y-axis) on the left side, but parallel to the easy axis on the right side. The local minima and the first order saddle point are marked with white dots.

The two wells corresponding to the stable states are not equally deep. For transitions from the metastable state to the ground state, the activation energy is again $\Delta E/V = K_1(1-h)^2$. Note that the positions of the minima and saddle point as well as the activation energy do not depend on the in-plane anisotropy, K_2. The direction of the MEP is along $\theta = \pi/2$, also independent of K_2. However, K_2 affects the shape of the energy surface, the variation of the energy with respect to θ when ϕ is constant, so the rate constant ends up being dependent on K_2, see below.

3. Rate constant

Within TST, the rate of transitions can be found as the product of the probability of reaching the transition state, a thin ribbon of configuration space around the dividing surface, $F(\theta, \phi) = 0$, and the flux out of the transition state. The key approximation of TST is that a dynamical trajectory starting from the initial state only crosses the dividing surface once until the system thermalizes in the product state. Recrossing events during the traversal over the energy barrier are neglected. Dynamical trajectories started at the transition state, can be used to correct the TST estimate of the rate constant. The TST estimate of the rate constant is

$$k^{TST} = \frac{1}{Z} \iint_S e^{-E(\theta,\phi)/k_B T} V_\perp \sin\theta d\theta d\phi, \tag{4}$$

where S denotes the dividing surface and

$$Z = \iint_A e^{-E(\theta,\phi)/k_B T} \sin\theta d\theta d\phi \tag{5}$$

is the configuration integral for the system in the initial state, A, and $V_\perp$ is the projection of the velocity vector, $\vec{V}$, onto the local normal of the dividing surface (that points to the final state B),

$$V_\perp = \frac{\nabla \vec{F}}{||\nabla \vec{F}||} \cdot \vec{V}. \tag{6}$$

When the harmonic approximation is used, i.e. in HTST, the dividing surface is taken to be a hyperplane going through the first order saddle point with normal pointing along the MEP. A quadratic approximation of the energy surface in terms of θ and ϕ around the initial state minimum and the first order saddle point are used to estimate the activation energy and the flux out of the transition state. In order to eliminate mixed terms in the quadratic approximation, it is convenient to define a new coordinate system in terms of the eigenvectors of the Hessian matrix, the vibrational normal coordinates q_1^β and q_2^β, where $\beta = s$ at the saddle point and $\beta = m$ at the initial state minimum

$$E(q_1^\beta, q_2^\beta) = E(\theta_\beta, \phi_\beta) + \frac{1}{2}[\epsilon_{\beta 1}(q_1^\beta)^2 + \epsilon_{\beta 2}(q_2^\beta)^2], \tag{7}$$

where, $\epsilon_{\beta 1}$ and $\epsilon_{\beta 2}$ are the eigenvalues of the Hessian matrix at the saddle point or initial state minimum. The velocity is given by the Landau-Lifshitz equation, which in the vicinity of the first order saddle point, can be written in terms of the normal coordinates as

$$\dot{q}_1^s = \frac{\gamma \epsilon_{s2}}{V M_0 \sin\theta_s} q_2^s \tag{8}$$

and

$$\dot{q}_2^s = -\frac{\gamma \epsilon_{s1}}{V M_0 \sin\theta_s} q_1^s. \tag{9}$$

where γ is the gyromagnetic ratio. If at the saddle point $\epsilon_{s1} < 0$ and $\epsilon_{s2} > 0$, then $V_\perp = \dot{q}_1^s \sin(\theta_s)$. Otherwise, if $\epsilon_{s1} > 0$ and $\epsilon_{s2} < 0$, then $V_\perp = \dot{q}_2^s \sin\theta_s$. The integral over the dividing surface in eqn. (4) needs to be carried out only for regions where $V_\perp > 0$, i.e. for trajectories that are heading away from the initial state and towards the product state [11]. The velocity is zero at the saddle point, but non-zero contributions to the flux are obtained from one half of the hyperplanar dividing surface. Integration gives

$$k^{HTST} = \frac{\gamma\sqrt{\epsilon_{m1}\epsilon_{m2}}}{2\pi M_0 V \sin\theta_m} \, e^{-\Delta E/k_B T}. \tag{10}$$

It is interesting to note that the pre-exponential factor does not depend on the Hessian at the saddle point, only at the initial minimum through the eigenvalues ϵ_{m1} and ϵ_{m2}. This occurs for two-dimensional energy surfaces because $V_\perp > 0$ is proportional to the one positive eigenvalue of the Hessian at the saddle point, but the same eigenvalue also appears in the denominator and thus cancels out. The pre-exponential factor also does not depend on the volume, V, because the eigenvalues of the Hessian at the minimum are proportional to the volume, and the volume also appears in the denominator, so it cancels out.

For the cases when the applied magnetic field is directed either parallel or perpendicular to the easy axis, an analytical expression for the rate constant in terms of the parameters characterizing the energy surface can be obtained. When the magnetic field is perpendicular to the easy axis, the result is

$$k_\perp^{HTST} = f_{0\perp} \, e^{-\Delta E/k_B T} = \frac{\gamma K_1 \sqrt{(1-h^2)(2c+1)}}{\pi M_0} \exp\left[-\frac{V K_1}{k_B T}(1-h)^2\right], \tag{11}$$

and when it is parallel to the easy axis, the result is

$$k_\parallel^{HTST} = f_{0\parallel} \, e^{-\Delta E/k_B T} = \frac{\gamma K_1 \sqrt{(1-h)(2c-h+1)}}{\pi M_0} \exp\left[-\frac{V K_1}{k_B T}(1-h)^2\right]. \tag{12}$$

Figure 4 shows the dependence of the pre-exponential factor, f_0, on the anisotropy parameters, K_1 and K_2 in the absence of an external magnetic field, when $M_0 = 200$ kA/m. A decrease of K_1 leads to a decrease of the pre-exponential factor but reduces at the same time the activation energy. These results show that a value of 10^9 Hz as was assumed in refs. [31,32] gives reasonable approximation.

4. Conclusion

We have presented here simple equations that can be easily evaluated to estimate to estimate the rate constant for remagnetization transitions in a single domain magnetic particle where the transition occurs by uniform rotation. While the saddle point needs to be found in order to estimate the activation energy, ΔE, the eigenvalues of the Hessian are not needed there, only at the initial state minimum.

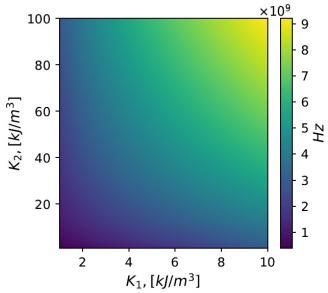

FIG. 4. Dependence of the pre-exponential factor on the anisotropy parameters K_1 and K_2 when the saturation magnetization is $M_0 = 200$ kA/m and no external magnetic field is present, $H = 0$

Especially simple analytical equations were obtained for the cases where the applied field is directed in either a parallel or perpendicular manner to the easy axis, or is absent. All that is needed to evaluate the rate constant in such cases is the saturation magnetization of the material and the two anisotropy constants. The rate constant turns out to be independent of the volume of the magnetic particle.

These results should be of value for theoretical estimates of magnetic transition rates in, for example, artificial spin ice systems, where previously, values of the pre-exponential factor have usually simply been assumed to have some value without relating to the basic properties of the individual islands. The approach presented here has already been shown to be accurate in calculations of the lifetime of single and double kagome rings [18].

For large enough islands compared with the strength of the magnetic interaction between the spins within the island, a uniform rotation is not the preferred transition mechanism, but rather a temporary domain wall. The results presented here do not apply to such situations. Calculations of Fe islands indicate that the pre-exponential factor can be substantially larger in such cases [15]. The reason may be that lower frequency modes then appear at the saddle point. Further analysis of the systematic trends in the pre-exponential factor in such cases as a function of the materials properties and the size and shape of the islands remains a topic of future studies.

Also, for low enough temperatures, quantum mechanical tunneling as opposed to the over-the-barrier mechanism considered here, will become the preferred transition mechanism. Recently, general equations for estimating the onset temperature for tunneling have been presented [35, 36] and can be used to give a lower bound on the temperature range for which the equations presented here remain reliable approximations.

5. Acknowledgements

This work was supported by the Icelandic Research Fund, the Academy of Finland (grant 278260) and the Government of the Russian Federation (grant 074-U01) and by grant 16-11-10330 of Russian Science Foundation.

References

[1] Coffey W.T., Garanin D.A. and McCarthy D.J. Crossover formulas in the Kramers theory of thermally activated escape rates - Application to spin systems.*Advances in Chemical Physics*, 2001, **117**, P. 483.
[2] Braun H.B. Topological effects in nanomagnetism: from superparamagnetism to chiral quantum solitons. *Advances in Physics*, 2012, **61**, P. 1.
[3] Wigner E. The transition state method. *Trans. Faraday Soc.*, 1938, **34**, P. 29–41.
[4] Kramers H.A. Brownian motion in a field of force and the diffusion model of chemical reactions. *Physica*, 1940, **7**, P. 284–304.
[5] Vineyard G.H. Frequency factors and isotope effects in solid state rate processes. *J. Phys. Chem. Solids*, 1957, **3**, P. 121.
[6] Brown Jr.W.F. Thermal fluctuations of a single-domain particle. *Phys. Rev.*, 1963, **130**, P. 1677.
[7] Brown Jr.W.F. Thermal Fluctuations of Fine Ferromagnetic Particles. *IEEE Trans. Magn.*, 1979, **MAG-15**, P. 1196–1208.
[8] Braun H.-B. Kramers's rate theory, broken symmetries and magnetization reversal. *J. Appl. Physics*, 1994, **76**, P. 6310–6315.
[9] Visscher P.B., Zhu R. Low-dimensionality energy landscapes: Magnetic switching mechanisms and rates. *Physica B*, 2012, **407**, P. 1340–1344.
[10] Fiedler G., Fidler J., Lee J., Schrefl T., Stamps R.L., Braun H.B. and Suess D., Direct calculation of the attempt frequency of magnetic structures using the finite element method. *J. Appl. Phys.*, 2012, **111**, P. 093917(7).

[11] Bessarab P.F., Uzdin V.M. and Jónsson H. Harmonic Transition State Theory of Thermal Spin Transitions. *Phys. Rev. B*, 2012, **85**, P. 184409(4).
[12] Bessarab P.F., Uzdin V.M. and Jónsson H. Potential Energy Surfaces and Rates of Spin Transitions. *Z. Phys. Chem.*, 2013, **227**, P. 1543–1557.
[13] Bessarab P.F., Uzdin V.M. and Jónsson H. Calculations of magnetic states and minimum energy paths of transitions using a noncollinear extension of the Alexander-Anderson model and a magnetic force theorem. *Phys. Rev. B*, 2014, **89**, P. 214424(12).
[14] W. Wernsdorfer, E. Bonet Orozco, K. Hasselbach, A. Benoit, B. Barbara, N. Demoncy, A. Loiseau, H. Pascard and D. Mailly. Experimental evidence of the Néel-Brown model of magnetization reversal. *Phys. Rev. Lett.*, 1997, **78**, P. 1791.
[15] Bessarab P.F., Uzdin V.M. and Jónsson H. Size and Shape Dependence of Thermal Spin Transitions in Nanoislands. *Phys. Rev. Lett.*, 2013, **110**, P. 020604(5).
[16] Krause S., Herzog G., Stapelfeldt T., Berbil-Bautista L., Bode M., Vedmedenko E. Y., Wiesendanger R. Magnetization reversal of nanoscale islands: How size and shape affect the Arrhenius Pprefactor. *Phys.Rev. Lett.*, 2009, **103**, P. 127202(4).
[17] Farhan A., Derlet P.M., Kleibert A., Balan A., Chopdekar R.V., Wyss M., Anghinolfi L., Nolting F., Heyderman L.J. Exploring hyper-cubic energy landscapes in thermally active finite artificial spin-ice systems. *Nature Physics*, 2013, **9**, P. 375(8).
[18] Liashko S.Y., Uzdin V.M. and Jónsson H. The effect of temperature and external field on transitions in elements of kagome spin ice. *New J. Phys.*, 2017, (accepted) DOI: 10.1088/1367-2630/aa8b96.
[19] Ivanov A., Bessarab P.F., Uzdin V.M. and Jónsson H. Magnetic exchange force microscopy: Theoretical analysis of induced magnetization reversals. *Nanoscale*, 2017, **9**, P. 13320–13325.
[20] Schmidt R., Schwarz A., Wiesendanger R. Magnetization switching utilizing the magnetic exchange interaction. *Phys. Rev. B*, 2012, **86**, P. 174402(6).
[21] Lobanov I.S., Jónsson H. and Uzdin V. M. Mechanism and activation energy of magnetic skyrmion annihilation obtained from minimum energy path calculations. *Phys. Rev. B* , 2016, **94**, P. 174418(7).
[22] Uzdin V.M., Potkina M.N., Lobanov I.S., Bessarab P.F., Jónsson H. The effect of confinement and defects on the thermal stability of skyrmions. *Physica B*, 2017, (in press), DOI; 10.1016/j.physb.2017.09.040.
[23] Uzdin V.M., Potkina M.N., Lobanov I.S., Bessarab P.F., Jónsson H. Energy surface and lifetime of magnetic skyrmions. *J. Magn. Magn. Mat.*, (accepted). Manuscript available at https://arxiv.org/pdf/1707.00124.pdf.
[24] Bessarab P.F., Uzdin V.M. and Jónsson H. Method for finding mechanism and activation energy of magnetic transitions, applied to skyrmion and antivortex annihilation. *Comp. Phys. Commun.*, 2015, **196**, P. 335–347.
[25] Bessarab P. F. Comment on “Path to collapse for an isolated Néel skyrmion”. *Phys. Rev. B* , 2017, **95**, P. 136401(2).
[26] Moskalenko M. , Bessarab P.F., Uzdin V.M. and Jónsson H. Qualitative Insight and Quantitative Analysis of the Effect of Temperature on the Coercivity of a Magnetic System. *AIP Advances*, 2016, **6**, P. 025213(8).
[27] Stoner E.C., Wohlfarth E.P. A mechanism of magnetic hysteresis in heterogeneous alloys. *Phil. Trans. Roy. Soc. A*, 1948, **240**, P. 599–642.
[28] Coffey W.T, Crothers D.S.F., Dormann J.L., Kalmykov Y.P., Kennedy E.C., Thermally activated relaxation time of a single domain ferromagnetic particle subjected to a uniform field at an oblique angle to the easy axis: Comparison with experimental observations. *Phys. Rev. Lett.*, 1998, **80**, P. 5655–5568.
[29] Poperechny I.S., Raikher Yu.L., Stepanov V.I. Dynamic magnetic hysteresis in single-domain particles with niaxial anisotropy. *Phys.Rev. B*, 2010, **82**, P. 174423(14).
[30] Franco V., Conde A. Thermal effects in a StonerWohlfarth model and their influence on magnetic anisotropy determination. *J. Magn. Magn. Mat.*, 2004, **278**, P. 28–38.
[31] De Vries J., Bolhuis T., Abelmann L. Temperature dependence of the energy barrier and switching field of sub-micron magnetic islands with perpendicular anisotropy. *New J. Phys.*, 2017, (accepted) DOI:10.1088/1367-2630/aa8082.
[32] Engelen J.B.C., Delalande M., le Febre A.J., Bolhuis T., Shimatsu T., Kikuchi N., Abelmann L., Lodder J.C. Thermally induced switching field distribution of a single CoPt dot in a large array. *Nanotechnology*, 2010, **21**, P. 035703(7).
[33] Jónsson H., Mills G., Jacobsen K.W. *Classical and Quantum Dynamics in Condensed Phase Simulations*, edited by Berne B.J., Ciccotti G., Coker D.F. (World Scientific, Singapore, 1998), P. 385–404.
[34] Henkelman G., Uberuaga B.P., Jónsson H. A climbing image nudged elastic band method for finding saddle points and minimum energy paths. *J. Chem. Phys.*, 2000, **113**, P. 9901–9904.
[35] Vlasov S., Bessarab P.F., Uzdin V.M. and Jónsson H. Classical to quantum mechanical tunneling mechanism crossover in thermal transitions between magnetic states. *Faraday Discuss.*, 2016, **195**, P. 93–109.
[36] Vlasov S., Bessarab P.F., Uzdin V.M. and Jónsson H. Calculations of the onset temperature for tunneling in multispin systems. *Nanosystems: Physics, Chemistry, Mathematics*, 2017, **8**, P. 454–461.

Article III

Calculations of switching field and energy barrier for magnetic islands with perpendicular anisotropy

S.Y. Liashko, H. Jónsson, V.M. Uzdin

Nanosystems: Physics, Chemistry, Mathematics (accepted for publication)

NANOSYSTEMS: PHYSICS, CHEMISTRY, MATHEMATICS, 2017, 0 (0), P. 1–10

Calculations of switching field and energy barrier for magnetic islands with perpendicular anisotropy

S. Y. Liashko[1,2], H. Jónsson[2,3], V. M. Uzdin[1,4]

[1]ITMO University, Kronverkskiy, 49, St. Petersburg, 197101, Russia
[2]Science Institute and Faculty of Physical Sciences, Univ. of Iceland
107 Reykjavík, Iceland
[3]Center for Nonlinear Studies, Los Alamos, NM 87545, USA
[4]St. Petersburg State University, St. Petersburg, 198504, Russia

Calculations of the magnetic field required to reverse the magnetization of islands with out-of-plane anisotropy are carried out using a model describing nucleation followed by rapid domain wall motion. The calculations are based on an extension of the Stoner-Wohlfarth model where thermal activation is taken into account as well as the applied magnetic field. Calculated switching field distribution (SFD) is compared with recently reported experimental measurements of de Vries *et al.* [New J. Phys. 19, 093019 (2017)] on circular 220 nm CoPt islands. The measured results can be reproduced closely by choosing appropriate values of two parameters, the nucleation volume, and the effective anisotropy. Both the position of SDF peaks and their width at high and low temperature, 300 K and 10 K, are described well with the same set of parameter values for a given island, while there is a large difference between islands with weak and strong magnetic anisotropy. There is no need to introduce temperature dependence of the activation energy at zero field. This is in contrast with the estimates obtained from the so-called diamond model used by de Vries *et al.* in their data analysis where multiple adjustable parameters are introduced, and a three- to fourfold change in the zero field activation energy is invoked.

Keywords: activation volume, pre-exponential factor, magnetic islands, activation energy, rate theory, spin ice.

1. Introduction

The large research effort has over the past decades been dedicated to studies of small magnetic particles. Advances in the technology for fabricating such particles of various forms, such as powder samples and ferrofluids, as well as ordered arrangements of magnetic particles have led to a wide range of interesting experiments. As a result, new physical phenomena have been discovered and technological advances made, such as high anisotropy nanoparticles [1], single-domain magnetic dots [2] and devices for spin manipulation [3]. There is a large potential for such materials in new applications from high-density data storage and logic devices to magnetic sensors. New applications are constantly found, for example in medicine for transportation of chemical substances or transfer of energy to defined target regions in biological systems, both for diagnostics and therapeutics.

One of the most important issues is the description of the magnetization reversal processes in such systems. The bulk magnetic material consists of multiple regions with homogeneous magnetization - domains, that are separated by domain walls. The structure and the shape of the domains are strongly dependent on the combination of exchange, magnetostatic and anisotropy energy. If one would decrease the volume of the magnetic system, the size of the domains and the width of the domain walls intend to decrease either. As the size of the magnetic particles is decreased sufficiently, the formation of the domain wall becomes unfavorable, and only a single magnetic domain is found within the particles [4].

This critical size depends on the saturation magnetization, the exchange energy between the spins and the anisotropy energy. For spherical particles, the critical diameter is on the order of 10-800 nm [5]. For example, the critical diameter of Fe and Co particles has been estimated to be 15 nm and 35 nm, respectively, while for $SmCo_5$ an estimate of 750 nm has been given [6].

Even if the particles have a single magnetic domain, there can be variations in magnetic properties within the particle due to impurities, changes in elemental composition and due to the shape of the particle. As a result, the anisotropy and exchange energy, for example, can be different in different regions of the particle. A reversal of the magnetization in the presence of an applied field can start in regions where the spins can more easily be flipped and then propagate rapidly from there throughout the particle. The field needed to reverse the magnetization, the switching field H_{sw}, is then strongly affected by imperfections in the particle that lower the activation energy for spin flips. Experiments on continuous [7] as well as patterned [8] magnetic devices including random access memory devices [9] have been interpreted successfully in terms of such a nucleation and propagation mechanism for the magnetization reversal. The switching field is then largely determined by the volume of the critical nucleus, which in turn determines the activation energy for the magnetization reversal.

Even carefully prepared samples of thin magnetic films on non-magnetic surfaces and magnetic islands patterned from such films have been found to have a wide distribution of nucleation volumes [10–12]. For example, experiments on Co/Pd islands as large as 5 μm [12] have shown that the switching field distribution (SFD) of patterned islands is a reflection of the spatial variation of the nucleation volume of the continuous film from which the islands were formed. The measurements could be described by a model where the continuous film reverses by nucleation of a low anisotropy volume followed by rapid domain wall propagation. While it might be assumed that high exchange coupling in patterned islands would lead to narrow SFD, compared for example to the thin films, this is not what has been found experimentally [12, 13]. Experiments, where the angle, θ, between the applied field and the anisotropy axis was varied, showed the well-known $1/\cos\theta$ dependence for the continuous film, consistent with a mechanism where the reversal rate is limited by wall propagation, but a minimum in the critical field at 45° was found for magnetic islands consistent with the Stoner-Wohlfarth model [14], which describes the rotation of a single magnetic moment of a homogeneous magnetic particle. This indicates that the rotation of the magnetic moment of the critical nucleus can be described by the Stoner-Wohlfarth model.

In recent experiments, de Vries *et al.* were able to measure the SFDs of individual magnetic islands and found a large variation in the properties of the islands even though the shape and size were the same [15]. In these experiments, the SFD is only a reflection of the stochastic nature of the thermal activation since the measurements are carried out for one island at a time but with repeated sweeps of the magnetic field. The experiments were based on the highly sensitive anomalous Hall effect and were carried out for disk-like islands of 220 nm diameter patterned from a Co/Pt multilayer film. A large difference was found in the maximum field needed to switch the magnetization of different islands, likely due to variations in the thickness and composition of the metallic layers from one island to another. "Weak" islands had, for example, a maximum in the SFD at a field of 84 kA/m while "strong" islands a maximum at 184 kA/m in measurements carried out at 10 K [15]. As the temperature was increased to 300 K, the peaks shifted to the lower field by ca. 50 kA/m and 30 kA/m for weak and strong islands, respectively.

These experiments were analyzed by a so-called diamond model where the shape of the islands is approximated by a square, and the activation energy is related to the length of a domain wall that starts at one corner and then propagates through the island. Several parameters in the model were adjusted in order to reproduce the experimental measurements, including a fairly strong drop in the saturation magnetization, by 7%, and the anisotropy constant, by 16%, as the temperature is increased from 10 K to 300 K. de Vries *et al.* concluded from their analysis that the energy barrier for magnetization reversal in zero field is a factor of three to four lower at 300 K than at 10 K. This is a very large factor and would mean that this fundamental and important parameter could not be obtained from measurements of remagnetization rates over a range in temperature, as is frequently done to establish Arrhenius rate expressions.

In the present article, we present calculations using an extended Stoner-Wohlfarth model [16] where the effect of thermal activation has been added and analyze the experimental measurements reported by de Vries *et al.* An analytical expression for the remagnetization rate, both pre-exponential factor, and activation energy is used to evaluate the SFD for both weak and strong islands. By adjusting two parameters in the model, the effective anisotropy constant and the nucleation volume, to reproduce the measured SFD peak positions, the full shape of the SFD at both 10 K and 300 K is found to be in close agreement with the experiments, without the need to vary the values of the parameters with temperature. Contrary to the conclusions described above, we find that a temperature independent energy barrier at zero field can be consistent with the experimental observations of de Vries *et al.* While the saturation magnetization and anisotropy should, of course, vary to some extent with temperature, our results indicate that it is only a small effect.

In the next section, the model is described including the method for calculating the SFDs. The results on the fitting of the peak positions are then described, followed by a comparison with the full shape of the SFDs. Calculated hysteresis loops for weak and strong islands are presented. Finally, the effect of temperature dependence is illustrated and discussed. The article closes with a conclusion section.

2. Model

The calculations are based on an extended Stoner-Wohlfarth model that takes into account thermal fluctuations [16]. This model was recently used to analyze remagnetization in elements of kagome spin ice [17]. In order to mimic the islands measured by de Vries *et al.*, the easy axis is taken to be perpendicular to the surface plane, and the applied magnetic field is directed parallel to the easy axis and opposite to the initial direction of the magnetization. A schematic of an island and a critical nucleus for the reversal are shown in Fig. 1 along with the coordinate system used. It is chosen in the same way as in ref. [16] for consistency. In the present case, the magnetic moment entering the model represents a critical nucleus for the remagnetization transition not the total magnetic moment of the island. It is assumed that the remagnetization transition starts in a small region within the island where for some reason it is easier to reverse the magnetic moments. Once the critical nucleus has formed, the domain of reversed magnetization grows quickly. A key parameter of the model is the volume of the nucleus, V, from which the magnetic moment of the nucleus, M, can be obtained from the saturation magnetization, M_s, as $M=VM_s$. The other key parameter in the model is the anisotropy constant, K_1. It represents an effective anisotropy that indirectly takes into account interfacial effects between the nucleus and the rest of the island. The experimental measurements of Thomson *et al.* [12] support the use of such a model to describe remagnetization in magnetic islands that are too large for uniform

rotation of all the magnetic moments in the island to be feasible. The parameters V and K_1 are treated as adjustable model parameters.

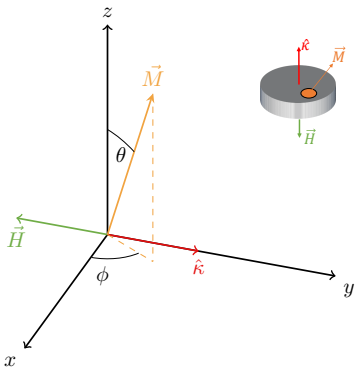

FIG. 1. Schematic representation of a magnetic island and the coordinate system used in the calculations. The out-of-plane anisotropy dominates over the in-plane anisotropy, and the magnetization is pointing along the surface normal, $\hat{\kappa}$. The external magnetic field, **H**, is directed opposite to the initial state magnetization. The model focuses on the magnetic moment of the critical nucleus of the remagnetization transition, **M**, pointing in the direction given by θ and ϕ.

For an applied magnetic field, H, pointing in the direction of the out-of-plane anisotropy axis the extended Stoner-Wohlfarth model gives an analytical expression for the rate of magnetization reversals [16]

$$k_{\parallel}^{HTST} = f_0\, e^{-\Delta E/k_B T} = \frac{\gamma K_1 \sqrt{(1-h)(2c-h+1)}}{\pi M_s} \exp\left[-\frac{K_1 V}{k_B T}(1-h)^2\right] \qquad (1)$$

where γ is the gyromagnetic ratio, $h \equiv HM_0/2K_1$, and c is the ratio of the out-of-plane, K_1, and in-plane, K_2, anisotropy constants, $c \equiv K_2/K_1$. The value of c does not affect the calculated results significantly and is simply assumed here to be 0.1. This expression can be used to estimate the magnetic field needed to reverse the magnetization at a given temperature and for a given timescale. A similar model has been used to analyze the reversal of magnetization in a spring magnet [18].

In typical experimental measurements, including those of de Vries *et al.*, the magnetic field is increased at a constant rate, $R = \Delta H/\Delta t$ until the magnetization reverses. Since the transition is thermally activated, in addition to being aided by the applied field, the field strength at the point when the reversal occurs varies from one measurement to another. Given the pre-exponential factor, f_0 and activation energy, ΔE, as in the expression for the rate constant above, the probability density for the value of H when the magnetization

switches can be estimated as [19]

$$p_{sw}(H) = \frac{f_0(H)}{R} \exp\left(-\frac{\Delta E(H)}{k_B T}\right) \times \exp\left[-\frac{1}{R}\int_{-H_{sat}}^{H'} f_0(H') \exp\left(-\frac{\Delta E(H')}{k_B T}\right) dH'\right] \quad (2)$$

The value of $p_{sw}(H)dH$ gives the probability that the magnetization switching will occur when the field strength is within the interval [H, H+dH] (the first two factors in 2), given the condition that it has not occurred at a smaller value of the field (the last factor in eq 2). This distribution can be compared with a histogram of the switching field in repeated measurements of a single magnetic island, as in the experiments of de Vries *et al.*. The M_s was chosen to have the reported value, M_s= 829 kA/m [15]. The islands where estimated have a diameter of d=220 nm and thickness t=20 nm, giving total volume of V_{isl}=760·10^3 nm^3, but these dimensions of the islands do not enter the calculations presented here since the focus is on the critical nucleus and its volume rather than the whole island. Only when the ratio of the volume of the nucleus and the total volume of the island is calculated for presentation purposes are the estimated total volume of the islands needed.

Each island is within this model described by the two parameters K_1 and V. Even if all the islands in the array have the same size and round shape, the effective anisotropy and, thereby, nucleation volume can differ significantly, for example, due to variations in the thickness of the metallic layers. Below, a detailed comparison is made between calculations using the model described above and the experimental measurements of de Vries *et al.* on weak and strong islands at a temperature of 10 K and 300 K.

3. Results

The maxima in the SFD at 10 K and at 300 K, $H^m_{10\,K}$ and $H^m_{300\,K}$, were calculated over a range of values for the two model parameters, K_1 and V. The results are shown in Fig. 2. The contour graph shows the value of the difference, ΔH^m=$H^m_{10\,K}$-$H^m_{300\,K}$, and the two colored curves show the values of K_1 and V that give $H^m_{10\,K}$ in agreement with the values obtained by de Vries *et al.* for weak and strong islands. The measured shift, ΔH^m, is ca. 50 kA/m for weak islands and 30 kA/m for strong islands. The low-temperature peaks, $H^m_{10\,K}$, are largely determined by K_1 but V affects the calculated temperature dependence of the peak positions.

For one particular set of parameters, K_1 and V, the measured values of both $H^m_{10\,K}$ and $H^m_{300\,K}$ can be reproduced for each type of island. The peak in the SFD at 10 K is largely determined by the anisotropy parameter and is weakly dependent on the nucleation volume (thus the small slope of the colored lines). The temperature shift, however, depends also on V and the isolines of constant temperature shift in H^m are nearly straight lines with a significant slope.

Fig. 3 shows the measured and calculated SFDs. It is evident from the figure that close agreement between the calculated and measured peak positions can be obtained by adjusting the two parameters. The optimal values are K_1=99.28 kJ/m^3 and V=0.036 V_{isl} for strong islands, and K_1=49.46 kJ/m^3 and V=0.0067 V_{isl} for weak islands.

Not only are the measured peak positions reproduced well, but also the shape of the calculated SDFs is in close correspondence with the measurements of de Vries *et al.* [15]. Since the width of the SFD peaks is not part of the fitting procedure, this lends strong support for the appropriateness of the present model for this system. Also, it is interesting that this close agreement with the experimental data can be obtained with the same values of K_1 and V over such widely different temperature values, 10 K and 300 K. The shift in peak position and the

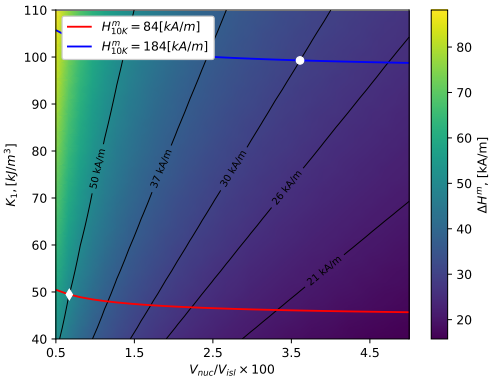

FIG. 2. Contour graph of the calculated shift in SFD peak positions when the temperature is increased from 10 K to 300 K, i.e., $\Delta H^m = H^m_{10\,K} - H^m_{300\,K}$, as a function of the two adjustable parameters, the anisotropy constant, K_1, and the nucleation volume, V (given as the fraction of the total volume $V_{isl} = 760 \cdot 10^3$ nm^3). Parameter values that give peak positions at 10 K, i.e., $H^m_{10\,K}$ in agreement with experimental observations [15] are shown with lines (red for a weak island, blue for a strong island). White diamond and disk identify parameter values that give peak positions in agreement with experiments at both 10 K and 300 K for weak and strong islands, respectively. The figure illustrates how a unique set of the two adjustable parameters can be found in such a way as to obtain agreement between the calculated and measured position of maxima in the SFD.

increased width of the peaks as temperature is increased is accurately described by harmonic transition state theory for magnetic systems [20] on which the extended Stoner-Wohlfarth model is based.

The zero field activation energy obtained from the model using these values of the parameters is 1.6 eV for weak and 17.0 eV for strong islands. The difference is indeed very large showing that the inhomogeneity is strong. The calculated pre-exponential factors in the rate expression, eqn. (1), at zero field are $3.5 \cdot 10^9$ Hz and for weak and $7.1 \cdot 10^9$ Hz for strong islands. These values are close to what has been assumed for Arrhenius rate expressions in the previous analysis [15, 21]. However, in the present approach, these values are obtained from the extended Stoner-Wohlfarth model.

Calculated hysteresis loops for weak and strong islands are shown in Fig. 4. The SFD is used there to produce loops for each type of island representing averages obtained in repeated scans of the applied field. The narrowing of the loops as the temperature is increased from 10 K to 300 K is clearly seen as well as the rounding of the corners due to the stochastic nature of the thermal activation. While the applied field lowers the activation energy the system needs to overcome to reverse the magnetization, the transitions eventually

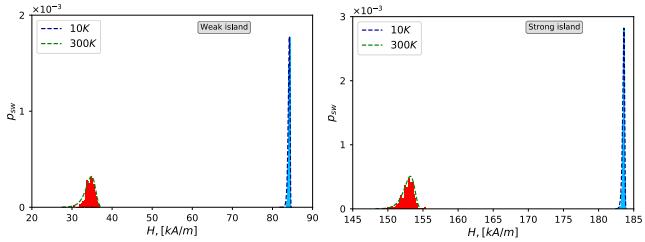

FIG. 3. Comparison of calculated (dashed lines) and measured (histograms) [15] SFDs for weak and strong islands at 10 K and at 300 K. The values of the two parameters, K_1 and V, in the theoretical model were obtained by adjusting the positions of the maxima of the SFD (see Fig. 2), but the shape of the SDFs then turns out to also be in close agreement with the experimental measurements.

occur due to thermal fluctuations. So, different values of the critical field are obtained in different scans of the field strength.

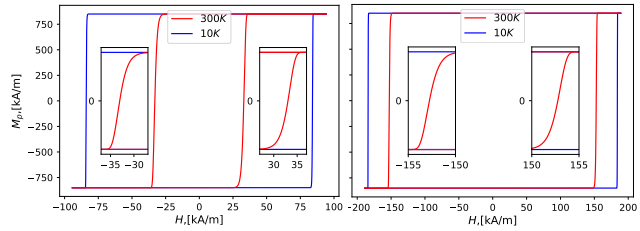

FIG. 4. Calculated hysteresis for a weak (left) and strong (right) island obtained from the calculated SFDs. The insets show on an expanded scale the rounding of the corners due to the stochastic nature of the thermal activation.

It is interesting that such close agreement with the experimental data can be obtained without changing the values of K_1 and V as well as M_s at the two values for the temperature, 10 K to 300 K. There will, of course, be some temperature dependence of these parameters, but the model used here indicates that it should be small. de Vries *et al.* estimated from their analysis a decrease in M_s by about 7% and a decrease in K_1 by about 16% as the temperature is increased from 10 K to 300 K [15]. It is indeed possible to reproduce the positions of the peaks in the SFDs with such a strong temperature dependence of these parameter values, but the nucleation volume, V, then needs to become 4 to 5 times larger at 300 K than at 10 K. As a result, the width of the SFD becomes much too narrow, by more than an order of magnitude, in strong disagreement with the experimental measurements. Within the present model, the decrease in the values of K_1 and V as well as M_s must be

much smaller than the estimate of de Vries *et al.* in order to reproduce the experimental observations.

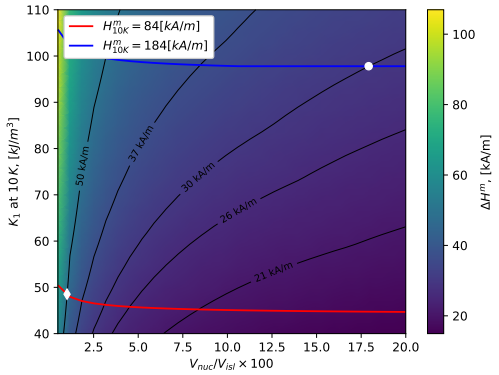

FIG. 5. Contour graph similar to Fig. 2 except here the saturation magnetization, M_s, is assumed to drop by 7% and the anisotropy constant, K_1, by 16% as the temperature is increased from 10 K to 300 K, as estimated by de Vries *et al.* [15]. Parameter values that give peak positions at 10 K, i.e., $H^m_{10\,K}$ in agreement with experimental observations [15] are shown with lines (red for a weak island, blue for a strong island). The value of the nucleation volume, V, needed to reproduce the shift in SDF peak position as the temperature is increased from 10 K to 300 K is much larger and the contour lines are more curved than when the parameters are temperature independent (see Fig. 2).

4. Conclusion

A simple model based on an extended Stoner-Wohlfarth equation for magnetization reversal in an island where the transition mechanism involves nucleation followed by rapid domain wall motion is found to reproduce well the elegant measurements of de Vries *et al.* [15] of SFDs of individual magnetic islands. The two adjustable parameters in the model, the anisotropy constant and the nucleation volume can be determined from the SFD peak positions at 10 K and 300 K. It is not necessary to include temperature dependence of the parameters. The shape of the SFD is then also found to be in close agreement with the measurements. The conclusion from this analysis of the experimental data is that the activation energy in zero field can be taken to be independent of temperature. This is in contradiction to the conclusion of de Vries *et al.* based on the diamond model where the zero field activation energy is decreased by a factor of three to four (for weak vs. strong islands) as the temperature is increased from 10 K to 300 K. This represents a large and important difference in the analysis of the experimental data. If indeed the zero field activation energy were to change so much with temperature, the standard methodology for determining activation energy from measurements taken over a wide temperature interval could not be applied when

determining this important quantity. Instead, our analysis indicates that the standard approach is applicable and can give the proper characterization of the magnetization reversal transition.

Our analysis does not assume the value of the pre-exponential factor, f_0, in the rate expression, eqn. (1). Rather, it is obtained from the model. While the magnitude of the pre-exponential factor turns out to be between 10^9 Hz and 10^{10} Hz in the present case, similar to what is often assumed for magnetic transitions, it is important to realize that harmonic transitions state theory has in some cases been found to give quite different values for pre-exponential factors in magnetic reversals (see, for example, [22, 23]). In general, it is important to evaluate the pre-exponential factor rather than just to assume some value.

5. Acknowledgements

This work was supported by the Icelandic Research Fund, the Academy of Finland (grant 278260) and the Government of the Russian Federation (grant 074U01).

References

[1] Sun S., Murray C. B., Weller D., Folks L., Moser A. Monodisperse FePt nanoparticles and ferromagnetic FePt nanocrystal superlattices. *Science*, 2000, **287(5460)**, P. 1989 – 1992.

[2] Allwood, D. A., Xiong, G., Faulkner, C. C., Atkinson, D., Petit, D., Cowburn, R. P. Magnetic domain-wall logic. *Science*, 2005, **309(5741)**, P. 1688–1692.

[3] Katine, J. A., Albert, F. J., Buhrman, R. A., Myers, E. B., Ralph, D. C. Current-driven magnetization reversal and spin-wave excitations in Co/Cu/Co pillars. *Physical review letters*, 2000, **84(14)**, P. 3149.

[4] Jacobs S., Bean C. P. Fine Particles, Thin Films and Exchange Anisotropy. *Magnetism vol. III, ed. Rado G. T. and Suhl H. (New York: Academic)*, 1963, P. 275.

[5] Zijlstra H. Permanent magnets, theory. *Handbook of Magnetic Materials, vol. 3, ed. Wohlfarth E. P. (Amsterdam: North-Holland)*, 1982, P. 37–107.

[6] Givord, D., Lu, Q., Rossignol, M. F. Coercivity in hard magnetic materials. *In Science and Technology of Nanostructured Magnetic Materials, Springer US* , 1991, P. 635–656.

[7] Zhu, J. G., Peng, Y., Laughlin, D. E. Toward an understanding of grain-to-grain anisotropy field variation in thin film media. *IEEE transactions on magnetics*, 2005, **41(2)**, P. 543–548.

[8] Terris, B. D., Thomson, T. Nanofabricated and self-assembled magnetic structures as data storage media. *Journal of physics D: Applied physics*, 2005, **38(12)**, P. R199.

[9] Engel, B. N., Akerman, J., Butcher, B., Dave, R. W., DeHerrera, M., Durlam, M., Slaughter, J. M. and others. A 4-Mb toggle MRAM based on a novel bit and switching method. *IEEE Transactions on Magnetics*, 2005, **41(1)**, P. 132–136.

[10] Jang, H. J., Eames, P., Dahlberg, E. D., Farhoud, M., Ross, C. A. Magnetostatic interactions of single-domain nanopillars in quasistatic magnetization states. *Applied Physics Letters*, 2005, **86(2)**, P. 023102.

[11] Kitade, Y., Komoriya, H., Maruyama, T. Patterned media fabricated by lithography and argon-ion milling. *IEEE transactions on magnetics*, 2004, **40(4)**, P. 2516–2518.

[12] Thomson T., Hu G., Terris B. D. Intrinsic Distribution of Magnetic Anisotropy in Thin Films Probed by Patterned Nanostructures. *Phys. Rev. Lett.*, 2006, **96**, P. 257204.

[13] Shaw, J. M., Rippard, W. H., Russek, S. E., Reith, T., Falco, C. M. Origins of switching field distributions in perpendicular magnetic nanodot arrays. *Journal of Applied Physics*, 2007, **101(2)**, P. 023909.

[14] Stoner E. C., Wohlfarth E. P. A mechanism of magnetic hysteresis in heterogeneous alloys. *Phil. Trans. Roy. Soc. A*, 1948, **240**, P. 599–642.

[15] de Vries J., Bolhuis T., Abelmann L. Temperature dependence of the energy barrier and switching field of sub-micron magnetic islands with perpendicular anisotropy. *New J. Phys.*, 2017, **19**, P. 093019.

[16] Liashko S. Y., Uzdin V. M., Jónsson H. Thermal stability of magnetic states in submicron magnetic islands. *Nanosystems: Physics, Chemistry, Mathematics*, 2017, **8(5)**, P. 572–578.

[17] Liashko S. Y, Jónsson H., Uzdin V. M. The effect of temperature and external field on transitions in elements of kagome spin ice. *New J. Phys.*, 2017, **19**, P. 113008.

[18] Moskalenko M., Bessarab P. F., Uzdin V. M., Jónsson H. Qualitative Insight and Quantitative Analysis of the Effect of Temperature on the Coercivity of a Magnetic System. *AIP Advances*, 2016, **6(2)**, P. 025213.

[19] Engelen J.B., Delalande M., Le Febre A.J., Bolhuis T., Shimatsu T., Kikuchi N., Abelmann L., Lodder J.C. Thermally induced switching field distribution of a single CoPt dot in a large array. *Nanotechnology*, 2009, **21(3)**, P. 035703.

[20] Bessarab P. F., Uzdin V. M. Jónsson H. Harmonic Transition State Theory of Thermal Spin Transitions. *Phys. Rev. B*, 2012, **85(18)**, P. 184409.

[21] Engelen J. B. C., Delalande M., le Febre A. J., Bolhuis T., Shimatsu T., Kikuchi N., Abelmann L., Lodder J. C. Thermally induced switching field distribution of a single CoPt dot in a large array. *Nanotechnology*, 2010, **21(3)**, P. 035703.

[22] Bessarab P. F., Uzdin V. M. Jónsson H. Size and Shape Dependence of Thermal Spin Transitions in Nanoislands. *Phys. Rev. Lett.*, 2013, **110(2)**, P. 020604.

[23] Ivanov A. A., Bessarab P. F., Uzdin V. M., Jónsson H. Magnetic exchange force microscopy: Theoretical analysis of induced magnetization reversals. *Nanoscale*, 2017, **9(35)**, P. 13320–13325.

References

[1] **J. L. Kirschvink**, **A. Kobayashi-Kirschvink** and **B. J. Woodford**. *Magnetite biomineralization in the human brain.* Proceedings of the National Academy of Sciences, 89(16), (1992), 7683.

[2] **C. Reig**, **S. Cardoso** and **S. C. Mukhopadhyay**. *Giant magnetoresistance (GMR) sensors*. SSMI6, pp. 157–180.

[3] **J. Denardin**, **M. Knobel**, **X. Zhang** and **A. Pakhomov**. *Giant Hall effect in superparamagnetic granular films*. Journal of magnetism and magnetic materials, 262(1), (2003), 15.

[4] **M. Julliere**. *Tunneling between ferromagnetic films*. Physics letters A, 54(3), (1975), 225.

[5] **J. Ding**, **P. McCormick** and **R. Street**. *Remanence enhancement in mechanically alloyed isotropic Sm 7 Fe 93-nitride*. Journal of magnetism and magnetic materials, 124(1), (1993), 1.

[6] **C. Leighton**, **J. Nogués**, **B. Jönsson-Åkerman** and **I. K. Schuller**. *Coercivity enhancement in exchange biased systems driven by interfacial magnetic frustration*. Physical review letters, 84(15), (2000), 3466.

[7] **R. McMichael**, **J. Ritter** and **R. Shull**. *Enhanced magnetocaloric effect in Gd3Ga5- x Fe x O12*. Journal of applied physics, 73(10), (1993), 6946.

[8] **C. Sangregorio**, **T. Ohm**, **C. Paulsen**, **R. Sessoli** and **D. Gatteschi**. *Quantum tunneling of the magnetization in an iron cluster nanomagnet*. Physical review letters, 78(24), (1997), 4645.

[9] **M. Respaud**, **J. Broto**, **H. Rakoto**, **A. Fert**, **L. Thomas**, **B. Barbara**, **M. Verelst**, **E. Snoeck**, **P. Lecante**, **A. Mosset** *et al. Surface effects on the magnetic properties of ultrafine cobalt particles*. Physical Review B, 57(5), (1998), 2925.

[10] **D. Cox**, **D. Trevor**, **R. Whetten**, **E. Rohlfing** and **A. Kaldor**. *Magnetic behavior of free-iron and iron oxide clusters*. Physical Review B, 32(11), (1985), 7290.

[11] **F. E. Luborsky** and **P. E. Lawrence**. *Saturation Magnetization and Size of Iron Particles Less than 100 A in Diameter*. Journal of Applied Physics, 32(3), (1961), S231.

[12] **T. Furubayashi**, **I. Nakatani** and **N. Saegusa**. *Magnetic moment and hyperfine field in colloidal fine particles of iron*. Journal of the Physical Society of Japan, 56(5), (1987), 1855.

[13] **J. Chen**, **C. Sorensen**, **K. Klabunde** and **G. Hadjipanayis**. *Enhanced magnetization of nanoscale colloidal cobalt particles*. Physical Review B, 51(17), (1995), 11527.

[14] **W. A. de Heer**, **P. Milani** and **A. Chtelain**. *Spin relaxation in small free iron clusters*. Physical review letters, 65(4), (1990), 488.

[15] **J. Bucher**, **D. Douglass** and **L. Bloomfield**. *Magnetic properties of free cobalt clusters*. Physical review letters, 66(23), (1991), 3052.

[16] **D. Douglass**, **A. Cox**, **J. Bucher** and **L. Bloomfield**. *Magnetic properties of free cobalt and gadolinium clusters*. Physical Review B, 47(19), (1993), 12874.

[17] **A. Cox**, **J. Louderback** and **L. Bloomfield**. *Experimental observation of magnetism in rhodium clusters*. Physical review letters, 71(6), (1993), 923.

[18] **I. M. Billas**, **A. Chatelain**, **W. A. De Heer** *et al. Magnetism from the atom to the bulk in iron, cobalt, and nickel clusters*. SCIENCE-NEW YORK THEN WASHINGTON-, pp. 1682–1682.

[19] **S. Apsel**, **J. Emmert**, **J. Deng** and **L. Bloomfield**. *Surface-enhanced magnetism in nickel clusters*. Physical review letters, 76(9), (1996), 1441.

[20] **F. Liu**, **M. Press**, **S. Khanna** and **P. Jena**. *Magnetism and local order: Ab initio tight-binding theory*. Physical Review B, 39(10), (1989), 6914.

[21] **J. Merikoski**, **J. Timonen**, **M. Manninen** and **P. Jena**. *Ferromagnetism in small clusters*. Physical review letters, 66(7), (1991), 938.

[22] **S. Khanna** and **S. Linderoth**. *Magnetic behavior of clusters of ferromagnetic transition metals*. Physical review letters, 67(6), (1991), 742.

[23] **B. Reddy**, **S. Khanna** and **B. Dunlap**. *Giant magnetic moments in 4d clusters*. Physical review letters, 70(21), (1993), 3323.

[24] **Z.-q. Li** and **B.-l. Gu**. *Electronic-structure calculations of cobalt clusters*. Physical Review B, 47(20), (1993), 13611.

[25] **W. F. Brown**. *Micromagnetics*. 18. Interscience Publishers, 1963.

[26] **J. Jacob** and **C. Bean**. *Magnetism Vol. III*. by Rado, GT and Suhl, H., Academic Press, New York, pp. 371–371.

[27] **E. C. Stoner** and **E. Wohlfarth**. *A mechanism of magnetic hysteresis in heterogeneous alloys*. Philosophical Transactions of the Royal Society of London A: Mathematical, Physical and Engineering Sciences, 240(826), (1948), 599.

[28] **S. Krupicka**, **P. Novak** and **E. Wohlfarth**. *Ferromagnetic Materials, Vol. 3*. ed. EP Wohlfarth, North-Holland publishing Co., Amsterdam, Holland, pp. 80090–2.

[29] **C. Chien** and **G. Hadjipanayis**. *Science and technology of nanostructured magnetic materials*. Plenum Press, New York, p. 4772.

[30] **J.-L. Dormann**, **D. Fiorani** and **E. Tronc**. *Magnetic relaxation in fine-particle systems*. Advances in Chemical Physics, Volume 98, pp. 283–494.

[31] **C. Bean**. *Hysteresis loops of mixtures of ferromagnetic micropowders*. Journal of Applied Physics, 26(11), (1955), 1381.

[32] **J. D. Jackson**. *Classical electrodynamics*. AAPT, 1999.

[33] **D. J. Griffiths**. *Introduction to quantum mechanics*. Cambridge University Press, 2016.

[34] **A. G. Gurevich** and **G. A. Melkov**. *Magnetization oscillations and waves*. CRC press, 1996.

[35] **A. Hubert** and **R. Schäfer**. *Magnetic domains: the analysis of magnetic microstructures*. Springer Science & Business Media, 2008.

[36] **J. M. Coey**. *Magnetism and magnetic materials*. Cambridge University Press, 2010.

[37] **A. Aharoni**. *Introduction to the Theory of Ferromagnetism*, volume 109. Clarendon Press, 2000.

[38] **A. Berger**, **U. Linke** and **H. Oepen**. *Symmetry-induced uniaxial anisotropy in ultrathin epitaxial cobalt films grown on Cu (1 1 13)*. Physical review letters, 68(6), (1992), 839.

[39] **B. Clark**, **R. Herman** and **R. Wallis**. *Theoretical mean-square displacements for surface atoms in face-centered cubic lattices with applications to nickel*. Physical Review, 139(3A), (1965), A860.

[40] **J. H. van Vleck**. *On the anisotropy of cubic ferromagnetic crystals*. Physical Review, 52(11), (1937), 1178.

[41] **J. Osborn**. *Demagnetizing factors of the general ellipsoid*. Physical review, 67(11-12), (1945), 351.

[42] **A. Aharoni**. *Demagnetizing factors for rectangular ferromagnetic prisms*. Journal of applied physics, 83(6), (1998), 3432.

[43] **A. Thiaville**, **J. M. García**, **J. Miltat**, **T. Schrefl** *et al. Micromagnetic study of Bloch-point-mediated vortex core reversal*. Physical Review B, 67(9), (2003), 094410.

[44] **A. Lyberatos**, **D. V. Berkov** and **R. W. Chantrell**. *A method for the numerical simulation of the thermal magnetization fluctuations in micromagnetics*. Journal of Physics: Condensed Matter, 5(47), (1993), 8911.

[45] **D. A. Garanin**. *Fokker-Planck and Landau-Lifshitz-Bloch equations for classical ferromagnets*. Physical Review B, 55(5), (1997), 3050.

[46] **S. Parkin** and **D. Mauri**. *Spin engineering: Direct determination of the Ruderman-Kittel-Kasuya-Yosida far-field range function in ruthenium*. Physical Review B, 44(13), (1991), 7131.

[47] **I. A. Sergienko** and **E. Dagotto**. *Role of the Dzyaloshinskii-Moriya interaction in multiferroic perovskites*. Physical Review B, 73(9), (2006), 094434.

[48] **M. Heide**, **G. Bihlmayer** and **S. Blügel**. *Dzyaloshinskii-Moriya interaction accounting for the orientation of magnetic domains in ultrathin films: Fe/W (110)*. Physical Review B, 78(14), (2008), 140403.

[49] **L. Lopez-Diaz**, **D. Aurelio**, **L. Torres**, **E. Martinez**, **M. Hernandez-Lopez**, **J. Gomez**, **O. Alejos**, **M. Carpentieri**, **G. Finocchio** and **G. Consolo**. *Micromagnetic simulations using graphics processing units*. Journal of Physics D: Applied Physics, 45(32), (2012), 323001.

[50] **X. Batlle** and **A. l. Labarta**. *Finite-size effects in fine particles: magnetic and transport properties*. Journal of Physics-London-D Applied Physics, 35(6), (2002), R15.

[51] **R. Victora**. *Predicted time dependence of the switching field for magnetic materials*. Physical review letters, 63(4), (1989), 457.

[52] **H. Pfeiffer**. *Influence of thermal fluctuations on the magnetic properties of particle assemblies*. physica status solidi (a), 122(1), (1990), 377.

[53] **W. Wernsdorfer**, **B. Doudin**, **D. Mailly**, **K. Hasselbach**, **A. Benoit**, **J. Meier**, **J.-P. Ansermet** and **B. Barbara**. *Nucleation of magnetization reversal in individual nanosized nickel wires*. Physical Review Letters, 77(9), (1996), 1873.

[54] **W. Wernsdorfer**, **E. B. Orozco**, **B. Barbara**, **K. Hasselbach**, **A. Benoit**, **D. Mailly**, **B. Doudin**, **J. Meier**, **J. Wegrowe**, **J.-P. Ansermet** *et al. Mesoscopic effects in magnetism: Submicron to nanometer size single particle measurements*. Journal of applied physics, 81(8), (1997), 5543.

[55] **W. Wernsdorfer**, **K. Hasselbach**, **A. Benoit**, **B. Barbara**, **B. Doudin**, **J. Meier**, **J.-P. Ansermet** and **D. Mailly**. *Measurements of magnetization switching in individual nickel nanowires*. Physical Review B, 55(17), (1997), 11552.

[56] **W. Wernsdorfer**, **E. B. Orozco**, **K. Hasselbach**, **A. Benoit**, **D. Mailly**, **O. Kubo**, **H. Nakano** and **B. Barbara**. *Macroscopic quantum tunneling of magnetization of single ferrimagnetic nanoparticles of barium ferrite*. Physical Review Letters, 79(20), (1997), 4014.

[57] **W. Wernsdorfer**, **E. B. Orozco**, **K. Hasselbach**, **A. Benoit**, **B. Barbara**, **N. Demoncy**, **A. Loiseau**, **H. Pascard** and **D. Mailly**. *Experimental evidence of the Néel-Brown model of magnetization reversal*. Physical Review Letters, 78(9), (1997), 1791.

[58] **W. Coffey**, **D. Crothers**, **J. Dormann**, **Y. P. Kalmykov**, **E. Kennedy** and **W. Wernsdorfer**. *Thermally activated relaxation time of a single domain ferromagnetic particle subjected to a uniform field at an oblique angle to the easy axis: Comparison with experimental observations*. Physical review letters, 80(25), (1998), 5655.

[59] **M. Lederman**, **S. Schultz** and **M. Ozaki**. *Measurement of the dynamics of the magnetization reversal in individual single-domain ferromagnetic particles*. Physical review letters, 73(14), (1994), 1986.

[60] **T. Chang** and **J. G. Zhu**. *Angular dependence measurement of individual barium ferrite recording particles near the single domain size*. Journal of Applied Physics, 75(10), (1994), 5553.

[61] **A. Kent**, **S. v. Molnár**, **S. Gider** and **D. Awschalom**. *Properties and measurement of scanning tunneling microscope fabricated ferromagnetic particle arrays*. Journal of Applied Physics, 76(10), (1994), 6656.

[62] **V. Cros**, **S.-F. Lee**, **G. Faini**, **A. Cornette**, **A. Hamzic** and **A. Fert**. *Detection of the magnetization reversal in submicron Co particles by GMR measurements*. Journal of magnetism and magnetic materials, 165(1-3), (1997), 512.

[63] **W. Gallagher**, **S. S. Parkin**, **Y. Lu**, **X. Bian**, **A. Marley**, **K. Roche**, **R. Altman**, **S. Rishton**, **C. Jahnes**, **T. Shaw** *et al. Microstructured magnetic tunnel junctions*. Journal of Applied Physics, 81(8), (1997), 3741.

[64] **B. Doudin**, **G. Redmond**, **S. Gilbert** and **J.-P. Ansermet**. *Magnetoresistance governed by fluctuations in ultrasmall Ni/NiO/Co junctions*. Physical review letters, 79(5), (1997), 933.

[65] **S. Guéron**, **M. M. Deshmukh**, **E. Myers** and **D. Ralph**. *Tunneling via individual electronic states in ferromagnetic nanoparticles*. Physical review letters, 83(20), (1999), 4148.

[66] **W. Wernsdorfer**, **K. Hasselbach**, **D. Mailly**, **B. Barbara**, **A. Benoit**, **L. Thomas** and **G. Suran**. *DC-SQUID magnetization measurements of single magnetic particles*. Journal of magnetism and magnetic materials, 145(1-2), (1995), 33.

[67] **W. Wernsdorfer**, **D. Mailly** and **A. Benoit**. *Single nanoparticle measurement techniques*. Journal of Applied Physics, 87(9), (2000), 5094.

[68] **W. Wernsdorfer**, **K. Hasselbach**, **A. Benoit**, **W. Wernsdorfer**, **B. Barbara**, **D. Mailly**, **J. Tuaillon**, **J. Perez**, **V. Dupuis**, **J. Dupin** *et al. High sensitivity magnetization measurements of nanoscale cobalt clusters*. Journal of applied physics, 78(12), (1995), 7192.

[69] **E. Bonet**, **W. Wernsdorfer**, **B. Barbara**, **A. Benoit**, **D. Mailly** and **A. Thiaville**. *Three-dimensional magnetization reversal measurements in nanoparticles*. Physical review letters, 83(20), (1999), 4188.

[70] **W. Coffey**, **D. Garanin** and **D. McCarthy**. *Crossover formulas in the kramers theory of thermally activated escape rates—application to spin systems*. Advances in Chemical Physics, Volume 117, pp. 483–765.

[71] **H.-B. Braun**. *Topological effects in nanomagnetism: from superparamagnetism to chiral quantum solitons*. Advances in Physics, 61(1), (2012), 1.

[72] **J. M. Shaw**, **W. H. Rippard**, **S. E. Russek**, **T. Reith** and **C. M. Falco**. *Origins of switching field distributions in perpendicular magnetic nanodot arrays*. Journal of Applied Physics, 101(2), (2007), 023909.

[73] **J. de Vries**, **T. Bolhuis** and **L. Abelmann**. *Temperature dependence of the energy barrier and switching field of sub-micron magnetic islands with perpendicular anisotropy*. New Journal of Physics, 19(9), (2017), 093019.

[74] **E. Meijer**. *Jacobus Henricus van't Hoff; Hundred years of impact on stereochemistry in the Netherlands*. Angewandte Chemie International Edition, 40(20), (2001), 3783.

[75] **R. Marcus**. *Solvent Dynamics and RRKM Theory of Clusters*. In *Advances in Chemical Physics: Chemical Reactions and their Control on the Femtosecond Time Scale: 20th Solvay Conference on Chemistry, Volume 101*, pp. 391–408. Wiley Online Library, 1997.

[76] **G. Billing** and **K. Mikkelsen**. *Introduction to Molecular Dynamics and Chemical Kinetics*. Wiley, 1996.

[77] **P. Hänggi**, **P. Talkner** and **M. Borkovec**. *Reaction-rate theory: fifty years after Kramers*. Reviews of modern physics, 62(2), (1990), 251.

[78] **N. G. Van Kampen**. *Stochastic processes in physics and chemistry*, volume 1. Elsevier, 1992.

[79] **H. Eyring**. *The activated complex in chemical reactions*. The Journal of Chemical Physics, 3(2), (1935), 107.

[80] **E. Wigner**. *The transition state method*. Transactions of the Faraday Society, 34, (1938), 29.

[81] **H. A. Kramers**. *Brownian motion in a field of force and the diffusion model of chemical reactions*. Physica, 7(4), (1940), 284.

[82] **H. Brinkman**. *Brownian motion in a field of force and the diffusion theory of chemical reactions. II*. Physica, 22(1-5), (1956), 149.

[83] **R. Landauer** and **J. Swanson**. *Frequency factors in the thermally activated process*. Physical Review, 121(6), (1961), 1668.

[84] **J. Langer**. *Statistical theory of the decay of metastable states*. Annals of Physics, 54(2), (1969), 258.

[85] **T. Ala-Nissila** and **S. Ying**. *Theory of classical surface diffusion*. Progress in surface science, 39(3), (1992), 227.

[86] **W. T. Coffey** and **Y. P. Kalmykov**. *Rotational diffusion and dielectric relaxation in nematic liquid crystals*. Advances in Chemical Physics, Volume 113, pp. 487–551.

[87] **M. Grant** and **J. Gunton**. *Theory for the nucleation of a crystalline droplet from the melt*. Physical Review B, 32(11), (1985), 7299.

[88] **L. P. Csernai** and **J. I. Kapusta**. *Nucleation of relativistic first-order phase transitions*. Physical Review D, 46(4), (1992), 1379.

[89] **L. Néel**. *Théorie du traînage magnétique de diffusion*. J. phys. radium, 13(5), (1952), 249.

[90] **W. F. Brown Jr**. *Thermal fluctuations of a single-domain particle*. Physical Review, 130(5), (1963), 1677.

[91] **I. Klik** and **L. Gunther**. *First-passage-time approach to overbarrier relaxation of magnetization*. Journal of Statistical Physics, 60(3-4), (1990), 473.

[92] **I. Klik** and **L. Gunther**. *Thermal relaxation over a barrier in single domain ferromagnetic particles*. Journal of Applied Physics, 67(9), (1990), 4505.

[93] **R. F. Grote** and **J. T. Hynes**. *The stable states picture of chemical reactions. II. Rate constants for condensed and gas phase reaction models*. The Journal of Chemical Physics, 73(6), (1980), 2715.

[94] **J. C. Keck**. *Variational theory of reaction rates*. Wiley Online Library, 1966.

[95] **P. F. Bessarab**, **V. M. Uzdin** and **H. Jónsson**. *Harmonic transition-state theory of thermal spin transitions*. Physical Review B, 85(18), (2012), 184409.

[96] **I. S. Lobanov**, **H. Jónsson** and **V. M. Uzdin**. *Mechanism and activation energy of magnetic skyrmion annihilation obtained from minimum energy path calculations*. Physical Review B, 94(17), (2016), 174418.

[97] **V. Uzdin**, **M. Potkina**, **I. S. Lobanov**, **P. Bessarab** and **H. Jonsson**. *The effect of confinement and defects on the thermal stability of skyrmions*.

[98] **V. Uzdin**, **M. Potkina**, **I. S. Lobanov**, **P. Bessarab** and **H. Jonsson**. *Energy surface and lifetime of magnetic skyrmions*. Journal of Magnetism and Magnetic Materials.

[99] **S. Liashko**, **H. Jonsson** and **V. M. Uzdin**. *The effect of temperature and external field on transitions in elements of kagome spin ice*. New Journal of Physics.

[100] **P. F. Bessarab**, **V. M. Uzdin** and **H. Jónsson**. *Size and shape dependence of thermal spin transitions in nanoislands*. Physical review letters, 110(2), (2013), 020604.

[101] **M. Moskalenko**, **P. F. Bessarab**, **V. M. Uzdin** and **H. Jónsson**. *Qualitative insight and quantitative analysis of the effect of temperature on the coercivity of a magnetic system*. AIP Advances, 6(2), (2016), 025213.

[102] **A. Ivanov**, **P. F. Bessarab**, **V. M. Uzdin** and **H. Jónsson**. *Magnetic exchange force microscopy: theoretical analysis of induced magnetization reversals*. Nanoscale, 9(35), (2017), 13320.

[103] **P. F. Bessarab**, **V. M. Uzdin** and **H. Jónsson**. *Potential energy surfaces and rates of spin transitions*. Zeitschrift für Physikalische Chemie, 227(9-11), (2013), 1543.

[104] **P. F. Bessarab**, **V. M. Uzdin** and **H. Jónsson**. *Calculations of magnetic states and minimum energy paths of transitions using a noncollinear extension of the Alexander-Anderson model and a magnetic force theorem*. Physical Review B, 89(21), (2014), 214424.

[105] **G. Henkelman** and **H. Jónsson**. *Improved tangent estimate in the nudged elastic band method for finding minimum energy paths and saddle points*. The Journal of chemical physics, 113(22), (2000), 9978.

[106] **G. Henkelman**, **B. P. Uberuaga** and **H. Jónsson**. *A climbing image nudged elastic band method for finding saddle points and minimum energy paths*. The Journal of chemical physics, 113(22), (2000), 9901.

[107] **P. F. Bessarab**, **V. M. Uzdin** and **H. Jónsson**. *Method for finding mechanism and activation energy of magnetic transitions, applied to skyrmion and antivortex annihilation*. Computer Physics Communications, 196, (2015), 335.

[108] **J. B. C. Engelen**, **M. Delalande**, **A. Le Febre**, **T. Bolhuis**, **T. Shimatsu**, **N. Kikuchi**, **L. Abelmann** and **J. Lodder**. *Thermally induced switching field distribution of a single CoPt dot in a large array*. Nanotechnology, 21(3), (2009), 035703.

[109] **Y. Kitade**, **H. Komoriya** and **T. Maruyama**. *Patterned media fabricated by lithography and argon-ion milling*. IEEE transactions on magnetics, 40(4), (2004), 2516.

[110] **C. Haginoya**, **S. Heike**, **M. Ishibashi**, **K. Nakamura**, **K. Koike**, **T. Yoshimura**, **J. Yamamoto** and **Y. Hirayama**. *Magnetic nanoparticle array with perpendicular crystal magnetic anisotropy*. Journal of applied physics, 85(12), (1999), 8327.

[111] **T. Thomson**, **G. Hu** and **B. Terris**. *Intrinsic distribution of magnetic anisotropy in thin films probed by patterned nanostructures*. Physical Review Letters, 96(25), (2006), 257204.

[112] **M. Harris**, **S. Bramwell**, **D. McMorrow**, **T. Zeiske** and **K. Godfrey**. *Geometrical frustration in the ferromagnetic pyrochlore Ho 2 Ti 2 O 7*. Physical Review Letters, 79(13), (1997), 2554.

[113] **J. Snyder**, **J. Slusky**, **R. Cava** and **P. Schiffer**. *How 'spin ice' freezes*. Nature, 413(6851), (2001), 48.

[114] **J. Gardner**, **A. Keren**, **G. Ehlers**, **C. Stock**, **E. Segal**, **J. Roper**, **B. Fåk**, **M. Stone**, **P. Hammar**, **D. Reich** *et al. Dynamic frustrated magnetism in Tb 2 Ti 2 O 7 at 50 mK*. Physical Review B, 68(18), (2003), 180401.

[115] **I. Mirebeau**, **H. Mutka**, **P. Bonville**, **A. Apetrei** and **A. Forget**. *Investigation of magnetic fluctuations in Tb 2 Sn 2 O 7 ordered spin ice by high-resolution energy-resolved neutron scattering*. Physical Review B, 78(17), (2008), 174416.

[116] **. R. Wang**, **C. Nisoli**, **R. Freitas**, **J. Li**, **W. McConville**, **B. Cooley**, **M. Lund**, **N. Samarth**, **C. Leighton**, **V. Crespi** *et al. Artificial 'spin ice' in a geometrically frustrated lattice of nanoscale ferromagnetic islands*. Nature, 439(7074), (2006), 303.

[117] **E. Mengotti**, **L. Heyderman**, **A. F. Rodriguez**, **A. Bisig**, **L. Le Guyader**, **F. Nolting** and **H. Braun**. *Building blocks of an artificial kagome spin ice: Photoemission electron microscopy of arrays of ferromagnetic islands*. Physical Review B, 78(14), (2008), 144402.

[118] **Y. Qi**, **T. Brintlinger** and **J. Cumings**. *Direct observation of the ice rule in an artificial kagome spin ice*. Physical Review B, 77(9), (2008), 094418.

[119] **M. Tanaka**, **E. Saitoh**, **H. Miyajima**, **T. Yamaoka** and **Y. Iye**. *Magnetic interactions in a ferromagnetic honeycomb nanoscale network*. Physical Review B, 73(5), (2006), 052411.

[120] **C. Castelnovo**, **R. Moessner** and **S. L. Sondhi**. *Magnetic monopoles in spin ice*. Nature, 451(7174), (2008), 42.

[121] **C. Phatak**, **A. Petford-Long**, **O. Heinonen**, **M. Tanase** and **M. De Graef**. *Nanoscale structure of the magnetic induction at monopole defects in artificial spin-ice lattices*. Physical Review B, 83(17), (2011), 174431.

[122] **V. Kapaklis**, **U. B. Arnalds**, **A. Harman-Clarke**, **E. T. Papaioannou**, **M. Karimipour**, **P. Korelis**, **A. Taroni**, **P. C. Holdsworth**, **S. T. Bramwell** and **B. Hjörvarsson**. *Melting artificial spin ice*. New Journal of Physics, 14(3), (2012), 035009.

[123] **L. Anghinolfi**, **H. Luetkens**, **J. Perron**, **M. G. Flokstra**, **O. Sendetskyi**, **A. Suter**, **T. Prokscha**, **P. M. Derlet**, **S. Lee** and **L. J. Heyderman**. *Thermodynamic phase transitions in a frustrated magnetic metamaterial*. Nature communications, 6, (2015), 8278.

[124] **A. Farhan**, **A. Scholl**, **C. F. Petersen**, **L. Anghinolfi**, **C. Wuth**, **S. Dhuey**, **R. V. Chopdekar**, **P. Mellado**, **M. J. Alava** and **S. Van Dijken**. *Thermodynamics of emergent magnetic charge screening in artificial spin ice*. Nature communications, 7, (2016), 12635.

[125] **G. Möller** and **R. Moessner**. *Magnetic multipole analysis of kagome and artificial spin-ice dipolar arrays*. Physical Review B, 80(14), (2009), 140409.

[126] **G.-W. Chern**, **P. Mellado** and **O. Tchernyshyov**. *Two-stage ordering of spins in dipolar spin ice on the kagome lattice*. Physical review letters, 106(20), (2011), 207202.

[127] **A. Vansteenkiste**, **J. Leliaert**, **M. Dvornik**, **M. Helsen**, **F. Garcia-Sanchez** and **B. Van Waeyenberge**. *The design and verification of MuMax3*. Aip Advances, 4(10), (2014), 107133.

[128] **A. Farhan**, **P. Derlet**, **A. Kleibert**, **A. Balan**, **R. Chopdekar**, **M. Wyss**, **L. Anghinolfi**, **F. Nolting** and **L. J. Heyderman**. *Exploring hyper-cubic energy landscapes in thermally active finite artificial spin-ice systems*. Nature Physics, 9(6), (2013), nphys2613.

[129] **I. Gilbert**, **G.-W. Chern**, **S. Zhang**, **L. O'Brien**, **B. Fore**, **C. Nisoli** and **P. Schiffer**. *Emergent ice rule and magnetic charge screening from vertex frustration in artificial spin ice*. Nature Physics, 10(9), (2014), 670.